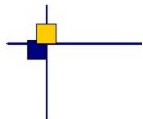


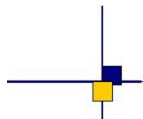


CalVal Jason-3



Jason-3 validation and cross calibration activities (Annual report 2018)

Contract No 160182-14026/00 Lot 1.6.3



Nomenclature : SALP-RP-MA-EA-23248-CLS

Issue : 1rev 1

Date : February 22, 2019

Chronology Issues:

Issue:	Date:	Reason for change:
	2018-12-15	Creation
1.0	2019-01-25	Draft version
1.1	2019-02-22	Delivery version

People involved in this issue :

	AUTHORS	COMPANY	DATE	INITIALS
Written by:	H. Roinard L. Michaud	CLS		
Checked by:		CLS		
Approved by:		CLS CLS		
Application authorised by:				

Index Sheet :

Context:	
Keywords:	
Hyperlink:	

Distribution:

Company	Means of distribution	Names
CLS/DOS	electronic copy	V.ROSMORDUC
CNES	electronic copy	thierry.guinle@cnes.fr nicolas.picot@cnes.fr gerald.dibarboure@cnes.fr aqgp_rs@cnes.fr dominique.chermain@cnes.fr delphine.vergnoux@cnes.fr francois.bignalet-cazalet@cnes.fr

List of tables and figures

List of Tables

1	<i>Events on Jason-3 mission</i>	11
2	<i>Acquisition mode</i>	12
3	<i>List of GDR version "D" standard</i>	16
4	<i>List of missing Jason-3 passes</i>	22
5	<i>Editing criteria over cycles 1 to 98</i>	27
6	<i>Seasonal variations of Jason SLA (cm) for years 2016 to 2018</i>	63
7	<i>Seasonal variations of Jason SLA standard deviation (cm) for years 2016 to 2018</i>	64

List of Figures

1	<i>Acquisition mode for cycle 060 (identical to acquisition mode automatic switch for cycles 6, 9, 11-19, 21-56, 58-98). 8 = autonomous acquisition / tracking, 9 = autonomous DIODE acquisition / tracking, 10 = DIODE + Digital Elevation Model tracking</i>	13
2	<i>Global GDRs data availability per cycle</i>	17
3	<i>Map of percentage of available measurements over land for Jason-3 (left) and for Jason-2 (right). Top: Jason-3 cycle 039 in DEM mode and Jason-2 cycle 320 in median mode. Bottom: Jason-3 cycle 031 in DEM mode and Jason-2 cycle 311 in DEM mode</i>	18
4	<i>Jason-2 and Jason-3 GDR data availability over ocean (per cycle)</i>	23
5	<i>Jason-3 data editing average by cycle.</i>	24
6	<i>Cycle per cycle monitoring of the percentage of edited measurements by ice flag criterion.</i>	25
7	<i>Top: Percentage of edited measurements by altimeter rain flag criterion. Bottom left: Map of global edited measurements without considering the rain flag. Bottom right: Map of global edited measurements using all criteria and considering the rain flag. All figures are computed over ocean and from cycle 62 to 98.</i>	26
8	<i>Jason-3 data editing by thresholds average by cycle.</i>	28
9	<i>Percentage of edited measurements by 20Hz range measurements threshold criterion (top) and by 20Hz range measurements standard deviation threshold criteria (bottom). Cycle per cycle monitoring compared with Jason-2 (left) and Jason-3 averaged map from cycle 62 to 98 (right).</i>	29
10	<i>Percentage of edited measurements by SWH threshold criterion. Left: Cycle per cycle monitoring compared with Jason-2 (Jason-2 DEM cycle in cyan. Jason-3 median tracker cycles in purple.) Right: Jason-3 averaged map from cycle 62 to 98 .</i>	30
11	<i>Percentage of edited measurements by backscatter coefficient threshold criterion (top) and by 20Hz backscatter coefficient standard deviation threshold criteria (bottom). Cycle per cycle monitoring compared with Jason-2 (left, Jason-2 DEM cycle in cyan. Jason-3 median tracker cycles in purple) and Jason-3 averaged map from cycle 62 to 98 (right).</i>	31
12	<i>Percentage of edited measurements by radiometer wet troposphere correction threshold criterion. Left: Cycle per cycle monitoring compared with Jason-2. Right: Jason-3 averaged map from cycle 62 to 98.</i>	32
13	<i>Percentage of edited measurements by ionospheric correction threshold criterion. Left: Cycle per cycle monitoring compared with Jason-2. Right: Jason-3 averaged map from cycle 62 to 98.</i>	32
14	<i>Percentage of edited measurements by wind speed threshold criterion. Left: Cycle per cycle monitoring compared with Jason-2. Right: Jason-3 averaged map from cycle 62 to 98.</i>	33
15	<i>Percentage of edited measurements by sea state bias threshold criterion. Left: Cycle per cycle monitoring compared with Jason-2. Right: Jason-3 averaged map from cycle 62 to 98.</i>	34

16	Percentage of edited measurements by ocean tide threshold criterion. Left: Cycle per cycle monitoring compared with Jason-2. Right: Jason-3 averaged map from cycle 62 to 98.	35
17	Percentage of edited measurements by square off nadir angle threshold criterion. Left: Cycle per cycle monitoring compared with Jason-2. Right: Jason-3 averaged map from cycle 62 to 98.	36
18	Percentage of edited measurements by sea surface height threshold criterion. Left: Cycle per cycle monitoring compared with Jason-2. Right: Jason-3 averaged map from cycle 62 to 98.	36
19	Percentage of edited measurements by sea level anomaly threshold criterion. Left: Cycle per cycle monitoring compared with Jason-2. Right: Jason-3 averaged map from cycle 62 to 98.	37
20	Top: Cyclic monitoring of number of elementary 20 Hz range measurements for Jason-2 and Jason-2 for Ku-band and C-band. Bottom: Jason-2 - Jason-3 difference daily monitoring of elementary 20 Hz range measurements number (until september 2017).	39
21	Map of number of 20 Hz range measurements for Jason-3 averaged over cycles 62 to 98, in Ku-band (left) and in C-band (right).	40
22	Top: Cyclic monitoring of elementary 20 Hz range measurements standard deviation for Jason-2 and Jason-3 for Ku-band and C-band. Bottom: Jason-2 - Jason-3 difference daily monitoring of elementary 20 Hz range measurements standard deviation.	41
23	Map of 20 Hz range measurements standard deviation for Jason-3 averaged over cycles 62 to 98, in Ku-band (left) and in C-band (right).	41
24	Left: Cyclic monitoring of the square off-nadir angle for Jason-2 and Jason-3 for GDRs (blue and red curves) and Jason-3 IGDRs (product IGDR for cycles 1 to 41 in light green, and IGDR L2P from cycle 25 to 68 in dark green). Right: Jason-2 - Jason-3 difference daily monitoring of the square off-nadir angle (GDR data).	42
25	Map of the square off-nadir angle for Jason-3 averaged over cycles 62 to 98.	43
26	Left: Mean per day of mispointing for Jason-3 from cycle 4. Right: Square off nadir angle against swh.	43
27	Top: Cyclic monitoring of backscatter coefficient for Jason-3 (Ku-band) OGDR/IGDR/GDR. Bottom: difference of atmospheric attenuation applied to sigma0 between IGDR and GDR products.	44
28	Top: Cyclic monitoring of backscatter coefficient for Jason-2 and Jason-3 for Ku-band (left) C-band (right). Bottom: daily monitoring of Jason-2 - Jason-3 GDR difference of the backscatter coefficient.	45
29	Map of backscatter coefficient for Jason-3 averaged over cycles 62 to 98, in Ku-band (left) and in C-band (right).	45
30	Cyclic monitoring of significant wave height for Jason-3 (Ku-band) OGDR/IGDR/GDR.	46
31	Cyclic monitoring of significant wave height for Jason-2 and Jason-3 for Ku-band (left) and for C-band (right). Jason-2 - Jason-3 difference daily monitoring of significant wave height (bottom).	46
32	Map of significant wave height for Jason-3 averaged over cycles 62 to 98, in Ku-band (left) and in C-band (right).	47
33	Cyclic monitoring of ionospheric correction for Jason-2 and Jason-3. (left). Cyclic monitoring of Jason-3 ionospheric correction for IGDR and GDR data (right). Jason-2 - Jason-3 difference daily monitoring of ionospheric correction (bottom).	48
34	Left: Map of ionospheric correction for Jason-3 averaged over cycles 62 to 98. Right: Map of dual-frequency minus GIM ionospheric correction solutions.	48
35	Cyclic monitoring of GIM ionosphere correction minus filtered altimeter ionosphere correction for Jason-2 and Jason-3. Left: mean, right: standard deviation.	49
36	Map of Jason-3 brightness temperatures averaged over cycles 62to 98: 18.7 Ghz channel (top left), 23.8 Ghz channel (top right) and 34.0 Ghz channel (bottom left). Map of AMR wet troposphere correction for Jason-3 averaged over cycles 62 to 98(bottom right)	50
37	Daily monitoring of AMR minus ECMWF model wet tropospheric correction. mean (left) and standard deviation (right)	51

38	<i>Cyclic monitoring of altimeter wind speed mean (left) and standard deviation (right). Top: for Jason-2 and Jason-3. Bottom: for Jason-3 GDR, IGDR and OGDR data.</i>	52
39	<i>Jason-2 - Jason-3 difference daily monitoring of altimeter wind speed mean (left) and standard deviation (right).</i>	52
40	<i>Cyclic monitoring of the sea state bias mean and standard deviation for Jason-2 and Jason-3</i>	53
41	<i>Jason-2 - Jason-3 difference daily monitoring of the sea state bias mean (left) and standard deviation (right).</i>	53
42	<i>Monitoring of mean of Jason-3 SSH crossover differences for OGDRs, IGDRs and GDRs. Only data with $latitude < 50^\circ$, bathymetry $< -1000m$ and low oceanic variability were selected.</i>	56
43	<i>Monitoring of mean of SSH crossover differences for Jason-2 and Jason-3 for GDRs. Only data with $latitude < 50^\circ$, bathymetry $< -1000m$ and low oceanic variability were selected, computed with got ocean tide (left) or fes ocean tide (right)</i>	56
44	<i>Map of SSH crossovers differences mean for Jason-3 cycle 0 to 98(left) and for Jason-2 cycle 281 to 506 (right)</i>	57
45	<i>Cyclic monitoring of Jason-2 - Jason-3 SSH crossover differences mean (left) and map over cycle 1 to 58 (right). Only data with $latitude < 50^\circ$, bathymetry $< -1000m$ and low oceanic variability were selected.</i>	57
46	<i>Cycle by cycle standard deviation of SSH crossover differences for Jason-2 and Jason-3 (left), and for Jason-3 using OGDRs, IGDRs and GDRs (right). Only data with $latitude < 50^\circ$, bathymetry $< -1000m$ and low oceanic variability were selected.</i>	58
47	<i>Monitoring (left) and periodogram (right) of pseudo time-tag bias estimated cycle by cycle from GDR products for Jason-2 and Jason-3</i>	59
48	<i>Daily monitoring of SSH bias between Jason-2 and Jason-3 before Jason-2 moved to interleaved ground-track in October 2016: SSH bias without applying geophysical corrections (black) and with corrections using radiometer wet troposphere correction (blue) or using ECMWF model wet troposphere correction (cyan).</i>	60
49	<i>GDR data. Caution: color map ranges are different between the two figures. Left: Map of SLA difference between Jason-2 and Jason-3 over tandem phase Right: Map of Jason-2 and Jason-3 SLA differences for Jason-3 cycles 025 to 058</i>	61
50	<i>Cyclic monitoring of along-track SLA standard deviation. Jason-3 OGDRs, IGDRs and GDRs (left). Jason-2 and Jason-3 GDRs (right)</i>	62
51	<i>Global (right) and regional (left) MSL trends from 1993 onwards.</i>	65
52	<i>Evolution of GMSL differences between altimeter and tide gauges for reference missions used in the GMSL indicator calculation (TOPEX/Poseidon, Jason-1, Jason-2 and Jason-3) with the GLOSS/CLIVAR network (blue line) and the PSMSL network (red line). Signal lower than 2 months and annual signals have been removed. The blue dashed line is the trend obtained applying a generalized least square method.</i>	66
53	<i>Evolution of global MSL differences from altimeter / tide gauges comparisons (GLOSS/CLIVAR and PSMSL network) from TOPEX/Poseidon, Jason-1, Jason-2 and Jason-3 L2P products linked together.</i>	67
54	<i>Left: Jason-3 net_instr_corr_sig0_ku flag. Right: Jason-2 and Jason-3 evolution of PTR power.</i>	68
55	<i>Jason-3 net_instr_corr_sig0_ku flag over ocean. Left: Jason-3 cycle 070. Right: Jason-3 cycle 095.</i>	68
56	<i>Left: Mean per day (blue) or per cycle (black) of standard deviation of sigma0 (left) and number of 20Hz measurements used to compute 1Hz sigma0 (right).</i>	69
57	<i>Mean and standard deviation of SSH difference at crossovers with geographical selection for Jason-3 GDR and IGDR reference data (using ocean tide sol1 = GOT4.8)</i>	70
58	<i>Periodogram for different orbit solutions using FES pure hydrodynamic model.</i>	71
59	<i>Yaw fix period impact</i>	72

60	<i>120 days signal against orbit solution</i>	72
61	<i>difference of variance at crossovers between CNES POE-E and CNES POE-F (OceanTide=FES14B, Ionospheric correction=filtered dual-freq. alti)</i>	73
62	<i>difference of variance at crossovers between CNES POE-F or JPL solutions (OceanTide=FES14B, Ionospheric correction=filtered dual-freq. alti). top: with operational JPL POE, bottom: with release18a JPL POE</i>	74
63	<i>Top : periodogram of along-track SLA cyclic mean (in green, blue and red - after remove of annual signal) and of cyclic mean of difference at crossovers (black). Bottom :along-track SLA cyclic mean (green for ascending passes only, blue for descending passes only and red taking into account all passes) after remove of annual signal - Ocean Tide = FES Left : CNES POE-F Right : JPL POE release18a</i>	75
64	<i>Difference between CNES POE-F and JPL POE release18a, separating odd and even passes</i>	75
65	<i>difference of variance at crossovers for SSH computed with or without internal tide solution</i>	76
66	<i>Difference of variance of along-track SLA for SSH computed with or without internal tide solution</i>	76
67	<i>Difference of trends for : Top left: SLA using Wahr85 with MPL2017 - SLA using GDR (Wahr85 and MPL legacy), Top right: SLA using Desai2015 with MPL2017 - SLA using GDR (Wahr85 and MPL legacy), Bottom: SLA using Wahr85 with MPL2017 - SLA using Desai2015 with MPL2017</i>	77

List of items to be defined or to be confirmed

Applicable documents / reference documents

Contents

1. Introduction	2
2. Processing status	8
2.1. Data Used	8
2.2. List of events	8
2.3. Tracking and acquisition mode	11
2.4. Models and standards	14
2.5. Processing versions	16
3. Data coverage and edited measurements	17
3.1. Missing measurements	17
3.1.1. Over land and ocean	17
3.1.2. Over ocean	22
3.2. Edited measurements	24
3.2.1. Global editing	24
3.2.2. Flagging quality criterion: Ice flag	25
3.2.3. Flagging quality criterion: Rain flag	25
3.2.4. Editing on thresholds criteria	26
3.2.4.1. Threshold criteria: 20-Hz range measurements number and standard deviation	28
3.2.4.2. Threshold criteria: Significant wave height (swh)	29
3.2.4.3. Threshold criteria: Backscatter coefficient (sigma0)	30
3.2.4.4. Threshold criteria: Radiometer wet troposphere correction	31
3.2.4.5. Threshold criteria: Ionospheric correction	32
3.2.4.6. Threshold criteria: Altimeter wind speed	33
3.2.4.7. Threshold criteria: Sea State Bias	34
3.2.4.8. Threshold criteria: Ocean tide	35
3.2.4.9. Threshold criteria: Square off nadir angle	36
3.2.4.10. Threshold criteria: Sea surface height	36
3.2.4.11. Threshold criteria: Sea level anomaly	37
4. Monitoring of altimeter and radiometer parameters	38
4.1. Methodology	38
4.2. 20Hz range measurements	38
4.2.1. 20 Hz range measurements number in Ku-Band and C-Band	39
4.2.2. 20 Hz range measurements standard deviation in Ku-Band and C-Band	40
4.3. Off-Nadir Angle from waveforms	42
4.4. Backscatter coefficient	44
4.5. Significant wave height	46
4.6. Dual-frequency ionosphere correction	47
4.7. AMR Wet Troposphere Correction	50
4.7.1. Overview	50
4.7.2. Comparison with the ECMWF model	51
4.8. Altimeter wind speed	52
4.9. Sea state bias	53

5. SSH crossover analysis	55
5.1. Overview	55
5.2. Mean of SSH crossover differences	56
5.3. Standard deviation of SSH crossover differences	58
5.4. Estimation of pseudo time-tag bias	58
6. Sea Level Anomalies (SLA) Along-track analysis	60
6.1. Overview	60
6.2. Mean of SLA differences between Jason-3 and Jason-2	60
6.3. Standard deviation of SLA differences between Jason-3 and Jason-2	61
6.4. Sea level seasonal variations	63
7. Mean Sea Level (MSL) calculation	65
7.1. Mean sea level (MSL) calculation of reference time serie and regional MSL trends	65
7.2. External data comparisons with tide gauges	66
8. Particular points and investigations	68
8.1. Caution about qual_inst_corr_1hz.sig0.ku	68
8.2. Impact of the centering of the echo on sigma0 std	69
8.3. 120 day signal on SSH difference at crossovers	70
8.3.1. Introduction	70
8.3.2. Ocean tide solution impact	71
8.3.3. Orbit solution impact	72
8.3.4. Variance at crossovers	73
8.3.5. Impact on SLA along-track	74
8.4. Internal tide solution	76
8.5. Pole tide solution	77
9. Conclusion	78
9.1. Poster on Global Jason-2 and Jason-3 Performances at OSTST	79
10. References	81

Glossary

AMR Advanced Microwave Radiometer

CLS Collecte Localisation Satellites

CNES Centre National d'Etudes Spatiales

CNG Consigne Numerique de Gain (= Automatic Gain Control)

DEM Digital Elevation Model

DIODE Détermination Immédiate d'Orbite par Doris Embarqué

ECMWF European Centre for Medium-range Weather Forecasting

GDR Geophysical Data Record

GIM Global Ionosphere Maps

GOT Global Ocean Tide

IGDR Interim Geophysical Data Record

JPL Jet Propulsion Laboratory (Nasa)

MLE Maximum Likelihood Estimator

MOE Medium Orbit Ephemeris

MQE Mean Quadratic Error

MSS Mean Sea Surface

PLTM PayLoad TeleMetry

POE Precise Orbit Ephemeris

OGDR Operational Geophysical Data Record

SALP Service d'Altimétrie et de Localisation Précise

SSH Sea Surface Height

SLA Sea Level Anomaly

SLR Satellite Laser Ranging

SSB Sea State Bias

SWH Significant Wave Height

TM TeleMetry

1. Introduction

This document presents the synthesis report concerning validation activities of Jason-3 data (Geophysical Data Records (GDRs), as well as Interim and Operational Data Records (O/IGDR)) under SALP contract (N° 160182/Lot 1.6.3) supported by CNES at the CLS Space Oceanography Division.

History

Jason-3 satellite was successfully launched on the 17th of January 2016. Since February 12th, Jason-3 is on its operational orbit to continue the long term climate data record on the primary TOPEX, Jason-1, and OSTM/Jason-2 ground track. Until October 2nd, 2016, Jason-3 and Jason-2 were in tandem flight, with only 80 seconds delay, before Jason-2 was moved to the same interleaved orbit that was used by TOPEX from 2002-2005 and Jason-1 from 2009-2012. Jason-2 was on its repetitive interleaved position until May 17th 2017, then was moved on a first Long Repeat Orbit from July 11th 2017 to July 18th 2017, and finally has been on a second interleaved long repeat orbit since July 25th 2018. After tandem phase with Jason-2, Jason-3 has become the reference mission in DUACS system from mid-september 2016 onwards.

CalVal activities

Since the beginning of the mission, Jason-3 data have been analyzed and monitored in order to assess the quality of Jason-3 products. Cycle per cycle reports summarizing mission performance are generated and made available through the AVISO web page ¹. This encompasses several points, which are either part of Cal/Val routine activities or following mission events:

- mono-mission validation and monitoring,
- Jason-3/Jason-2 cross-calibration,
- accuracy and stability of SLA measurements check,
- specific studies and investigations.

Overview

The present document assesses Jason-3 data quality and mission performance. After an executive summary, dedicated sections of this report deal with:

- description of data processing,
- data coverage / availability,
- monitoring of rejected spurious data,
- analysis of relevant parameters derived from instrumental measurements and geophysical corrections.
- system performance via analyses at crossover points,
- system performance via along-track Sea Level Anomalies monitoring,
- long-term monitoring and contribution to climat surveys.

¹<http://www.aviso.altimetry.fr/en/data/calval/systematic-calval/validation-reports.html>

Over all these parts , the document also focuses on Jason-3/Jason-2 cross-calibration:

- During the tandem flight (February, 12th to October 2nd 2016) both satellites were on the same ground track, which is a unique opportunity to precisely assess parameter discrepancies between both missions and detect geographically correlated biases, jumps or drifts.
- But even after Jason-2 move to interleaved orbit (formation flight phase, after the end of the tandem phase and until move to LRO),
- and also during Jason-2 flight on LRO, comparisons were still possible while Jason-2 data are available.

The difference at crossovers, SLA performances and consistency with Jason-2 are described. *Please note that in this document, only Jason-2 cycles 281 to 506 - corresponding to February 2016 to mid September 2017 - are used to compute Jason-2 GDR statistics.*

2018 executive summary on Jason-3

By succeeding to TOPEX/Poseidon, Jason-1 and Jason-2 on their primary ground track, Jason-3 has extended the high-precision ocean altimetry data record [1]. It was launched on January 17th 2016. During the tandem phase with Jason-2 (February 12th to October 2nd 2016), both satellites were on the same ground-track (with only 80 seconds delay), which is a unique opportunity to precisely assess parameter discrepancies between both missions and detect geographically correlated biases, jumps or drifts. OGDR and IGDR products have been publicly available since June 30th 2016. OGDRs were generated in version “T” until cycle 18/pass 137, and then turned into “D” version. Concerning IGDRs, they turned from “T” to “D” version at cycle 14/pass 143 on June 27th. GDR products have been available in version “T” on [2] or via [3] since early October 2016 (more details on products versions on Jason-3 handbook [4]). During each cycle, missing measurements were monitored, spurious data were edited and relevant parameters derived from instrumental measurements and geophysical corrections were analysed for OGDR, IGDR and GDR.

Jason-3 can use two on-board tracking modes: Diode/DEM (open loop) and median tracker (more details in complete annual report). In addition, a tracking automatic transition is possible, which means that when authorized: acquisition mode switches automatically from autonomous DIODE acquisition mode over land to Diode/DEM over ocean and referenced inland water. During 2017, an update of DEM (Digital Elevation Model) was uploaded on August (cycle 057). It aims at adding new hydrologic targets such as rivers and lakes: 110 lakes and more than 2700 virtual stations over lakes and rivers have been added (from 1644 virtual stations up to 4366). **Please note this year the change in orbit standard solution available in the products:**

- until Jason-3 cycle 094, POE-E (MOE-E) orbit standard is available in GDR (IGDR) products
- from Jason-3 cycle 095 onwards, orbit standard “F” is used for both POE and MOE.

Data availability

Data availability is excellent for Jason-3. Jason-3 presents 100% of data availability over ocean after removing specific events (99.96% for Jason-2, see figure 1). Such events occurred twice over Jason-3 full period:

- during cycle 3, where 21.02% of measurements are missing due to the GPS platform upload,
- during cycle 57, where 1.76% of measurements are missing due to the DEM-onboard upload.

¹<https://www.aviso.altimetry.fr/?id=601&L=0>

²<ftp://ftp.jason3.oceanobs.com>

³<http://www.class.noaa.gov>

⁴https://www.aviso.altimetry.fr/fileadmin/documents/data/tools/hdbk_j3.pdf

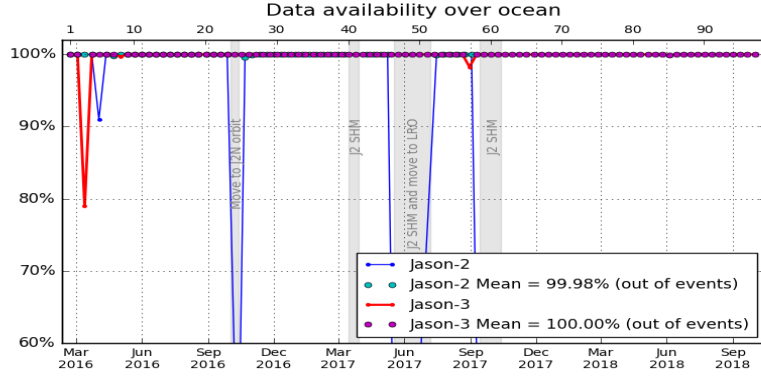


Figure 1 – Jason-2 and Jason-3 GDR data availability over ocean (per cycle)

Sea Level Anomalies

Over the tandem phase, mean SLA differences between Jason-2 and Jason-3 data is stable in time with variations close to 1 mm rms (left of figure 2) and shows no drift. It presents only a weak hemispheric bias as both satellites measure the same oceanic features only 1'20" apart (figure 2) that corresponds to orbital signatures observed on sea surface height. The global average SSH bias is close to 2.98 cm using SSH corrections (2.84 cm when using ECMWF instead of radiometer wet troposphere correction) and 2.23 cm without.

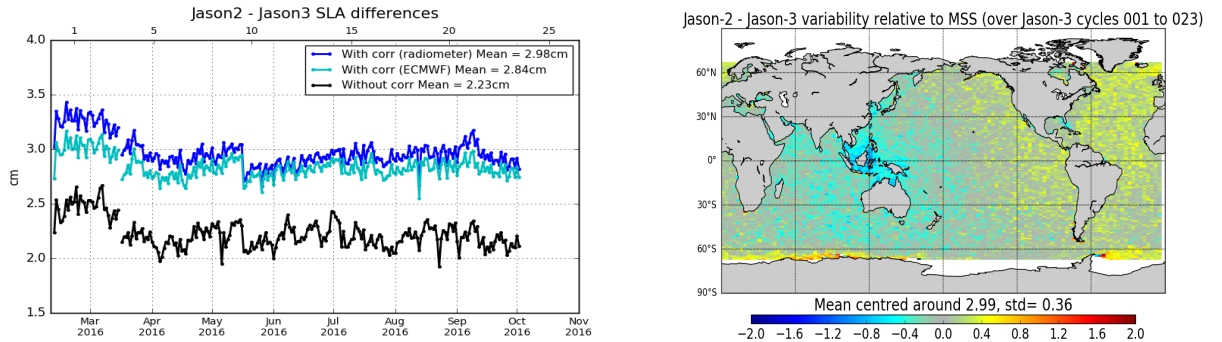


Figure 2 – Jason-3/Jason-2 tandem phase: until 02-10-2016. **Left:** Daily monitoring of SSH bias between Jason-2 and Jason-3 before Jason-2 moved to interleaved ground-track in October 2016: SSH bias without applying geophysical corrections (black) and with corrections using radiometer wet troposphere correction (blue) or using ECMWF model wet troposphere correction (cyan). **Right:** Map of SLA difference between Jason-2 and Jason-3 over tandem phase

During the formation flight (i.e. over cycles 25 to 46 from 12-10-2016 to 17-05-2017) and over Jason-2 LRO phase (until Jason-3 cycle 58, on 14-09-2017), average difference of gridded SLA for Jason-2 and Jason-3 shows high variability regions as Gulf Stream and Antarctic circumpolar currents are visible (figure 3). This difference is quite noisy as both satellites are shifted in time and sea state changes especially in regions of high ocean variability.

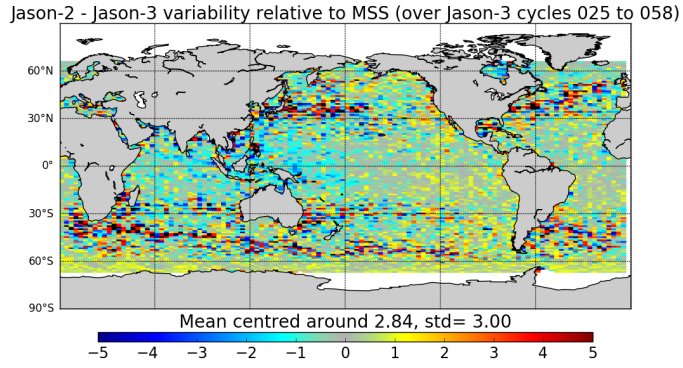


Figure 3 – GDR data. Map of Jason-2 and Jason-3 SLA differences for Jason-3 cycles 025 to 058

Performances at crossover points

Looking at SSH difference at crossovers (figure 4), a 120 day signal is visible on the mean for Jason-3 GDR data. Concerning SSH error at crossover points (standard deviation/ $\sqrt{2}$), Jason-3 missions show very good and stable performances with an error of 3.48 cm (3.47cm for Jason-2).

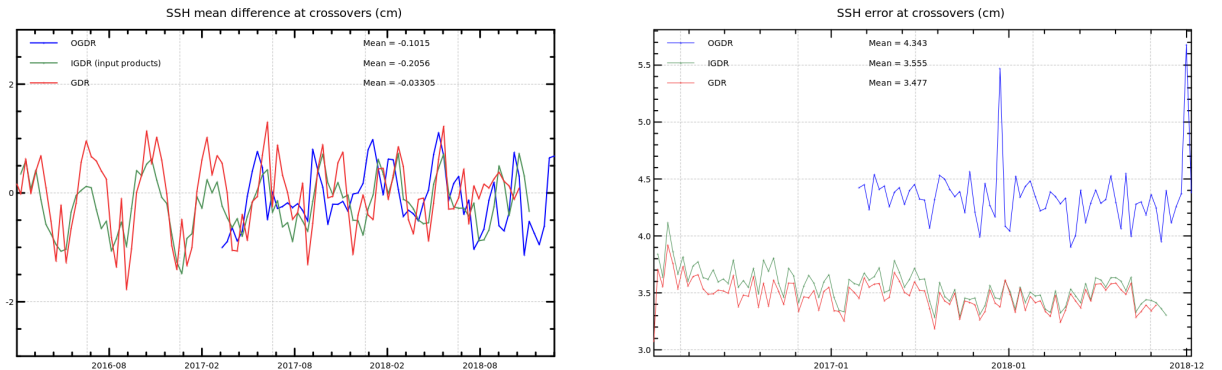


Figure 4 – Monitoring of SSH difference at crossovers for Jason-3 OGDR, IGDR and GDR. Mean of difference (**left**) and error at crossovers (**right**). Only data with $|latitude| < 50^\circ$, bathymetry $< -1000m$ and low oceanic variability were selected.

Mean SSH differences at Jason 3/Jason 2 crossovers is quite stable and around 3cm in average (figure 5, left). The geographical pattern indicates some hemispheric biases: positive to the west, negative to the east (figure 5, right). It corresponds to orbital signatures observed on sea surface height.

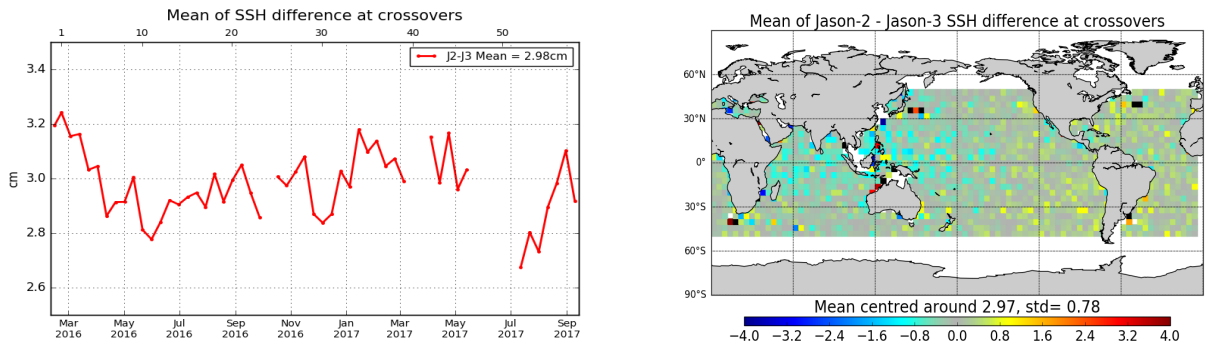


Figure 5 – Cyclic monitoring of Jason-2 - Jason-3 SSH crossover differences mean (left) and map over cycle 1 to 58 (right). Only data with $|latitude| < 50^\circ$, bathymetry $< -1000m$ and low oceanic variability were selected.

Contribution to Global Mean Sea Level

Since May 2016 (Jason-3 cycle 11), Jason-3 has been the reference altimetry mission to estimate the Global Mean Sea Level (GMSL), replacing Jason-2. Regional and global biases between missions have to be precisely estimated in order to ensure the quality of the reference GMSL serie. For more precisions, see the dedicated section on AVISO+ website [5].

⁵<https://www.aviso.altimetry.fr/en/data/products/ocean-indicators-products/mean-sea-level.html>

2. Processing status

2.1. Data Used

Metrics provided in this document are based on Jason-3 dataset from cycle 0 to 98 for GDR products (corresponding to February 12th 2016 to October 16th 2018). This period extends until cycle 104 (December 14th 2018) when IGDR data are considered. Cycle 0 is not included in many statistics because of its available data covering only 5 days.

After tandem phase with Jason-2, Jason-3 has become the reference mission in *DUACS* system from mid-september 2016 onwards. Note that in order to improve their product quality (and also to use as possible same corrections for multimission products), *DUACS* system applies some updates to IGDR data. If no precision is done, IGDR results that are presented in this document contains *DUACS* updates (also called here IGDR-L2P).

2.2. List of events

The following table shows the major events during the Jason-3 mission.

Start time → End time	Cycle	Event
15/02/2016 08:00:00 → 18:04:28	0	First calibration in DIODE + DEM mode
16/02/2016 16:07:00 → 16:38:59	0	Poseidon3B instrument CNG calibration
08/03/2016 20:00:00 → 09/03/2016 00:00:01	3	Gyro calibration
11/03/2016 05:14:00 → 05:34:00	3	AMR Cold Sky calibration maneuver
15/03/2016 → 17/03/2016	3	Platform GPS upload
25/03/2016 09:30:15	4	AMR OFF / ON
06/04/2016 06:05:00 → 06:36:59	5	Poseidon3B instrument CNG calibration
07/04/2016 00:21:27 → 22:19:56	6	DIODE DEM mode
08/04/2016 04:44:30 → 05:00:46 05:11:00 → 05:28:21	6	Poseidon3B instrument CAL2 calibration
27/04/2016 11:38:21 → 12:05:55	8	OPS error
..../....		

Start time → End time	Cycle	Event
02/05/2016 14:34:23 → 14:37:28	8	DEM patch upload.
06/05/2016 18:16:59 → 16/05/2016 16:15:29	9	DIODE DEM mode
12/05/2016 22:44:59 → 22:52:23	9	AMR Cold Sky calibration maneuver
16/05/2016 10:00:00 → 10:16:15	9	Poseidon3B instrument CAL2 calibration
17/05/2016 02:34:00 → 19/05/2016 03:34:16	10	Poseidon3B instrument CAL2 calibration (5 sequences)
25/06/2016 08:09:39 → 05/07/2016 06:08:10	14	DIODE DEM mode
07/07/2016 15:04:44 → 15:11:15	15	AMR internal error
12/07/2016 04:26:36 → 04:34:00	15	AMR Cold Sky calibration maneuver
05/09/2016 04:24:44 → 04:32:08	21	AMR Cold Sky calibration maneuver
10/2016	24	OSTM/Jason 2 moved to the interleaved orbit, end of the verification phase for Jason 3
07/11/2016 22:21:30 → 22:28:54	27	AMR Cold Sky calibration maneuver
27/11/2016 06:15:00 → 06:46:59	29	Poseidon3B instrument CNG calibration
08/12/2016 04:36:34 → 09/12/2016 12:58:47	30	AMR anomaly
10/01/2017 16:37:35 → 16:44:59	34	AMR Cold Sky calibration maneuver
23/02/2017 11:35:00 → 12:06:59	38	Poseidon3B instrument CNG calibration
26/02/2017 17:13:07 → 17:20:31	38	AMR Cold Sky calibration maneuver
27/04/2017 04:13:16 → 04:20:40	44	AMR Cold Sky calibration maneuver
.../...		

Start time → End time	Cycle	Event
03/06/2017 15:46:00 → 16:17:59	48	Poseidon3B instrument CNG calibration
28/06/2017 05:10:04 → 05:17:28	51	AMR Cold Sky calibration maneuver
14/08/2017 05:57:05 → 06:04:29	55	AMR Cold Sky calibration maneuver
29/08/2017 13:41:14 → 31/08/2017 16:24:07	57	DEM onboard upload
31/08/2017 21:33:00 → 22:04:59	57	Poseidon3B instrument CNG calibration
04/09/2017 17:32:09 → 17:39:33	58	AMR Cold Sky calibration maneuver
14/09/2017 16:54:56 → 17:52:18	59	Gyro calibration
14/10/2017 15:30:11 → 15:37:35	62	AMR Cold Sky calibration maneuver
02/11/2017 02:05:23 → 02:12:47	63	AMR Cold Sky calibration maneuver
02/12/2017 02:30:00 → 03:01:59	66	Poseidon3B instrument CNG calibration
16/12/2017 02:03:45 → 02:11:09	68	AMR Cold Sky calibration maneuver
05/01/2018 20:45:36 → 20:53:00	70	AMR Cold Sky calibration maneuver
04/02/2018 16:46:42 → 16:54:06	73	AMR Cold Sky calibration maneuver
26/02/2018 02:36:17 → 02:43:41	75	AMR Cold Sky calibration maneuver
01/03/2018 08:17:00 → 08:48:59	75	Poseidon3B instrument CNG calibration
07/04/2018 23:25:16 → 23:32:40	79	AMR Cold Sky calibration maneuver
25/04/2018 20:34:10 → 20:41:34	81	AMR Cold Sky calibration maneuver
.../...		

Start time → End time	Cycle	Event
29/05/2018 14:05:00 → 14:36:59	84	Poseidon3B instrument CNG calibration
30/05/2018 13:08:34 → 13:17:02 14:41:24 → 14:42:47	85	Poseidon BDR update (2 sequences)
10/06/2018 00:41:29 → 00:48:53	86	AMR Cold Sky calibration maneuver
07/07/2018 19:27:47 → 19:35:10	88	AMR Cold Sky calibration maneuver
31/07/2018 01:05:47 → 01:13:11	91	AMR Cold Sky calibration maneuver
22/08/2018 01:25:28 → 01:32:52	93	AMR Cold Sky calibration maneuver
29/08/2018 19:00:00 → 19:31:59	94	Poseidon3B instrument CNG calibration
02/10/2018 18:53:50 → 19:01:14	97	AMR Cold Sky calibration maneuver

Table 1 – Events on Jason-3 mission

2.3. Tracking and acquisition mode

Jason-3 can use two on-board tracking modes: Diode/DEM (open loop) and median tracker. In addition, a tracking automatic transition is possible, which means that when authorized: acquisition mode switches automatically from autonomous DIODE acquisition mode over land to Diode/DEM over ocean and referenced inland water. The status of tracking and acquisition modes are detailed in table 2.

Cycle	Acquisition Mode over land	Acquisition Mode over ocean and all referenced inland waters	Comment
Cycle 000	Median tracker + autonomous acquisition / tracking + DEM	Median tracker + autonomous acquisition / tracking + DEM	tracking automatic transition inhibited except for 7 passes
Cycles 001 to 005	Median tracker	Median tracker	tracking automatic transition inhibited.
Cycles 006	see dedicated point below	see dedicated point below	
			.../...

Cycle	Acquisition Mode over land	Acquisition Mode over ocean and all referenced inland waters	Comment
Cycles 007	Median tracker	Median tracker	tracking automatic transition inhibited everywhere.
Cycles 008	mainly Median tracker	mainly Median tracker	autonomous acquisition / tracking for passes 144 to 148 (DEM patch upload on 2016-05-02) . tracking automatic transition inhibited everywhere.
Cycle 009 Pass 001 to mid-248	Median tracker	DEM	mid-pass 248 = CAL2 event on 2016-05-16 10:00)
Cycle 009 Pass mid-248 to 254	Median tracker	Median tracker	mid-pass 248 = CAL2 event on 2016-05-16 10:00)
Cycle 010	Median tracker	Median tracker	tracking automatic transition inhibited
Cycles 011 to 019	Median tracker	DEM	tracking automatic transition authorized
Cycle 020	Median tracker	Median tracker	tracking automatic transition inhibited
Cycles 021 to 056	Median tracker	DEM	tracking automatic transition authorized
Cycle 057			DEM upload
Cycles 058 onwards	Median tracker	DEM	tracking automatic transition authorized

Table 2 – Acquisition mode

- About cycle 006: Altimeter state flag for tracking mode is set to 1 by three times (=0 everywhere else):
 - for passes 018 to 029 from 2016-04-07 16:32:57 to 2016-04-08 03:13:59 :

>DIODE Acquisition/Autonomous mode (Altimeter state flag for acquisition mode is set to 9) due to operation error after transponder calibration : back to DIODE DEM mode after the next routine calibration.
 - for passes 065 to 070, from 2016-04-09 12:46:05 to 2016-04-09 17:25:10 :

>Auto Acquisition/Autonomous tracking mode (Altimeter state flag for acquisition mode is set to 8) due to automatic reinitialisation in POS3B default mode, triggered on-board by GPS reinit : back to DIODE DEM mode after the next routine calibration
 - for passes 113 to 116, from 2016-04-11 10:03:37 to 2016-04-11 12:20:28 :

>Auto Acquisition/Autonomous tracking mode (Altimeter state flag for acquisition mode is set to

- 8) due to automatic reinitialisation in POS3B default mode, triggered on-board by GPS OFF-ON : back to DIODE DEM mode after the next routine calibration
- From cycle 21 onwards, except during DEM upload on cycle 057, tracking automatic transition is activated.

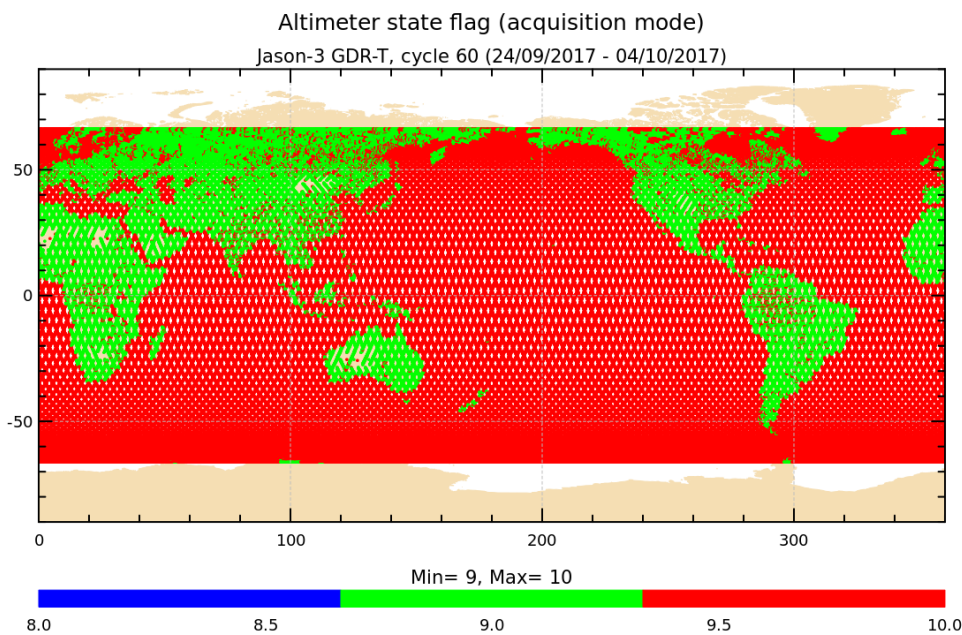


Figure 1 – Acquisition mode for cycle 060 (identical to acquisition mode automatic switch for cycles 6, 9, 11-19, 21-56,58-98). 8 = autonomous acquisition / tracking, 9 = autonomous DIODE acquisition / tracking, 10 = DIODE + Digital Elevation Model tracking

- About cycle 057, some passes are entirely autonomous acquisition / tracking, and some passes entirely median tracker. DEM upload during this cycle is detailed in [22].

2.4. Models and standards

The standards used for version “D” are listed in Table 3.

The main differences between the O/IGDRs versions “T” and “D” are summarized hereafter:

- CAL-2 calibration processing are based on typical ocean AGC values, correcting the negative squared-attitude values that were observed from the start of the mission.
- Backscatter (sigma-0) values are adjusted internally during ground processing. A calibration bias of +0.14 dB and +0.109 dB is added to the measured (and reported) MLE-4 and MLE-3 Ku-band sigma-0, respectively, prior to wind speed computation; a calibration bias of -0.231 dB and -0.012 dB is added to the measured (and reported) MLE-3 Ku- and C-band sigma-0, respectively, prior to rain flag computation and rain flag values. This ensure that they are properly aligned with the adopted algorithms, so that rain flagging and wind speed values are in-line with those from Jason-2.

Model	Product version “D”
Orbit	<p>Based on Doris onboard navigator solution for OGDRs.</p> <p>DORIS tracking data for IGDRs (orbit standard MOE-E until cycle 094 and MOE-F from cycle 095 onwards).</p> <p>DORIS and/or GPS tracking data for GDRs (orbit standard POE-E until cycle 094 and POE-F from cycle 095 onwards).</p>
Altimeter Retracking	<p>OceanMLE4 retracking: MLE4 fit from 2nd order Brown model: MLE4 simultaneously retrieves the following 4 parameters from the altimeter waveforms:</p> <ul style="list-style-type: none"> • Epoch (tracker range offset) → altimeter range • Composite Sigma → SWH • Amplitude → Sigma0 • Trailing Edge slope → Square of mispointing angle (Ku band only, a null value is used in input of the C band re-tracking algorithm) <p>OceanMLE3 retracking: MLE3 fit from first orderBrown analytical model: MLE3 simultaneously retrieves the 3 parameters that can be inverted from the altimeter waveforms:</p> <ul style="list-style-type: none"> • Epoch (tracker range offset) → altimeter range • Composite Sigma → SWH • Amplitude → Sigma0 <p>“Ice” retracking: Geometrical analysis of the altimeter waveforms, which retrieves the following parameters:</p> <ul style="list-style-type: none"> • Epoch (tracker range offset) → altimeter range • Amplitude → Sigma0
.../...	

Model	Product version "D"
Altimeter Instrument Corrections	Two sets: one set consistent with MLE4 retracking and one set consistent with MLE3 retracking
Jason3 Advanced Microwave Radiometer (AMR) Parameters	Using parameters derived from long term calibration tool developed and operated by NASA/JPL
Dry Troposphere Range Correction	From ECMWF atmospheric pressures and model for S1 and S2 atmospheric tides
Wet Troposphere Range Correction from Model	From ECMWF model
Ionosphere correction from model	Based on Global Ionosphere TEC Maps from JPL
Sea State Bias Model	Two empirical models: <ul style="list-style-type: none"> • MLE4 version derived from 1 year of MLE4 Jason-2 altimeter data with version "D" geophysical models • MLE3 version derived from 1 year of MLE3 Jason-2 altimeter data with version "D" geophysical models
Mean Sea Surface Model	MSS_CNES-CLS11 (reference 7 years)
Mean Dynamic Topography Model	MDT_CNES-CLS09
Geoid	EGM96
Bathymetry Model	DTM2000.1
Inverse Barometer Correction	Computed from ECMWF atmospheric pressures after removing S1 and S2 atmospheric tides
Non-tidal High-frequency De-aliasing Correction	Mog2D high resolution ocean model on I/GDRs. None on OGDRs. Ocean model forced by ECMWF atmospheric pressures after removing S1 and S2 atmospheric tides.
Tide Solution 1	GOT4.8 + S1 ocean tide. S1 load tide ignored
Tide Solution 2	FES2004 + S1 and M4 ocean tides. S1 and M4 load tides ignored
Equilibrium long-period ocean tide model.	From Cartwright and Taylor tidal potential.
Non-equilibrium long-period ocean tide model.	Mm, Mf, Mt, and Msqm from FES2004
Solid Earth Tide Model	From Cartwright and Taylor tidal potential.
Pole Tide Model	Equilibrium model
Wind Speed from Model	ECMWF model
Rain Flag	Derived from comparisons to thresholds of the radiometer-derived integrated liquid water content and of the difference between the measured and the expected Ku-band backscatter coefficient
.../...	

Model	Product version “D”
Ice Flag	Derived from comparison of the model wet tropospheric correction to a dual-frequency wet tropospheric correction retrieved from radiometer brightness temperatures, with a default value issued from a climatology table

Table 3 – List of GDR version “D” standard

2.5. Processing versions

OGDR and IGDR products are publicly available since June 30th 2016. OGDRs were generated in version “T” until cycle 18/pass 137, and then turned in “D” version.

→ The first OGDR “D” file is: *JA3_OPN_2PdS018_137_20160809_080914_20160809_100739.nc*

Concerning IGDRs, they turned from “T” to “D” version a few days before OGDRs on June 27th(cycle 14/pass 143).

→ The first IGDR “D” file is: *JA3_IPN_2PdP014_043_20160626_233040_20160627_002653.nc*

GDRs were generated in version “T” until cycle 021/pass 254, and then turned in “D” version.

→ The first GDR “D” file is: *JA3_GPN_2PdP022_001_20160912_155750_20160912_165403.nc*

3. Data coverage and edited measurements

3.1. Missing measurements

3.1.1. Over land and ocean

Determination of missing measurements relative to the theoretically expected orbit ground pattern is an essential tool to detect missing telemetry or satellite events for instance. Applying the same procedure for Jason-2 and Jason-3, the comparison of the percentage of missing measurements has been performed.

Figure 2 shows the percentage of available measurements for Jason-3 and Jason-2 for all kind of surfaces observed, computed with respect to a theoretical possible number of measurements. In average Jason-3 provides 99.05% of measurements over 98 cycles (without taking into accounts cycles with explained anomalies), which shows an improvement compared to Jason-2 tracking capabilities.

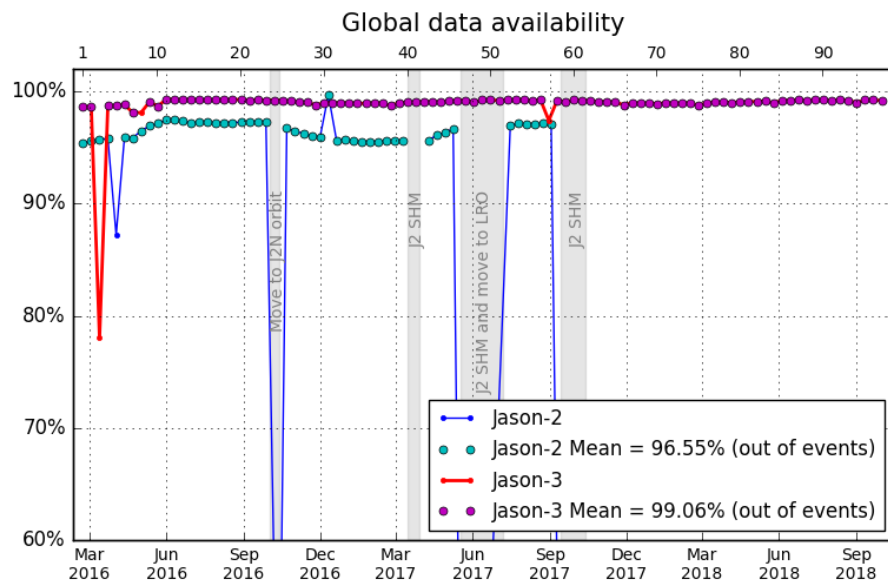


Figure 2 – Global GDRs data availability per cycle

Out of Jason-2 SHM or move of orbit, missing measurements on Jason-2 and Jason-3 since the beginning of Jason-3 mission are:

- **Jason-3 Cycle 3:** GPS platform upload interrupted the data production for two days.
- **Jason-3 Cycle 57:** DEM onboard upload interrupted the data production for few passes.
- **Jason-2 Cycle 285:** Data are missing in 2016 between April, 5 at 13:35:10 and April, 6 at 12:02:40. No scientific products have been processed during this period to allow the upload of new GPS On Board software.

Jason-2 in median tracker mode and Jason-3 in DEM mode: For almost all cycles, available data percentage is greater for Jason-3 than for Jason-2. This is due to differences in tracking and acquisition modes

(Jason-3 uses DEM mode over ocean and inland waters and Jason-2 uses median tracker everywhere): Jason-3 data coverage over land surface can be slightly different regarding to Jason-2 (as shown on top of figure 3).

Jason-2 and Jason-3 both in median tracker: Available data percentage is greater for Jason-3 than for Jason-2 even over cycles where median tracker is used on Jason-2 (all except Jason-2 cycle 311) and only median tracker is used on **Jason-3 (cycles 1 to 5, 7-8, 10 and 20: see 2.3.)**. This difference is probably due to a limitation imposed on Jason-2 tracking to avoid ghost echoes.

Jason-2 and Jason-3 both in DEM mode: Note that **Jason-2 cycle 311 (partly over Jason-3 cycles 30 and 31)** is in DEM mode, so that availability of measurements over this cycle is quite 100% (but more data are rejected). Bottom part of figure 3 shows that these additional measurements for Jason-2 (right) compared to Jason-3 (left) are mainly located over Asia.

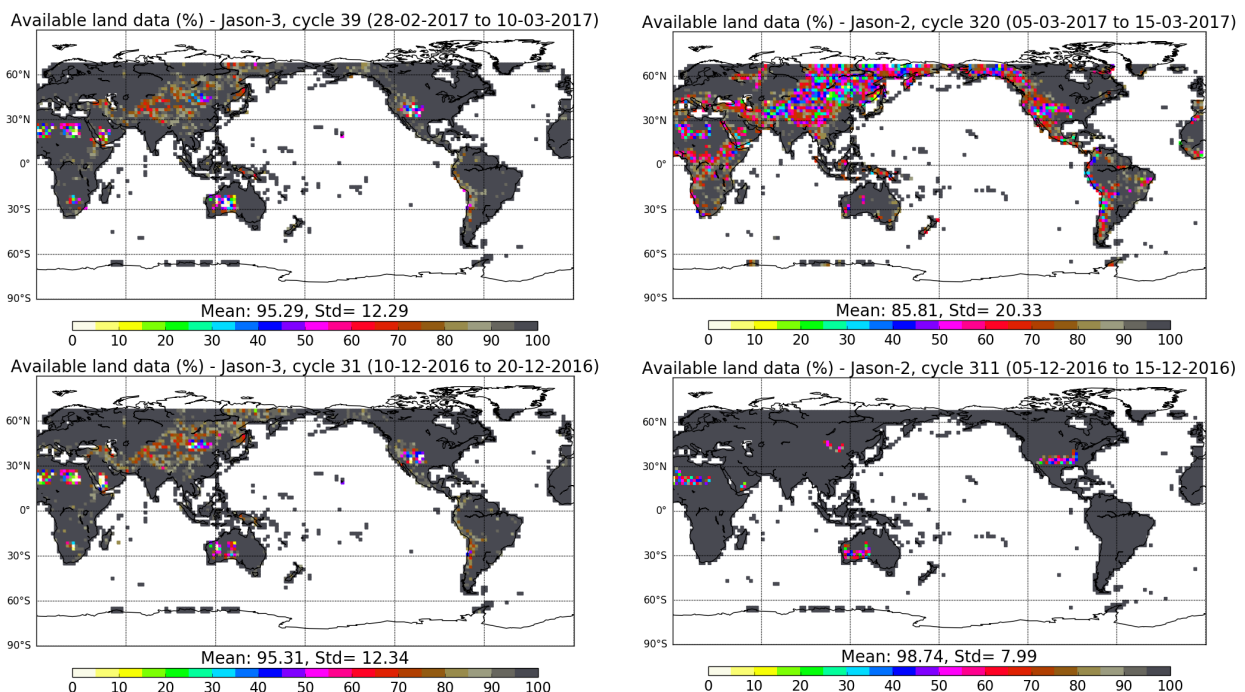


Figure 3 – Map of percentage of available measurements over land for Jason-3 (left) and for Jason-2 (right). **Top:** Jason-3 cycle 039 in DEM mode and Jason-2 cycle 320 in median mode. **Bottom:** Jason-3 cycle 031 in DEM mode and Jason-2 cycle 311 in DEM mode

Table 4 gives an overview of missing passes and reasons for Jason-3.

Date	Jason-3 Cycle/Pass	Reason
Before 12/02/2016 01:11:09	C000 / P001-116	Final ground-track reached on 12-02-2016 01:11:09
		.../...

Date	Jason-3 Cycle/Pass	Reason
	C000 / P201, 203, 236	Due to calibration events, passes 201 (~10%), 203 (~12%) and 236 (~8%) partly missing
08/03/2016 20:00:00 → 09/03/2016 00:00:01	C003	Due to Gyro calibration , data gap on pass 018.
11/03/2016 05:14:00 → 05:34:00	C003	AMR Cold Sky calibration maneuver
15/03/2016 07:15:04 to 17/03/2016 08:06:13	C003 / P181-233	Due to platform GPS software upload, passes 182 to 232 are entirely missing, as well as part of passes 181 and 233
06/04/2016 06:05:00 → 06:36:59	C005 / P235	Due to Poseidon3B instrument CNG calibration, data gap on pass 235, that mainly concerns land data acquisition and a portion of Red Sea.
26/04/2016 20:18:29 → 2016-05-06 18:16:59	C008	Due to Poseidon3B instrument CAL2 calibrations , data gaps over land on passes 55, 53, 27, 5, 38, 12 and 29
27/04/2016 11:38:11 to 12:05:55	C008 / P017	Due to OPS error, pass 017 has 49.39% of missing measurements (42.44% over ocean)
08/04/2016 04:44:30 → 05:00:46 05:11:00 → 05:28:21	C006	Due to Poseidon3B instrument CAL2 calibration, data gaps over land
02/05/2016 10:17:04 to 10:28:14 and 14:34:22 to 14:37:28	C008 / P144,148	Due to DEM upload: <ul style="list-style-type: none"> • Pass 144 has 20.33% of missing measurements (13.27% over ocean, Norwegian Sea) • Pass 148 has 6.60% of missing measurements over ocean (western african coast)
12/05/2016 22:44:59 → 22:52:23	C009	AMR Cold Sky calibration maneuver
16/05/2016 10:00:00 → 10:16:15	C009	Due to Poseidon3B instrument CAL2 calibration, data gap over land on pass 248
17/05/2016 02:34:00 → 19/05/2016 03:34:16	C010	Due to Poseidon3B instrument CAL2 calibration (5 sequences), data gaps over land on passes 31, 64, 38, 12, and 44
.../...		

Date	Jason-3 Cycle/Pass	Reason
12/07/2016 04:26:36 → 04:34:00	C015	AMR Cold Sky calibration maneuver
05/09/2016 04:24:44 → 04:32:08	C021	AMR Cold Sky calibration maneuver
07/11/2016 22:21:30 → 22:28:54	C027	AMR Cold Sky calibration maneuver
27/11/2016 06:15:00 to 06:46:58	C029 / P159, 160	Due to CNG calibration, parts of passes 159 and 160 are missing (mostly over land). Pass 159 has 54.73% of missing measurements (10.54% over ocean).
10/01/2017 16:37:35 → 16:44:59	C034	AMR Cold Sky calibration maneuver
23/02/2017 11:35:00 → 12:06:59	C038	Poseidon3B instrument CNG calibration
26/02/2017 17:13:07 → 17:20:31	C038	AMR Cold Sky calibration maneuver
27/04/2017 04:13:16 → 04:20:40	C044	AMR Cold Sky calibration maneuver
03/06/2017 from 15:46:00 to 16:17:59	C048 / P159	Due to CNG calibration, pass 159 has 56.55% of missing data mostly over land (10.54% over ocean)
28/06/2017 05:10:04 → 05:17:28	C051	AMR Cold Sky calibration maneuver
14/08/2017 05:57:05 → 06:04:29	C055	AMR Cold Sky calibration maneuver
30/08/2017 12:07:15 to 14:10:33	C057 / P123-125	Due to DEM upload: <ul style="list-style-type: none"> • Pass 123 has 23.91% of missing measurement (15.44% over ocean). • Pass 124 is missing • Pass 125 has 96.16% of missing measurement (100% over ocean).
.../...		

Date	Jason-3 Cycle/Pass	Reason
31/08/2017 14:22:58 to 16:26:10	C057 / P151-153	<p>Due to DEM upload:</p> <ul style="list-style-type: none"> • Pass 151 has 12.40% of missing measurement (8.57% over ocean). • Pass 152 has 100% of missing measurement over ocean • Pass 153 has 98.40% of missing measurement (100% over ocean).
31/08/2017 21:33:00 to 22:04:59	C057 / P159	Due to CNG calibration, pass 159 has 56.17% of missing measurement (10.54% over ocean).
04/09/2017 17:32:09 → 17:39:33	C058	AMR Cold Sky calibration maneuver
14/09/2017 from 16:54:56 to 17:52:18	C059 / P005	Due to Gyro calibration, pass 5 has 47.22% of missing measurements (0.07% over ocean)
14/10/2017 15:30:11 → 15:37:35	C062	AMR Cold Sky calibration maneuver
02/11/2017 02:05:23 → 02:12:47	C063	AMR Cold Sky calibration maneuver
02/12/2017 02:30:00 → 03:01:59	C066 / P235	Due to CNG calibration, pass 235 has 57.16% of missing measurement (8.33% over ocean).
16/12/2017 02:03:45 → 02:11:09	C068	AMR Cold Sky calibration maneuver
26/12/2017 23:03:32 → 23:06:25	C069	Pass 110 has 5.88% of missing measurement (5.66% over ocean) probably due to connection to Usingen anomaly.
05/01/2018 20:45:36 → 20:53:00	C070	AMR Cold Sky calibration maneuver
04/02/2018 16:46:42 → 16:54:06	C073	AMR Cold Sky calibration maneuver
26/02/2018 02:36:17 → 02:43:41	C075	AMR Cold Sky calibration maneuver
01/03/2018 08:17:00 → 08:48:59	C075 / P235	Due to CNG calibration, pass 235 has 57.03% of missing measurement (8.33% over ocean).
.../...		

Date	Jason-3 Cycle/Pass	Reason
07/04/2018 23:25:16 → 23:32:40	C079	AMR Cold Sky calibration maneuver
25/04/2018 20:34:10 → 20:41:34	C081	AMR Cold Sky calibration maneuver
29/05/2018 14:05:00 → 14:36:59	C084 / P235	Due to CNG calibration, pass 235 has 57.00% of missing measurement (8.33% over ocean).
30/05/2018 13:08:34 → 13:17:02 14:41:24 → 14:42:47	C085 / P006-007	Due to BDR update: <ul style="list-style-type: none"> • Pass 6 has 15.31% of missing measurement (10.80% over ocean). • Pass 7 has 2.84% of missing measurement (4.86% over ocean).
10/06/2018 00:41:29 → 00:48:53	C086	AMR Cold Sky calibration maneuver
07/07/2018 19:27:47 → 19:35:10	C088	AMR Cold Sky calibration maneuver
31/07/2018 01:05:47 → 01:13:11	C091	AMR Cold Sky calibration maneuver
22/08/2018 01:25:28 → 01:32:52	C093	AMR Cold Sky calibration maneuver
29/08/2018 19:00:00 → 19:31:59	C094 / P057	Due to CNG calibration, pass 057 has 57.00% of missing measurement (12.67% over ocean).
02/10/2018 18:53:50 → 19:01:14	C097	AMR Cold Sky calibration maneuver

Table 4 – List of missing Jason-3 passes

3.1.2. Over ocean

The behaviour of Jason-3 over ocean is excellent and conform to what is observed with Jason-2 during tandem phase (on the same ground track, with 80 seconds of difference), and even after on interleaved groundtrack.

Looking at data over ocean, Jason-3 is always available (ocean is fully covered) out of specific events (see figure 4)

- 21.03% of missing measurements due to GPS platform upload during cycle 3,

- 0.3% of missing measurements over cycle 8 due to operator error,
- 1.74% of missing measurements due to the DEM-onboard upload during cycle 57.

Jason-2 missing measurements reason until end of 2017 is detailed in Jason-2 2017 Annual report [115].

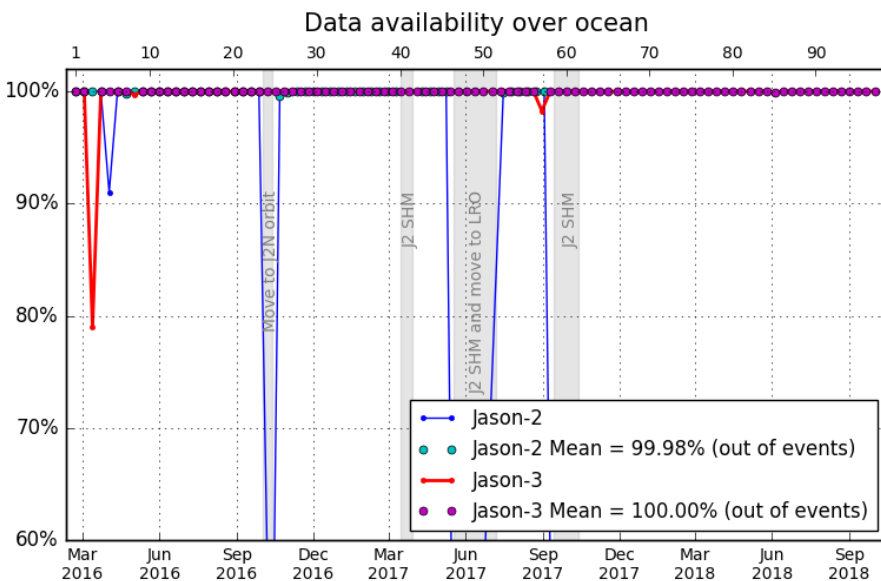


Figure 4 – Jason-2 and Jason-3 GDR data availability over ocean (per cycle)

3.2. Edited measurements

Editing criteria allow to select only measurements considered as valid over ocean. This editing process is structured in 4 main steps:

1. Measurements over land are removed, only measurements over ocean and lakes are kept
2. Measurements over ice are removed
3. Threshold criteria are applied on altimeter, radiometer and geophysical parameters as described in the following table 5. Except for the dual frequency ionosphere correction, only Ku-band measurements are used in this editing procedure, as they mainly represent the end user dataset.
4. A spline criterion is applied to remove the remaining spurious data.

3.2.1. Global editing

The percentage of total edited measurements is monitored on a cyclic basis. The average of total edited measurements is 37.7% (see Figure 5). A small annual cycle is visible due to ice coverage signal (see dedicated part 3.2.2.): the total percentage is slightly lower during March/April/May (30-35%), then increasing during May to July and remains around 38-42%, and start to slowly decrease in mid-September. This expected behaviour is related to sea ice coverage, and was already observed on previous altimetry missions such as OSTM/Jason 2. The peak detected on cycle 30 is due to an AMR anomaly that occurred from 08/12/2016 04:36:34 to 09/12/2016 12:58:47.

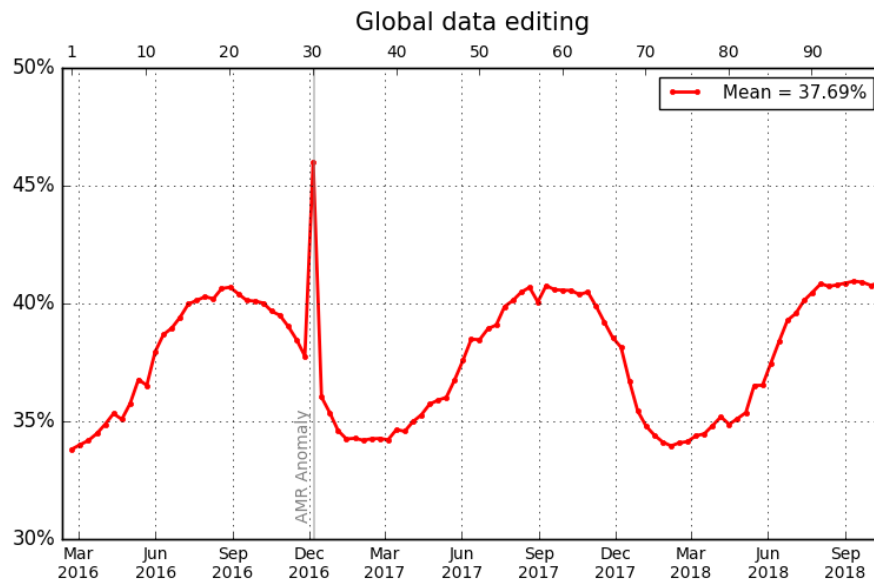


Figure 5 – Jason-3 data editing average by cycle.

3.2.2. Flagging quality criterion: Ice flag

The ice flag (from official product) is used to remove the ice and sea ice data. Figure 6 shows cycle per cycle percentage of measurements edited by this criterion in comparison with Jason-2 (only ocean and big lakes measurements are kept). Jason-2 and Jason-3 ice flag show similar features while on repetitive orbit. A small bias (< 0.2%) is visible since Jason-2 has been on its drifting orbit. This difference is due to the change in global number of ocean points for Jason-2 (that increased globally and everywhere from repetitive phase to LRO), so that ice flagged points percentage relatively to global number of points decreased.

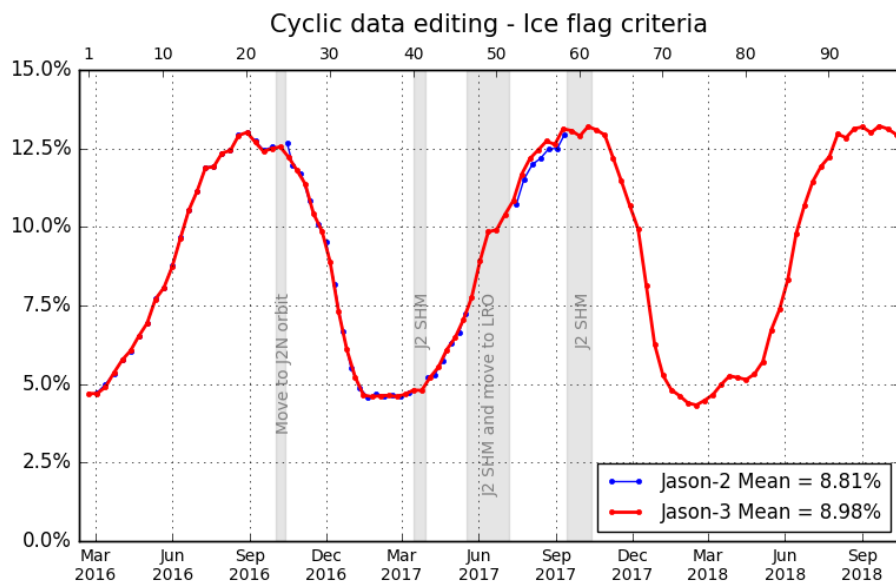


Figure 6 – Cycle per cycle monitoring of the percentage of edited measurements by ice flag criterion.

Over the shown period, no anomalous trend is detected but the nominal annual cycle is visible. Indeed, the maximum number of points over ice is reached during the southern winter (i.e. July - September). As Jason-3 takes measurements between 66° north and south, it does not detect thawing of sea ice (due to global warming), which takes place especially in northern hemisphere over 66°N.

3.2.3. Flagging quality criterion: Rain flag

Though the altimeter rain flag is available in GDR, it is not used hereafter during the editing procedure. The percentage of measurements where rain flag is set to 1 is plotted in figure 7 top pannel. Using the altimeter rain flag would lead to edit 6.5% of additional measurements (see figure 7 bottom pannels for comparison).

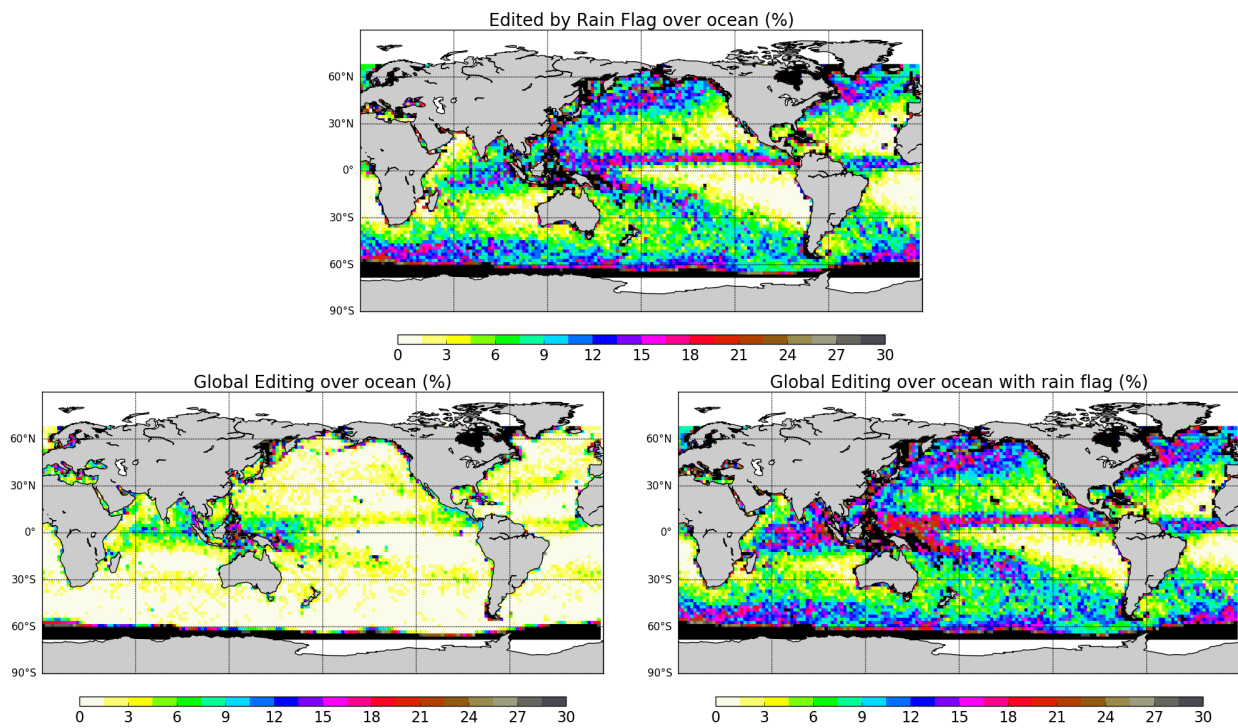


Figure 7 – Top: Percentage of edited measurements by altimeter rain flag criterion. Bottom left: Map of global edited measurements without considering the rain flag. Bottom right: Map of global edited measurements using all criteria and considering the rain flag. All figures are computed over ocean and from cycle 62 to 98.

3.2.4. Editing on thresholds criteria

After quality flag analysis, instrumental parameters have also been analyzed from comparison with thresholds. The average of total edited measurements following threshold criterion is around 3.3% (Figure 8). For each criterion, cycle percentage of edited measurements is monitored (detailed from part 3.2.4.1. to 3.2.4.11.). This allows detection of anomalies in the number of removed data, which could have instrumental, geophysical or algorithmic origins. In particular, note that no measurement is edited by the following corrections (these parameters are only verified in order to detect data at default values, which might happen during a processing anomaly):

- dry troposphere correction,
- inverted barometer correction (including DAC),
- equilibrium tide,
- earth tide,
- pole tide.

Threshold criteria applied on altimeter, radiometer and geophysical parameters are described in the following table 5. The last column represents the mean of rejected data on each criterion over GDR cycles 1 to 98.

Parameter	Min thresholds	Max thresholds	Mean edited
Sea surface height	-130 m	100 m	0.74%
Sea level anomaly	-2.0 m	2.0 m	0.96%
Number measurements of range	10	<i>Not applicable</i>	1.01%
Standard deviation of range	0	0.2 m	1.33%
Squared off-nadir angle	-0.2 deg ²	0.64 deg ²	0.57%
Dry troposphere correction	-2.5 m	-1.9 m	0.00%
Inverted barometer correction	-2.0 m	2.0 m	0.00%
AMR wet troposphere correction	-0.5m	-0.001 m	0.22%
Ionosphere correction	-0.4 m	0.04 m	1.15%
Significant wave height	0.0 m	11.0 m	0.57%
Sea State Bias	-0.5 m	0.0 m	0.50%
Number measurements of Ku-band Sigma0	10	<i>Not applicable</i>	1.00%
Standard deviation of Ku-band Sigma0	0	1.0 dB	2.04%
Ku-band Sigma0 ²	7.0 dB	30.0 dB	0.54%
Ocean tide	-5.0 m	5.0 m	0.01%
Equilibrium tide	-0.5 m	0.5 m	0.00%
Earth tide	-1.0 m	1.0 m	0.00%
Pole tide	-15.0 m	15.0 m	0.00%
Altimeter wind speed	0 m.s ⁻¹	30.0 m.s ⁻¹	1.02%
All together	-	-	3.26%

Table 5 – Editing criteria over cycles 1 to 98

The peak detected on cycle 30 (Figure 8) is due to an AMR anomaly that occurred from 08/12/2016 04:36:34 to 09/12/2016 12:58:47. Except this anomaly, the rate of rejected by thresholds data is quite stable.

²A bias of -2.38 dB is subtracting in order to be in agreement with TOPEX thresholds.

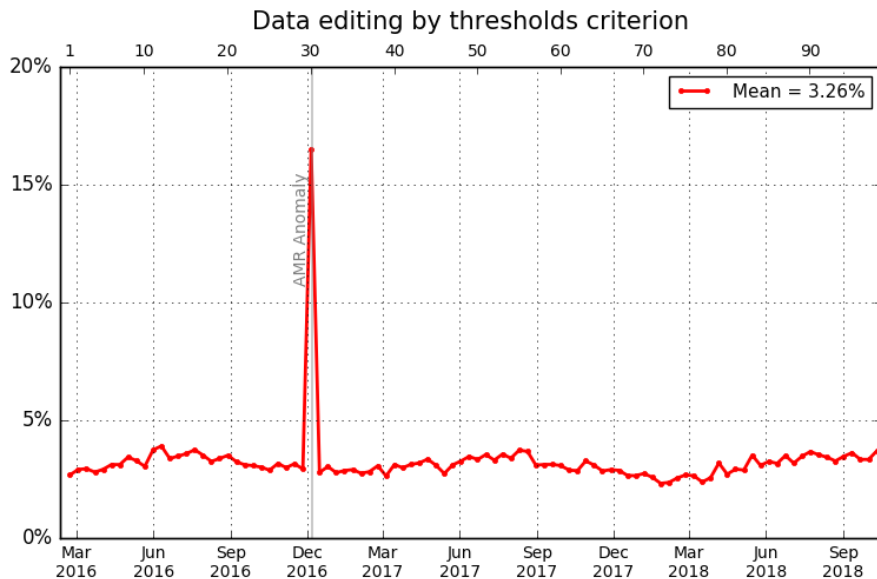


Figure 8 – Jason-3 data editing by thresholds average by cycle.

3.2.4.1. Threshold criteria: 20-Hz range measurements number and standard deviation

Range measurements computed with less than 10 full resolutions (20Hz, 20 measurements/seconds) are removed. Indeed they are considered as not consistent to compute 1Hz resolution range. Such situation usually occurs in regions with disturbed sea state or heavy rain, as shown on Figure 9 top right. Indeed waveforms are distorted by rain cells, which makes them often meaningless for SSH calculation. As a consequence, edited measurements due to several altimetric criteria are often correlated with wet areas.

For Jason-3, the average percentage of removed measurements using this criterion is 1.01% whereas it is 1.04% for Jason-2. The two missions provide very closed values (Figure 9 top right).

Using the threshold editing on 20Hz measurements standard deviation (Figure 9 bottom), 1.33% of data are removed in average for Jason-3, which is very close to Jason-2 (1.41%). An annual signal appears here for both missions. As for 20Hz range measurements number, edited measurements are correlated with wet areas.

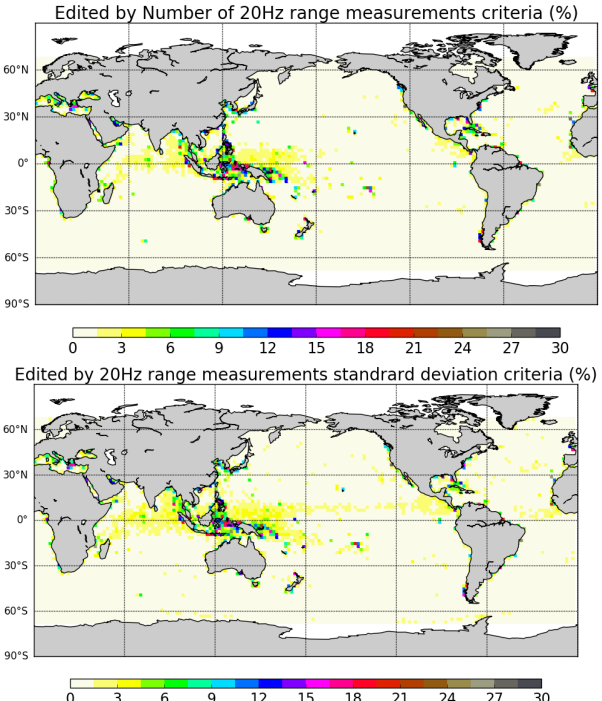
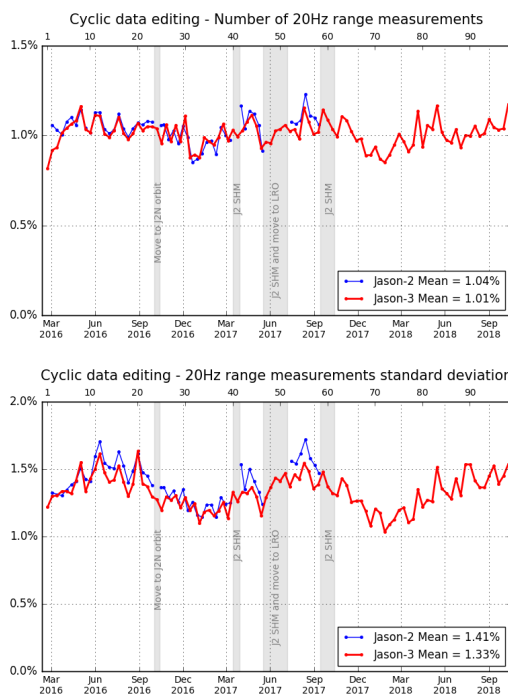


Figure 9 – Percentage of edited measurements by 20Hz range measurements threshold criterion (top) and by 20Hz range measurements standard deviation threshold criteria (bottom). Cycle per cycle monitoring compared with Jason-2 (left) and Jason-3 averaged map from cycle 62 to 98 (right).

3.2.4.2. Threshold criteria: Significant wave height (swh)

The percentage of edited measurements due to significant wave heights criterion is represented on Figure 10, and is about 0.57%. They are mostly due to set to default values data, and are located near coasts, in the equatorial regions and in circumpolar areas. Compared to Jason-2, the former removes globally more SWH data (0.64%), which seems to be linked to acquisition modes:

- For Jason-3 cycles 1 to 5, 7-8, 10, and 20, both missions are using median tracker: rejected data rate on this criterion are equivalent for both missions.
- For almost all cycles, Jason-2 uses meadian tracker and Jason-3 uses Diode/DEM automatic switch: there are less data removed for Jason-3 than for Jason-2.
- For Jason-2 cycle 311 (over Jason-3 cycles 30 and 31), both missions are in Diode/DEM mode: there are quite equivalent, with slightly less data removed on Jason-2.

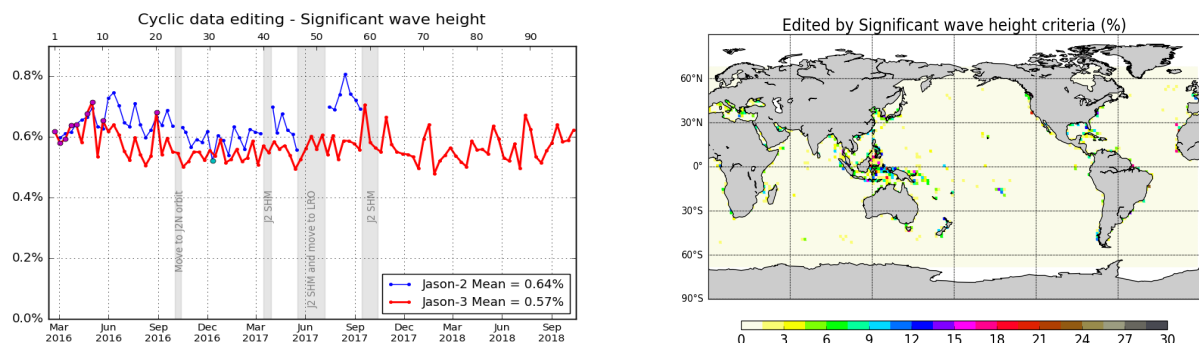


Figure 10 – Percentage of edited measurements by SWH threshold criterion. Left: Cycle per cycle monitoring compared with Jason-2 (Jason-2 DEM cycle in cyan. Jason-3 median tracker cycles in purple.) Right: Jason-3 averaged map from cycle 62 to 98 .

3.2.4.3. Threshold criteria: Backscatter coefficient (σ_0)

The percentage of edited measurements due to backscatter coefficient criterion is represented on top of Figure 11. It is about 0.54%, compared to 0.61% for Jason-2. The bottom part of Figure 11 shows again close values between the two missions for the 20Hz σ_0 standard deviation criterion. However, there are slightly more rejected measurements with this criterion on Jason-3 (2.04%) than Jason-2 (1.95%). Edited measurements are especially found in regions with disturbed waveforms, as shown on the maps. As for SWH criterion (3.2.4.2.), differences seem to be linked to acquisition modes:

- For Jason-3 cycles 1 to 5, 7-8, 10, and 20, both missions are using median tracker: rejected data rate on this criterion are equivalent for both missions.
- For almost all cycles, Jason-2 uses meadian tracker and Jason-3 uses Diode/DEM automatic switch: there are less data removed for Jason-2 than for Jason-3.
- For Jason-2 cycle 311 (over Jason-3 cycles 30 and 31), both missions are in Diode/DEM mode: there are quite equivalent.

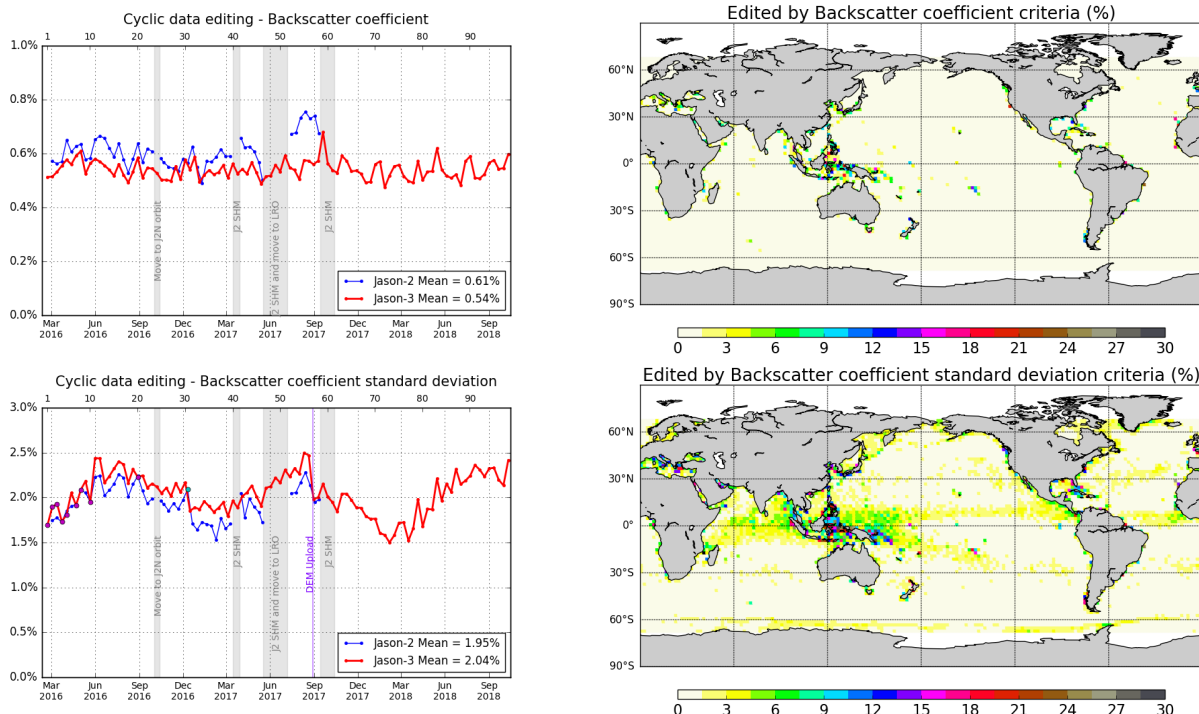


Figure 11 – Percentage of edited measurements by backscatter coefficient threshold criterion (top) and by 20Hz backscatter coefficient standard deviation threshold criteria (bottom). Cycle per cycle monitoring compared with Jason-2 (left, Jason-2 DEM cycle in cyan. Jason-3 median tracker cycles in purple) and Jason-3 averaged map from cycle 62 to 98 (right).

3.2.4.4. Threshold criteria: Radiometer wet troposphere correction

The percentage of edited measurements due to radiometer wet troposphere correction criterion is represented in figure 12. It is about 0.22%. When removing cycles which experienced problems, percentage of edited measurements drops to 0.08%. For some cycles, the percentage of edited measurements is higher than usual. For cycle 30, this unusual value (13.85%) is due to an AMR anomaly. Compared to Jason-2 values, they are within the same order of magnitude, except specific events or anomalies (Jason-2 AMR anomalies during cycle 285 and cycle 326, that correspond respectively to Jason-3 cycle 5 and cycle 45 datation).

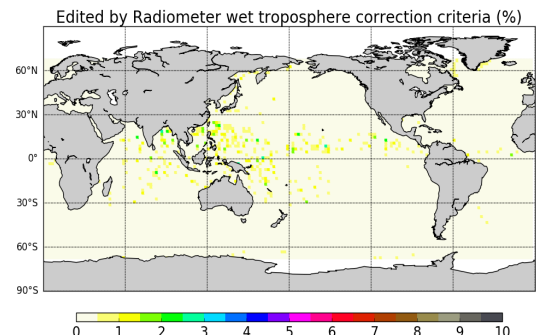
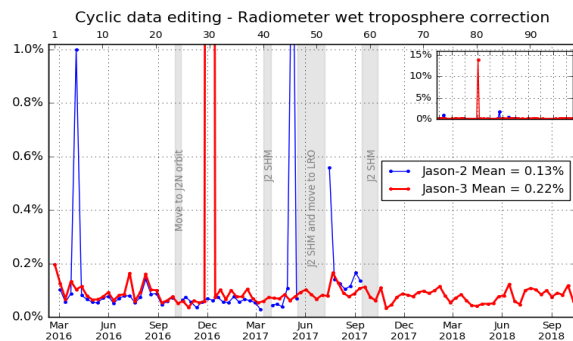


Figure 12 – Percentage of edited measurements by radiometer wet troposphere correction threshold criterion. Left: Cycle per cycle monitoring compared with Jason-2. Right: Jason-3 averaged map from cycle 62 to 98.

3.2.4.5. Threshold criteria: Ionospheric correction

The mean percentage of edited data by threshold criterion on ionospheric correction is 1.15% and is close to Jason-2 mean (1.18%). The map on figure 13 shows that measurements edited by dual frequency ionosphere correction are mostly found in equatorial regions.

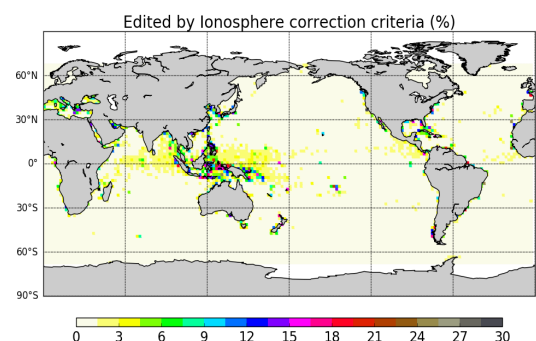
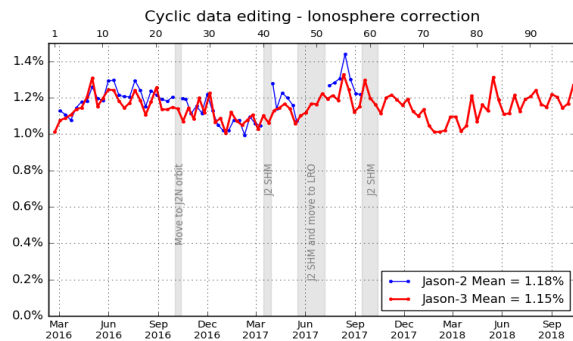


Figure 13 – Percentage of edited measurements by ionospheric correction threshold criterion. Left: Cycle per cycle monitoring compared with Jason-2. Right: Jason-3 averaged map from cycle 62 to 98.

3.2.4.6. Threshold criteria: Altimeter wind speed

The percentage of edited measurements due to altimeter wind speed criterion is represented on figure 14. It is about 1.02%, and in accordance with Jason-2 (1.03%). Measurements are usually edited because of default values. This is the case when sigma0 itself is at default value, or when it shows very high values (higher than 25 dB), which occurs during sigma bloom situations and also over sea ice. Indeed, the wind speed algorithm (which uses backscatter coefficient and significant wave height) can not retrieve values for sigma0 higher than 25 dB.

Wind speed is also edited when it includes negative values, which can occur in GDR products. Nevertheless, sea state bias is available even for negative wind speed values. Therefore, the percentage of edited altimeter wind speed data is higher than the percentage of edited sea state bias data (see 3.2.4.7.).

The map 14 showing percentage of measurements edited by altimeter wind speed criterion is correlated with maps 10 (swh) and 15 (ssb).

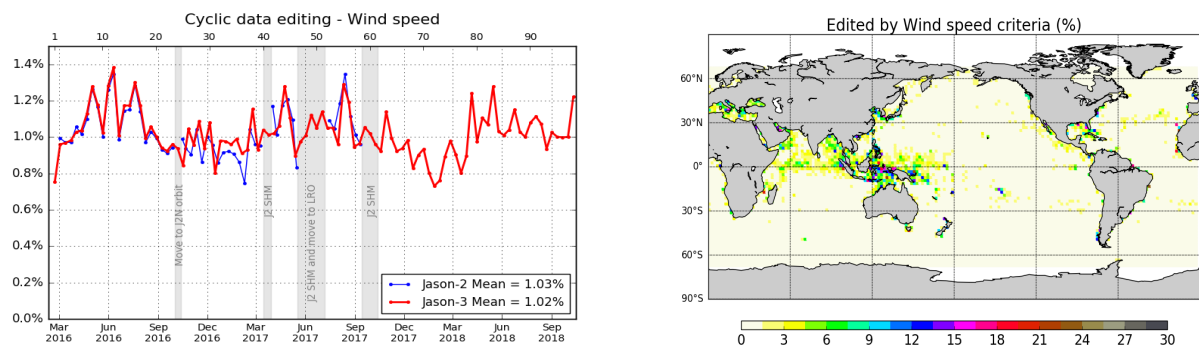


Figure 14 – Percentage of edited measurements by wind speed threshold criterion. Left: Cycle per cycle monitoring compared with Jason-2. Right: Jason-3 averaged map from cycle 62 to 98.

3.2.4.7. Threshold criteria: Sea State Bias

Regarding the sea state bias criterion, the percentage of Jason-3 edited measurements is about 0.50% and 0.63% for Jason-2. The difference can also be observed on the sigma0 and the significant wave height threshold criteria (which are both used for SSB computation).

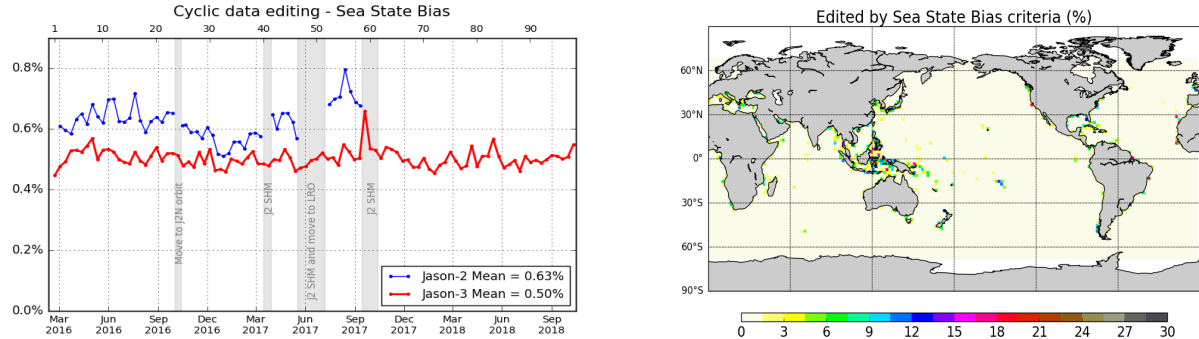


Figure 15 – Percentage of edited measurements by sea state bias threshold criterion. Left: Cycle per cycle monitoring compared with Jason-2. Right: Jason-3 averaged map from cycle 62 to 98.

3.2.4.8. Threshold criteria: Ocean tide

The percentage of edited measurements due to ocean tide is 0.01% for both missions. The ocean tide correction is a model output, there should therefore be no edited measurement. Indeed there are no measurements edited in open ocean areas, but only very few near coasts (Alaska, Kamchatka, Labrador). These measurements are mostly at default values. The level of edited measurements decreases or increases with move of orbit for Jason-2 : this is related to the new ground track, which no longer overflows the same areas.

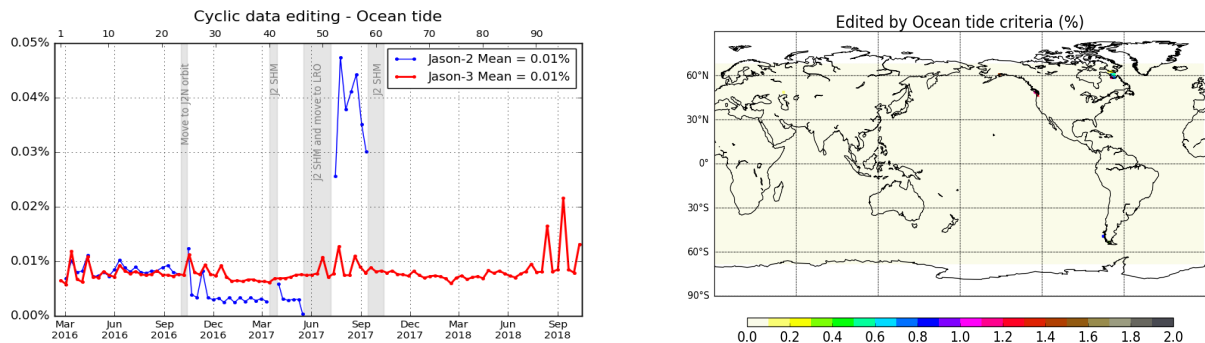


Figure 16 – Percentage of edited measurements by ocean tide threshold criterion. Left: Cycle per cycle monitoring compared with Jason-2. Right: Jason-3 averaged map from cycle 62 to 98.

3.2.4.9. Threshold criteria: Square off nadir angle

The percentage of edited data for both missions is almost similar (0.57% for Jason-3 and 0.58% for Jason-2). An increase in Jason-2 edited measurements is observed from July 2017 after Jason-2 move to drifting orbit.

The map 17 shows that edited measurements are mostly found in coastal regions and regions with disturbed waveforms.

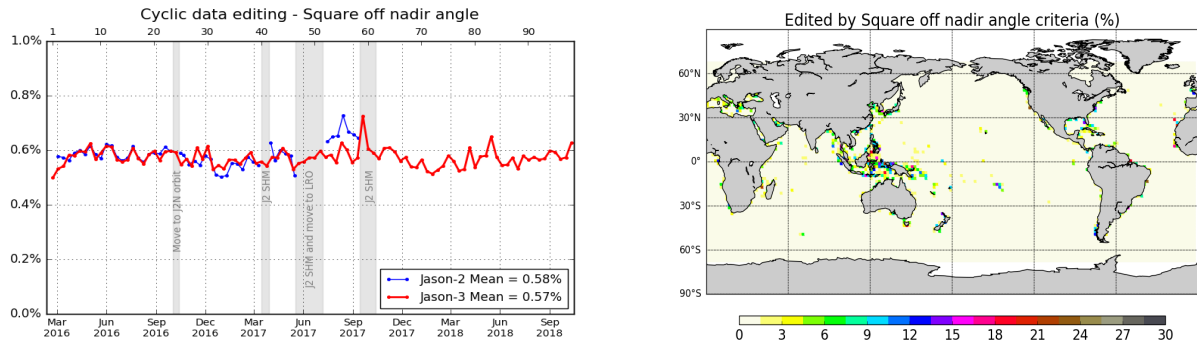


Figure 17 – Percentage of edited measurements by square off nadir angle threshold criterion. Left: Cycle per cycle monitoring compared with Jason-2. Right: Jason-3 averaged map from cycle 62 to 98.

3.2.4.10. Threshold criteria: Sea surface height

Sea surface height represents the difference between the orbit and the altimeter range in Ku band. Figure 18 summarizes the editing resulting from the sea surface height threshold criterion. It removes in average 0.74% of data for Jason 3 whereas it removes 0.77% of data for Jason 2. The editing is usually due to range measurements at default values near coast in equatorial and mid-latitude regions, as well as regions with low significant wave heights.

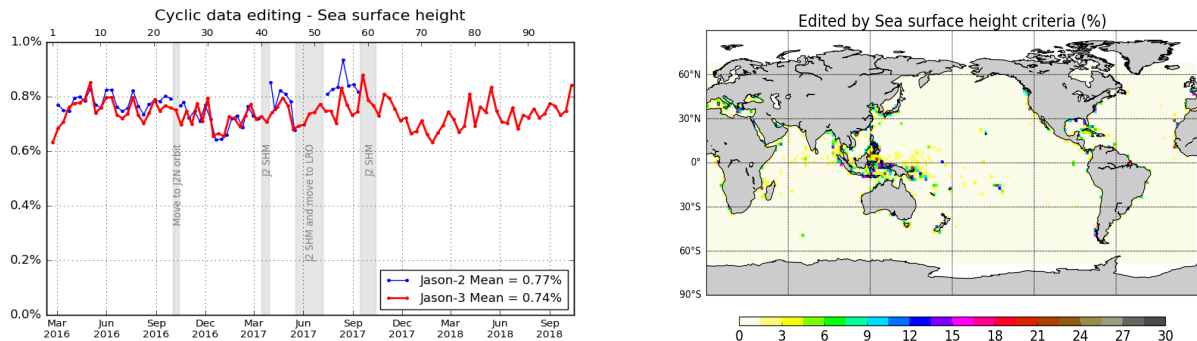


Figure 18 – Percentage of edited measurements by sea surface height threshold criterion. Left: Cycle per cycle monitoring compared with Jason-2. Right: Jason-3 averaged map from cycle 62 to 98.

3.2.4.11. Threshold criteria: Sea level anomaly

The percentage of edited data by threshold criterion is 0.96% for Jason-3. As the wet tropospheric correction is used in the SLA computation, percentage of edited SLA measurement presents the same peak on cycle 30. When removing this cycle, percentage of edited measurements drops to 0.81%. The rate of rejected data for Jason-3 is quite equivalent as for Jason-2 (0.93%). As in case of Jason-3, higher points on Jason-2 monitoring are mainly due to Jason-2 wet troposphere contribution, where AMR was unavailable during cycle 285 (Jason-3 cycle 5), cycle 326 (Jason-3 cycle 45), and for restart after SHM, leading to an increase of the quantity of edited data (point out of plot scale).

Otherwise the overall performance of Jason-3 system is in excellent agreement with Jason-2, and shows very close results in terms of edited data.

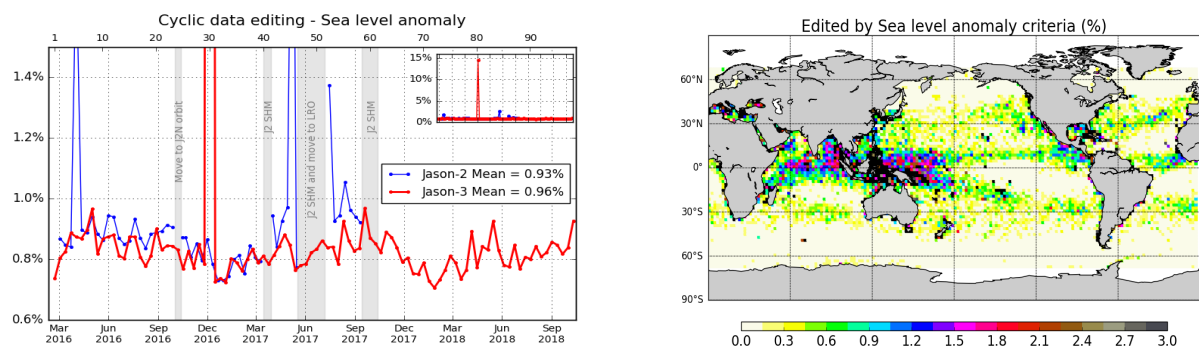


Figure 19 – Percentage of edited measurements by sea level anomaly threshold criterion. Left: Cycle per cycle monitoring compared with Jason-2. Right: Jason-3 averaged map from cycle 62 to 98.

4. Monitoring of altimeter and radiometer parameters

4.1. Methodology

Mean and standard deviation of Jason-3 main parameters have both been monitored since the beginning of the mission. Moreover, a comparison with Jason-2 parameters has been performed: it allows to monitor the bias between the parameters of the 2 missions.

- Till Jason-3 cycle 23, Jason-3 and Jason-2 are on the same ground track and are spaced out about 80 seconds apart (tandem phase), the mean of the Jason-2 - Jason-3 differences can be computed using a point by point repeat track analysis (referred as ‘residuals’ in plots).
- From Jason-3 cycle 24, a maneuver sequence was conducted (from end of Jason-2 cycle 303) to move Jason-2 to the new formation flight mission orbit. Jason-2 has a repeat ground-track which is interleaved with Jason-3. It is the same ground-track as already used by Topex/Poseidon during its formation flight phase with Jason-1, and Jason-1 with Jason-2. Because of a time shift of 5 days, geographical variations are then too strong to directly compare Jason-3 and Jason-2 parameters on a point by point basis. Therefore day per day global differences have been carried out to monitor differences between the two missions. A filter over 11 days was applied. Nevertheless the differences are still quite noisy, especially for corrections which vary rapidly in time and space. Therefore occasional small jumps might be covered by the noise of the differences. Nevertheless it should be possible to detect drifts and permanent jumps. Jason-3 and Jason-2 were in this formation flight phase from Jason-3 cycles 25 to 46 (Jason-2 cycles 305 to 327).

In March and May 2017, Jason-2 experienced several safe holds caused by gyro anomalies. It was decided to move Jason-2 to an End-of-Life (EOL) Long Repeat Orbit (LRO). Jason-2 mission phase is detailed in [115]. Science data on the first LRO are available from 11th of July 2017 to 16th of July 2018. Note that the first cycle on the new orbit starts with cycle 500 (this corresponds to mid-Jason-3 cycle 52) and this first interleaved ground track ends on cycle 537 (end of Jason-3 cycle 89). Note that after this first LRO, Jason-2 was moved to a second interleaved ground track (iLRO) on 18th of July 2018. Science data restart on 25th of July 2018 with cycle 600.

As during the formation flight phase, day per day global differences of the parameters have been carried out to monitor differences between the two missions (only until Jason-2 cycle 506 (14th of September 2017)): differences are done over Jason-3 cycles 1 to 58, corresponding to Jason-2 cycles 281 to 506.

4.2. 20Hz range measurements

The monitoring of the number and standard deviation of 20 Hz elementary range measurements used to derive 1 Hz data is presented here. These two parameters are computed during the altimeter ground processing. For both Jason-2 and Jason-3, before performing a regression to derive the 1 Hz range from 20 Hz data, a MQE (mean quadratic error) criterion is used to select valid 20 Hz measurements. This first step of selection consists in verifying that the 20 Hz waveforms can be approximated by a Brown echo model (Brown, 1977 [49]) (Thibaut et al. 2002 [101]).

Then, through an iterative regression process, elementary ranges too far from the regression line are discarded until convergence is reached. Thus, monitoring the number of 20 Hz range measurements and the standard deviation computed among them is likely to reveal changes at instrumental level.

4.2.1. 20 Hz range measurements number in Ku-Band and C-Band

Jason-3 number of elementary 20 Hz range measurements starts with values slightly higher than Jason-2 until cycle 3. During cycle 3, new calibration (CAL2) filter turned the square off-nadir angle to zero, which implies the absence of waveform mispointing, a higher MQE and a smaller number of elementary measurements. Then from cycle 4 onwards, Jason-3 number of elementary 20 Hz range measurements is very similar to Jason-2 with an average of 19.61 versus 19.60 in Ku-band (left of figure 20) and 19.24 versus 19.25 in C-band (right of figure 20).

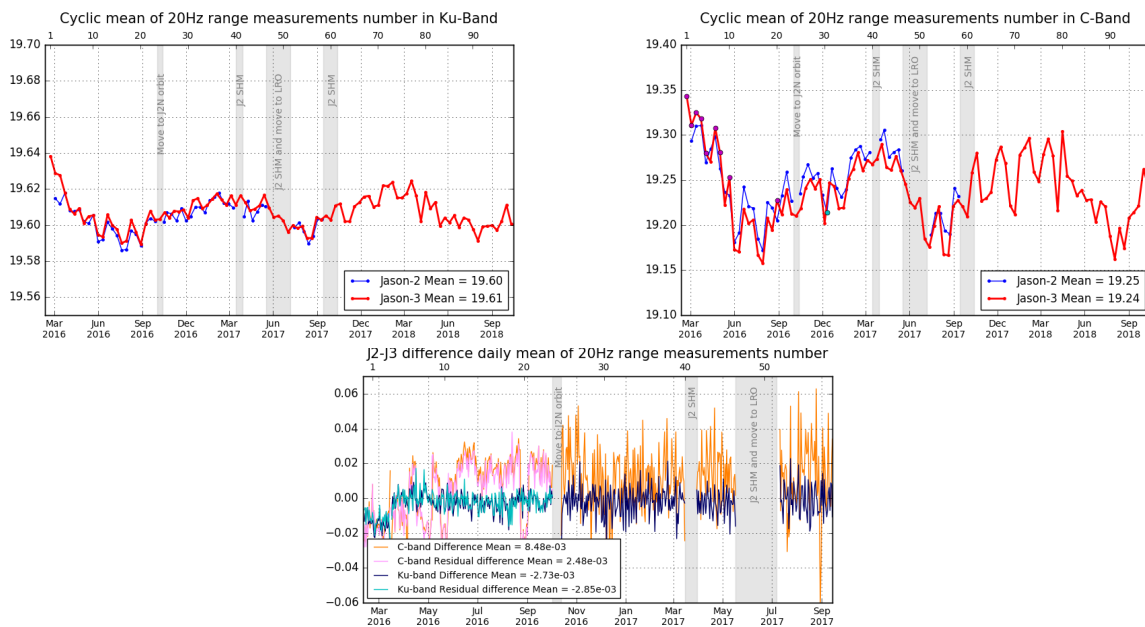


Figure 20 – **Top:** Cyclic monitoring of number of elementary 20 Hz range measurements for Jason-2 and Jason-3 for Ku-band and C-band. **Bottom:** Jason-2 - Jason-3 difference daily monitoring of elementary 20 Hz range measurements number (until september 2017).

Elementary number of measurements used to compute a 1Hz measurement is correlated to significant wave height (4.5.): figure 21 shows less elementary range measurements around Indonesia, the Mediterranean Sea and close to coasts, which are all regions of low significant wave heights.

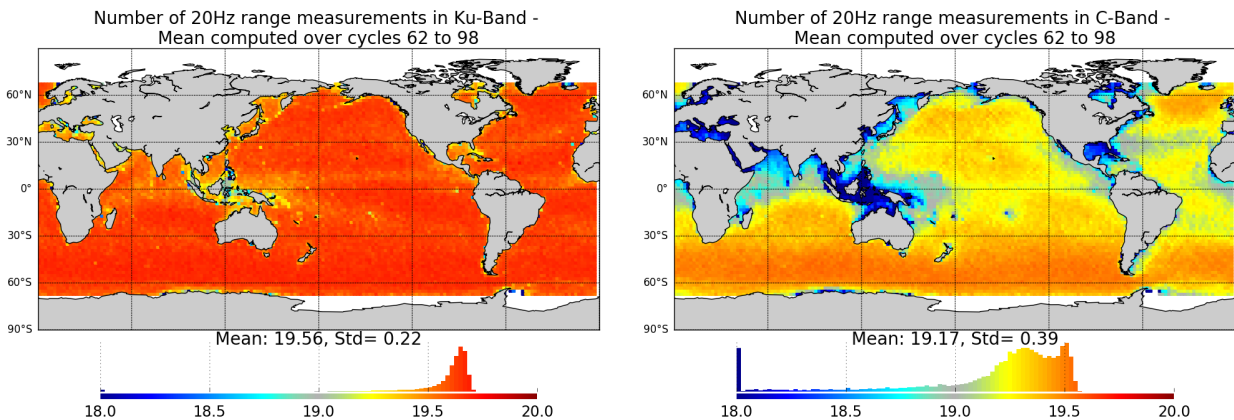


Figure 21 – Map of number of 20 Hz range measurements for Jason-3 averaged over cycles 62 to 98, in Ku-band (left) and in C-band (right).

4.2.2. 20 Hz range measurements standard deviation in Ku-Band and C-Band

Figure 22 shows the monitoring of Jason-3 and Jason-2 20 Hz range measurements standard deviation, in Ku-band (left) and C-band (right). Jason-3 standard deviation of the 20 Hz measurements is 7.98 cm for Ku-Band and 17.55 cm for C-Band. It is similar to Jason-2 data (8.00 cm in Ku-Band and 17.43 cm in C-Band). 20 Hz range measurements standard deviation is higher on C-band than on Ku-band due to the onboard averaging that is performed over less waveforms (onboard averaging of 90 measurements for each 20Hz Ku-band value, against 15 in case of C-band), which leads to an increased noise.

Standard deviation of measurements is correlated to significant wave height (swh dedicated part: 4.5.).

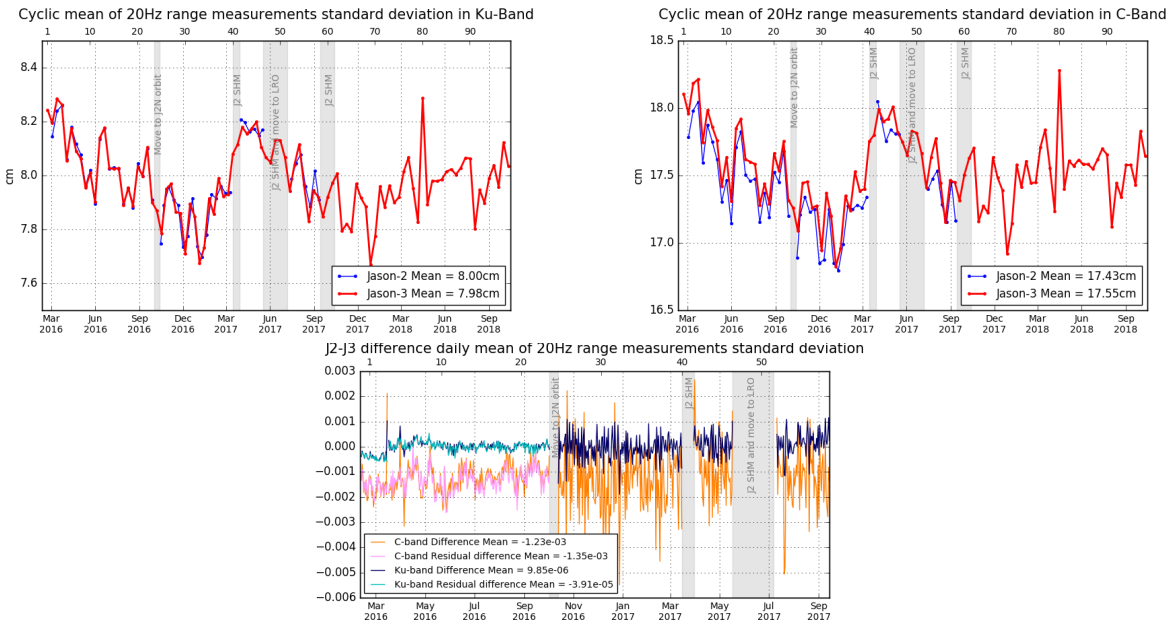


Figure 22 – Top: Cyclic monitoring of elementary 20 Hz range measurements standard deviation for Jason-2 and Jason-3 for Ku-band and C-band. **Bottom:** Jason-2 - Jason-3 difference daily monitoring of elementary 20 Hz range measurements standard deviation.

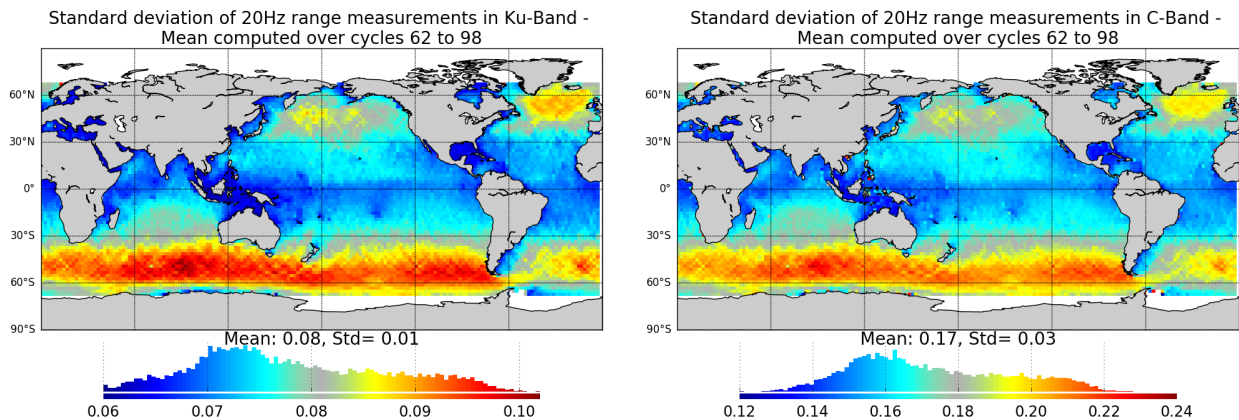


Figure 23 – Map of 20 Hz range measurements standard deviation for Jason-3 averaged over cycles 62 to 98, in Ku-band (left) and in C-band (right).

4.3. Off-Nadir Angle from waveforms

The off-nadir angle is derived from the slope of the trailing edge of the waveform during the altimeter processing: it can either be caused by real platform mispointing or by backscattering properties of the surface. The square of the off-nadir angle, averaged on a cyclic basis (taking into account valid measurements only), has been plotted for Jason-3 and Jason-2 on figure 24.

At the beginning of the mission, Jason-3 altimeter mispointing was deeply analysed to understand the negative values observed from cycle 3 after GPS upload. Mispointing is actually related to CAL2 filter shapes, which depends on automatic gain control settings for Jason-3. During the first cycles, the in-flight calibration (CAL2) filters were measured using a different Automatic Gain Control code than the one used during waveform acquisition over ocean, in order to optimize the CAL2 measurement numerical accuracy (quantification optimization). It has however an impact on the filter slope and fully explains the observed mispointing negative values. The filter slope was modified during cycle 14 (June 26th, 2016) and explains the jump to zero on the IGDR curve. This correction was applied during GDR production, which explains the difference between red and green curves between cycles 4 and 14, so that GDR mispointing has been close to zero from cycle 4.

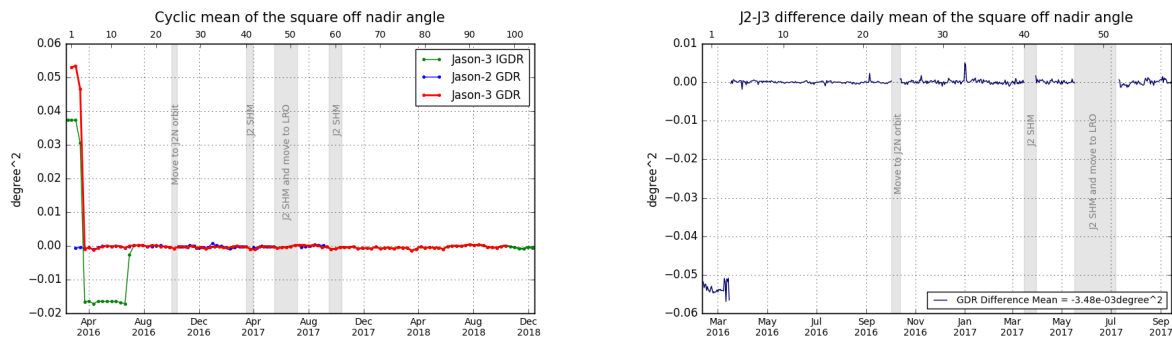


Figure 24 – Left: Cyclic monitoring of the square off-nadir angle for Jason-2 and Jason-3 for GDRs (blue and red curves) and Jason-3 IGDRs (product IGDR for cycles 1 to 41 in light green, and IGDR L2P from cycle 25 to 68 in dark green). *Right:* Jason-2 - Jason-3 difference daily monitoring of the square off-nadir angle (GDR data).

No mispointing event occurred on Jason-3 over the considered period. The map figure 25 is generally slightly negative, except for regions around Indonesia, and close to coasts.

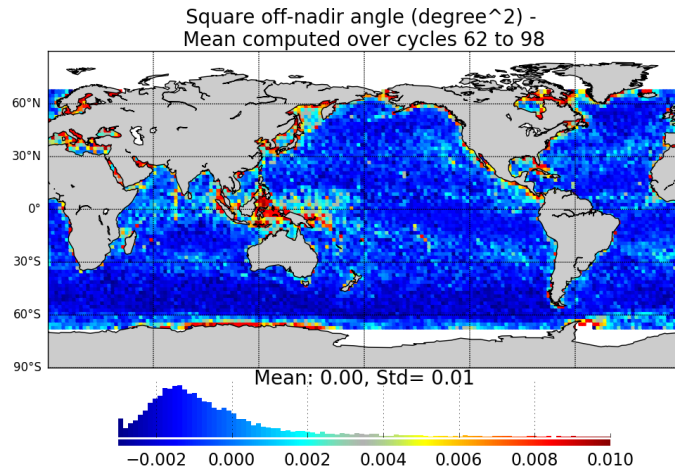


Figure 25 – Map of the square off-nadir angle for Jason-3 averaged over cycles 62 to 98.

Without taking into account the three third cycles, square off-nadir angle is monitored year by year on the left part of figure 26, highlighting a small annual signal (global mean is higher during summer). Square off-nadir angle slightly depends on significant wave height as shown on right part of figure 26: considering this monitoring for swh between 2m and 6m, slope is $-0.0005\text{deg}^2/\text{m}$.

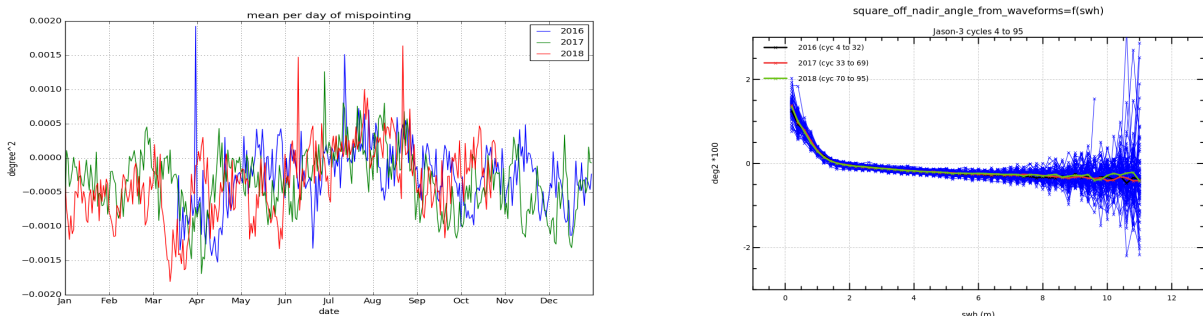


Figure 26 – Left: Mean per day of mispointing for Jason-3 from cycle 4. Right: Square off nadir angle against swh.

4.4. Backscatter coefficient

The Jason-3 Ku-band and C-band backscatter coefficients show good agreement with Jason-2 as visible on cyclic monitoring (figure 28). Jason-3 backscatter coefficient is about 13.76 dB for Ku-band (15.51 dB for C-band) while for Jason-2 it is about 13.51 dB (15.40 dB). The difference between the two missions is about -0.25 dB (-0.11 dB) and present a good stability. However, this was different from cycle 0 to cycle 4, where slight mispointing on Jason-3 caused higher differences of sigma0 between missions.

During the tandem flight, Jason-3 sigma0 was modified with a new altimeter characterization file, an update of the look up tables (Patch 6) and a new CAL2 filter (cycle 14, June 26th, 2016). All of them were applied on all GDR cycles. As a consequence, there is a bias between backscatter coefficient in GDR and IGDR products until cycle 14. In addition, a new AMR calibration file is applied for IGDR cycle 17 (see part 4.7.), so that IGDR and GDR sigma0 are slightly different until cycle 17 due to atmospheric attenuation applied to sigma0 (as the atmospheric attenuation is derived from radiometer parameters).

A special investigation on the standard deviation of the backscatter coefficient is presented in part 8.2..

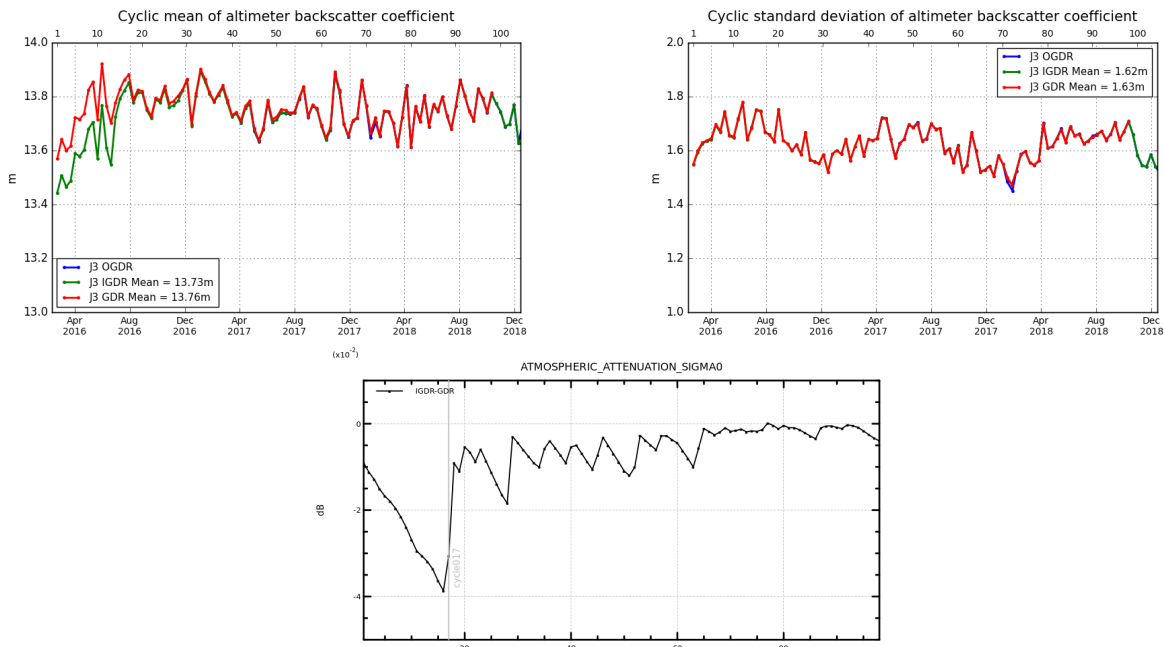


Figure 27 – Top: Cyclic monitoring of backscatter coefficient for Jason-3 (Ku-band) OGDR/IGDR/GDR. Bottom: difference of atmospheric attenuation applied to sigma0 between IGDR and GDR products.

Jason-3 validation and cross calibration activities (Annual report 2018)

Nomenclature : SALP-RP-MA-EA-23248-CLS

Page : 45

Document version: 1.1

Date : February 22, 2019

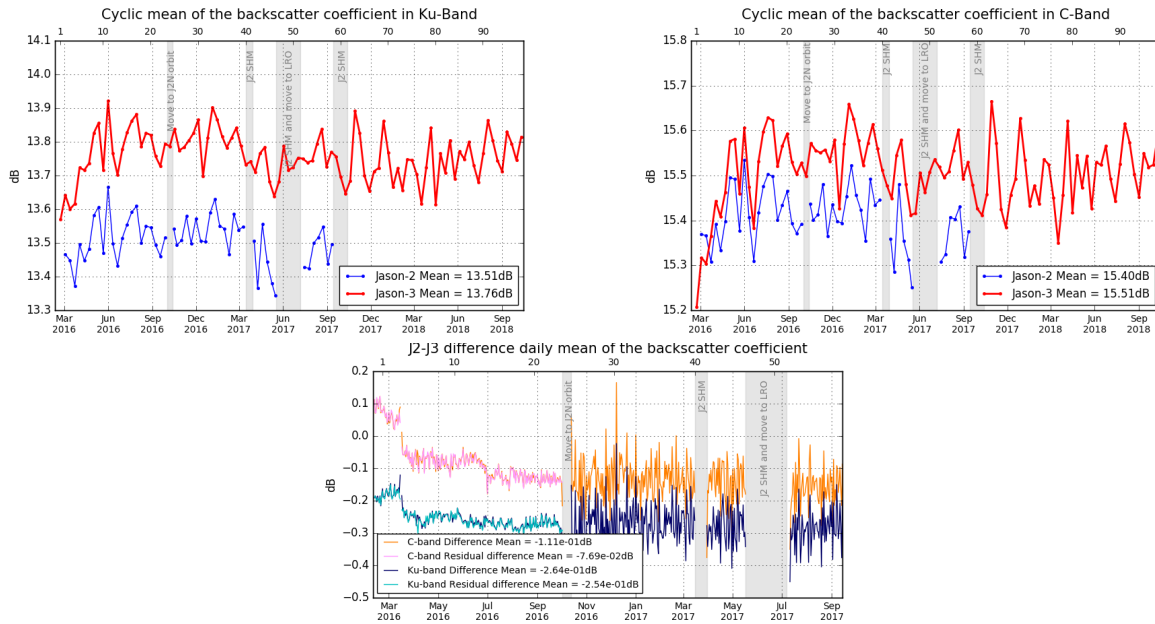


Figure 28 – Top: Cyclic monitoring of backscatter coefficient for Jason-2 and Jason-3 for Ku-band (left) C-band (right). **Bottom:** daily monitoring of Jason-2 - Jason-3 GDR difference of the backscatter coefficient.

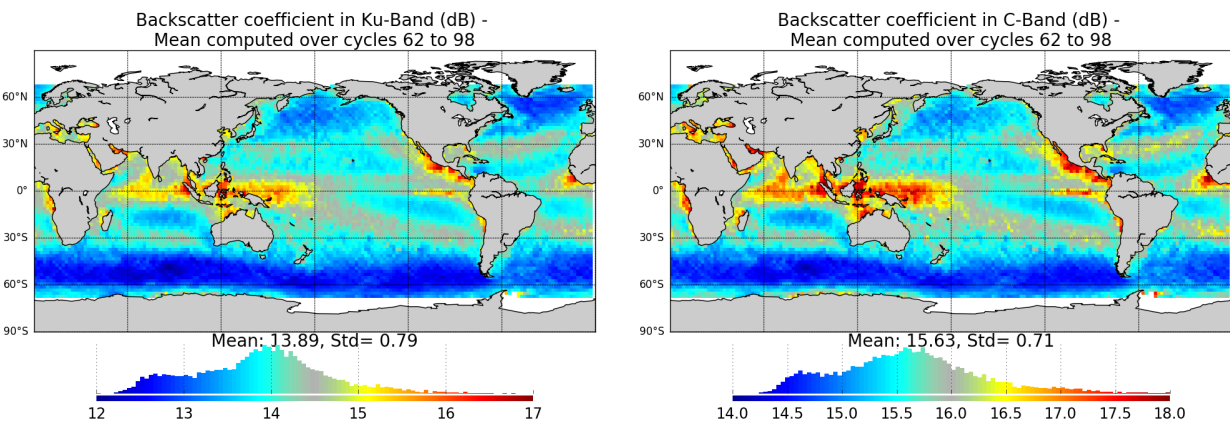


Figure 29 – Map of backscatter coefficient for Jason-3 averaged over cycles 62 to 98, in Ku-band (left) and in C-band (right).

4.5. Significant wave height

As for Sigma0 parameter, a very good consistency between both significant wave height is shown (see figure 31). In addition, until Jason-3 cycle 23 (tandem phase, observing the same ocean with only 1'20" apart), Jason-2 and Jason-3 measurements are identical. After Jason-2 move to interleaved orbit, the two missions are not as close as during tandem phase and measured swh are slightly different, but there is still no bias between Jason-2 and Jason-3 measured wave height in average (see bottom of figure 31).

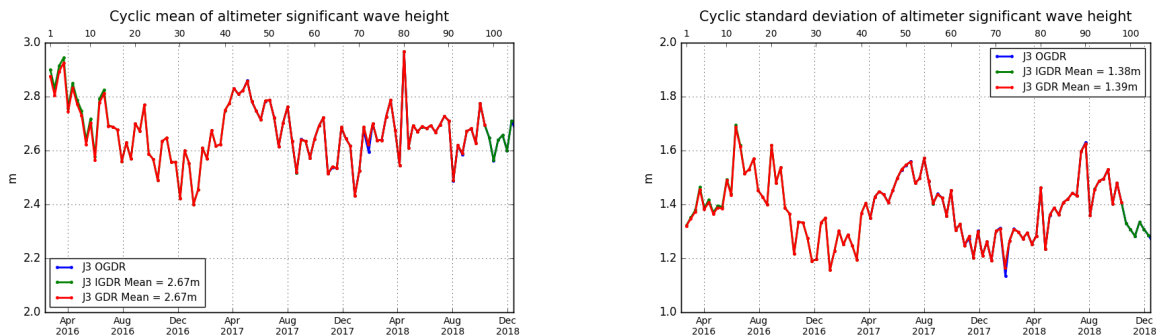


Figure 30 – Cyclic monitoring of significant wave height for Jason-3 (Ku-band) OGDR/IGDR/GDR.

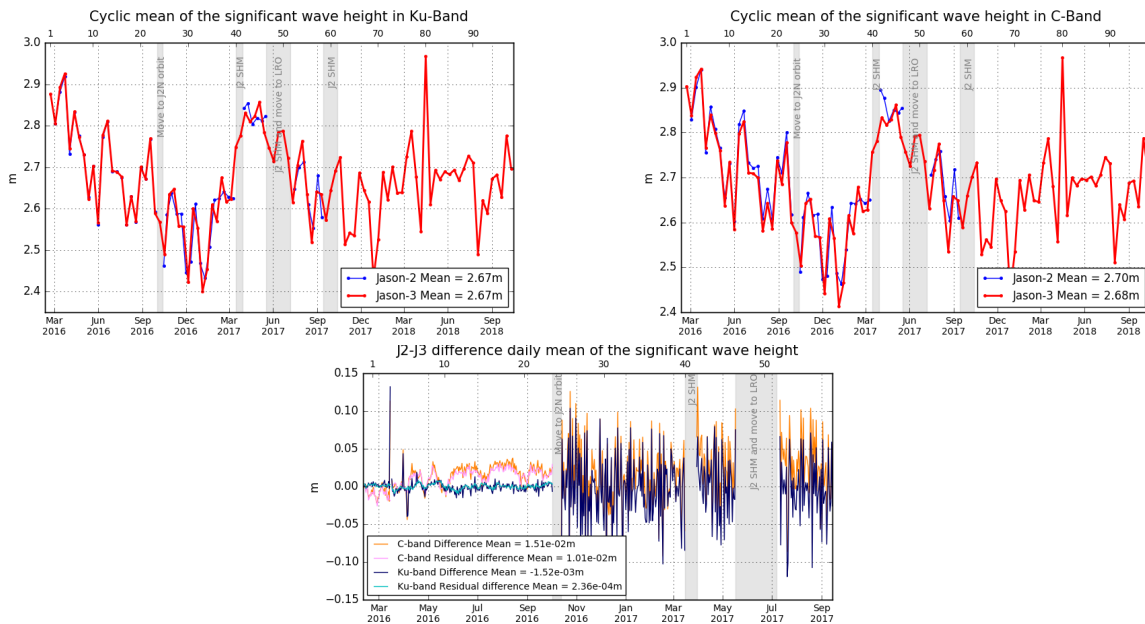


Figure 31 – Cyclic monitoring of significant wave height for Jason-2 and Jason-3 for Ku-band (left) and for C-band (right). Jason-2 - Jason-3 difference daily monitoring of significant wave height (bottom).

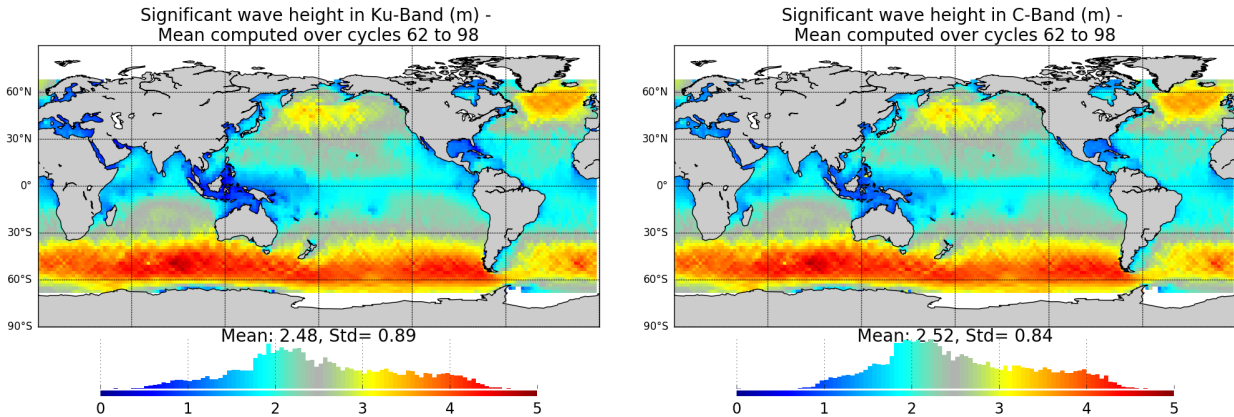


Figure 32 – Map of significant wave height for Jason-3 averaged over cycles 62 to 98, in Ku-band (left) and in C-band (right).

4.6. Dual-frequency ionosphere correction

The dual frequency ionosphere corrections derived from the Jason-3 and Jason-2 altimeters show a mean difference of about 0.56 cm (figure 33), with cycle to cycle variations lower than 1 mm.

Until the LUT changes that occurred during cycle 14 (for O/IGDRs), the mean bias between the two missions was 1 cm (for O/IGDRs). It turns then to 0.55 cm following “jumps” of Ku range (5 mm), C Range (1.5 cm) and sea state bias (0.1 mm). This event has an impact on Sea Level Anomalies retrieved from OGDRs and IGDRs products. For GDR products, the same LUT was used for the whole mission period, hence the absence of jump (see bottom and right of figure 33).

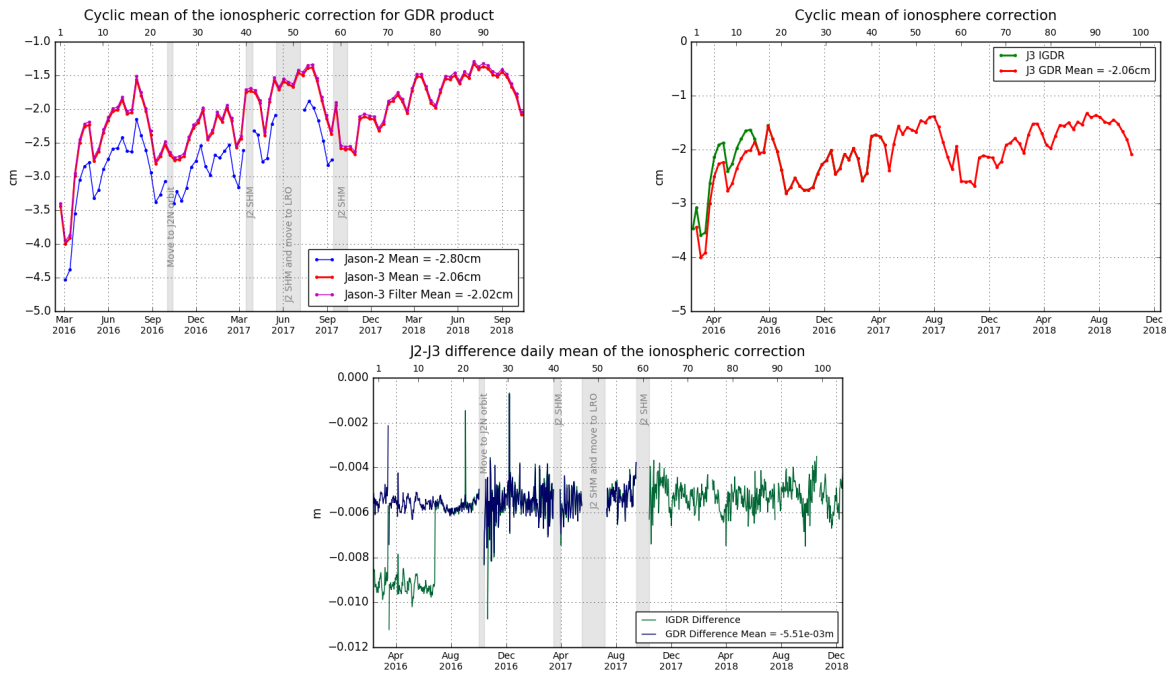


Figure 33 – Cyclic monitoring of ionospheric correction for Jason-2 and Jason-3. (left). Cyclic monitoring of Jason-3 ionospheric correction for IGDR and GDR data (right). Jason-2 - Jason-3 difference daily monitoring of ionospheric correction (bottom).

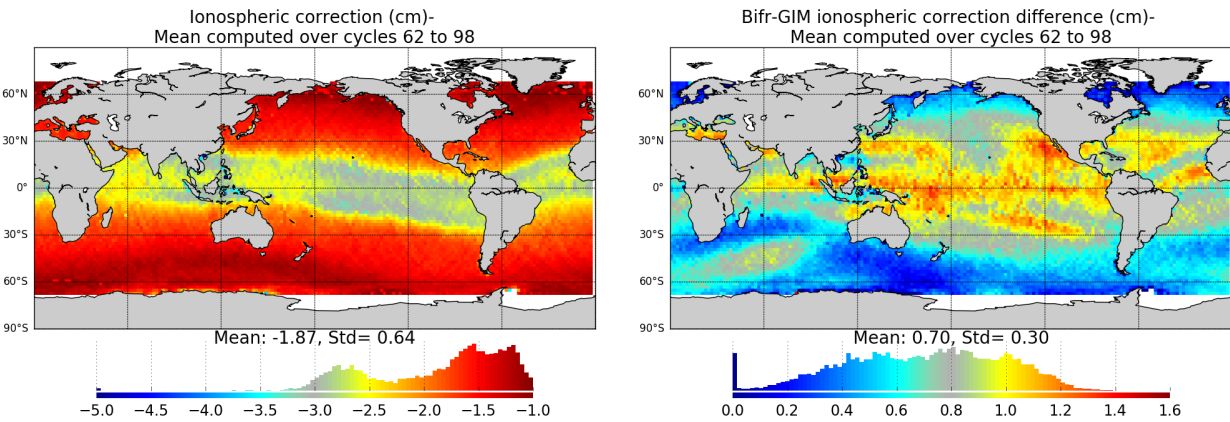


Figure 34 – Left: Map of ionospheric correction for Jason-3 averaged over cycles 62 to 98. Right: Map of dual-frequency minus GIM ionospheric correction solutions.

When comparing altimeter ionosphere correction to GIM correction (figure 35), mean as well as standard deviation of this difference present same variation for both missions.

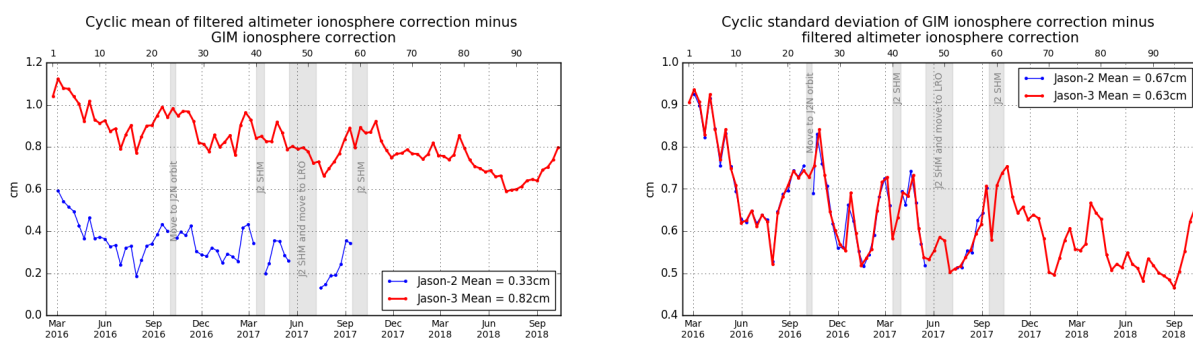


Figure 35 – Cyclic monitoring of GIM ionosphere correction minus filtered altimeter ionosphere correction for Jason-2 and Jason-3. Left: mean, right: standard deviation.

4.7. AMR Wet Troposphere Correction

4.7.1. Overview

In order to evaluate radiometer wet troposphere correction, liquid water content, water vapour content and atmospheric attenuation, Jason-3 uses a three-frequency AMR radiometer (18.7, 23.8 and 34.0 GHz), similar to the one used on Jason-2.

Note that the 23.8 GHz channel is the primary water vapor sensing channel, meaning higher water vapor concentrations leads to larger 23.8 GHz brightness temperature values. As a consequence, top right and bottom right parts of figure 36 are correlated. Moreover, the 34 GHz channel and the 18.7 GHz channel, which have less sensitivity to water vapor, facilitate the removal of the contributions from cloud liquid water and excess surface emissivity of the ocean surface due to wind, which also act to increase the 23.8 GHz brightness temperature.

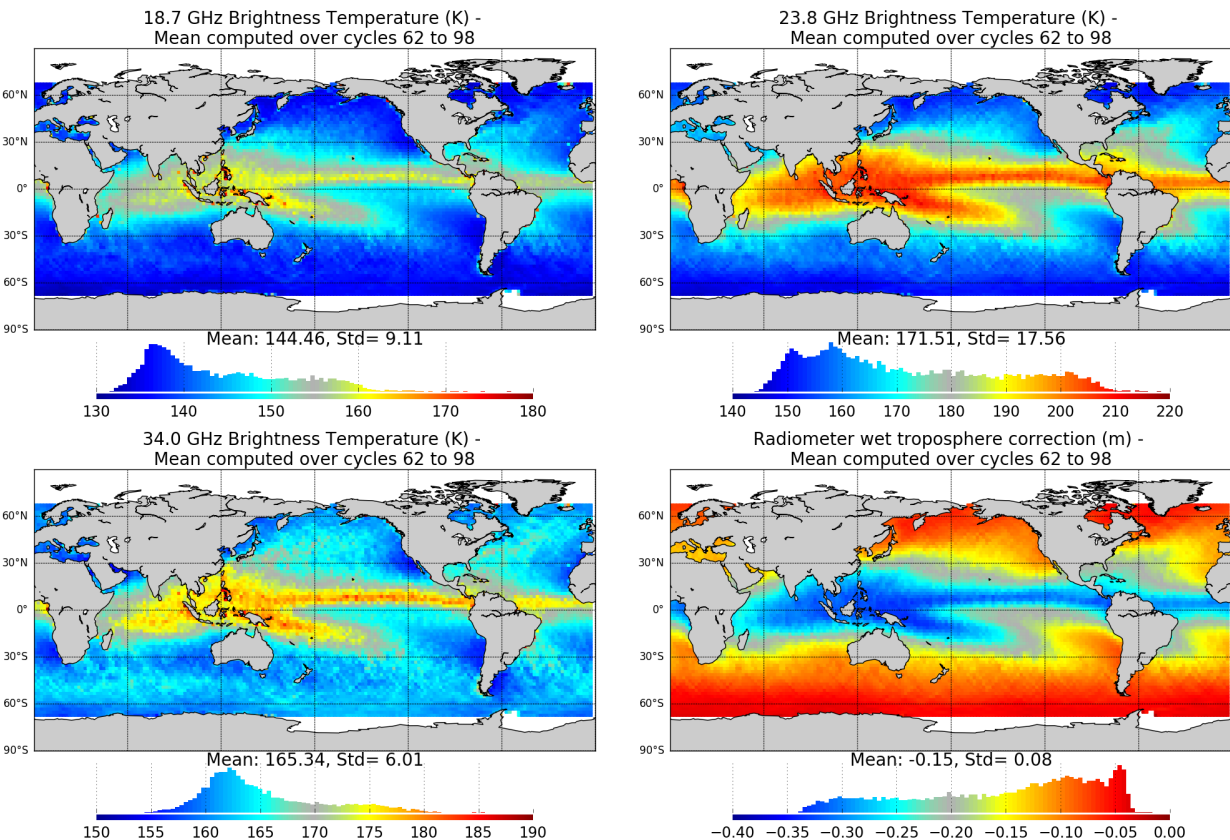


Figure 36 – Map of Jason-3 brightness temperatures averaged over cycles 62 to 98: 18.7 Ghz channel (top left), 23.8 Ghz channel (top right) and 34.0 Ghz channel (bottom left). Map of AMR wet troposphere correction for Jason-3 averaged over cycles 62 to 98 (bottom right)

4.7.2. Comparison with the ECMWF model

The ECMWF wet troposphere correction has been used to check the Jason-2 and Jason-3 radiometer corrections. The cross-comparison between all radiometers and models available is necessary to analyze the stability of each wet troposphere correction. An overview of the wet troposphere correction importance for mean sea level is given in Obligis et al. [84]. The difference between AMR and model data is computed on a daily basis and is plotted on figure 37 for Jason-3 IGDR and GDR, and Jason-2 GDR for comparisons. As observed, Jason-3 AMR correction has a drift of more than half a millimetre per cycle for IGDRs (and OGDRs, not shown). Such behaviour is routinely monitored by JPL instrument expert team. Impact of drift is corrected through ground calibration (ARCS, Autonomous Radiometer Calibration System), also accounting for cold sky calibration. The first ARCS calibration occurred at the end of cycle 17 and is visible on IGDR monitoring. As regards GDR data, AMR radiometer correction is calibrated at each cycle and the calibration coefficients are modified if necessary. It allows to correct the drift for GDR data (red curve on figure 37), nevertheless small drifts and jumps persist of up to 2 mm amplitude.

In GDR, Jason-3 AMR-ECMWF model daily difference is about 6.7 mm and about 5.3 mm for Jason-2. Though Jason-3 radiometer wet troposphere correction is more stable for GDRs, Jason-3 and Jason-2 do not have exactly the same behaviour, with an inflection point around cycle 13 and another one after Jason-2 moved to its new interleaved groundtrack on October 2016. With 2017 Safe Hold Modes, Jason-2 shows some jumps that are known to occur after restart.

Standard deviation of radiometer minus model wet troposphere correction is equivalent around 1.2 cm for both missions (right side of figure 37).

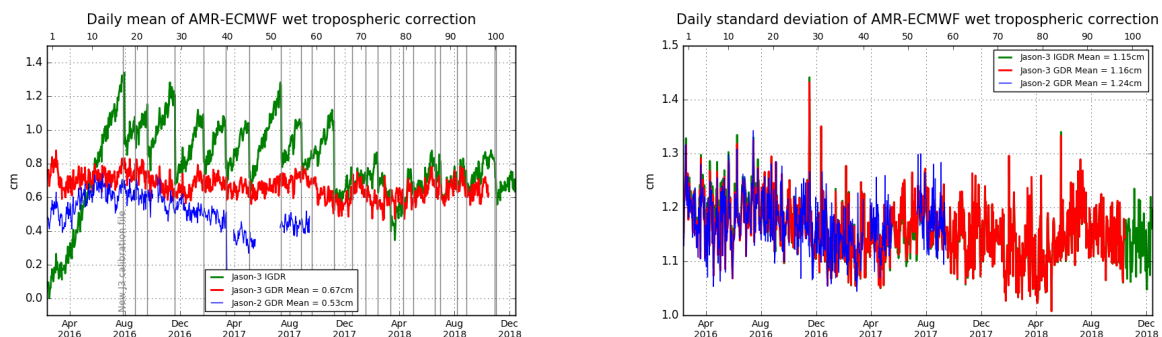


Figure 37 – Daily monitoring of AMR minus ECMWF model wet tropospheric correction. mean (left) and standard deviation (right)

4.8. Altimeter wind speed

Jason-3 and Jason-2 present very close results in terms of wind speed. Jason-2 provides higher wind values than Jason-3 (7.80 vs 7.55 m.s⁻¹, figure 38). The difference between the two missions is 0.25 m.s⁻¹ and can be separated in two phases: before and after GPS upload. The GPS upload occurred on March, 15th 2016 (Cycle 3) and corrected the square off nadir angle, i.e. the mispointing of the platform. Then from the restart of data production (March 18th) mispointing was set to value close to zero, which increases the sigma0 and decreases the wind speed.

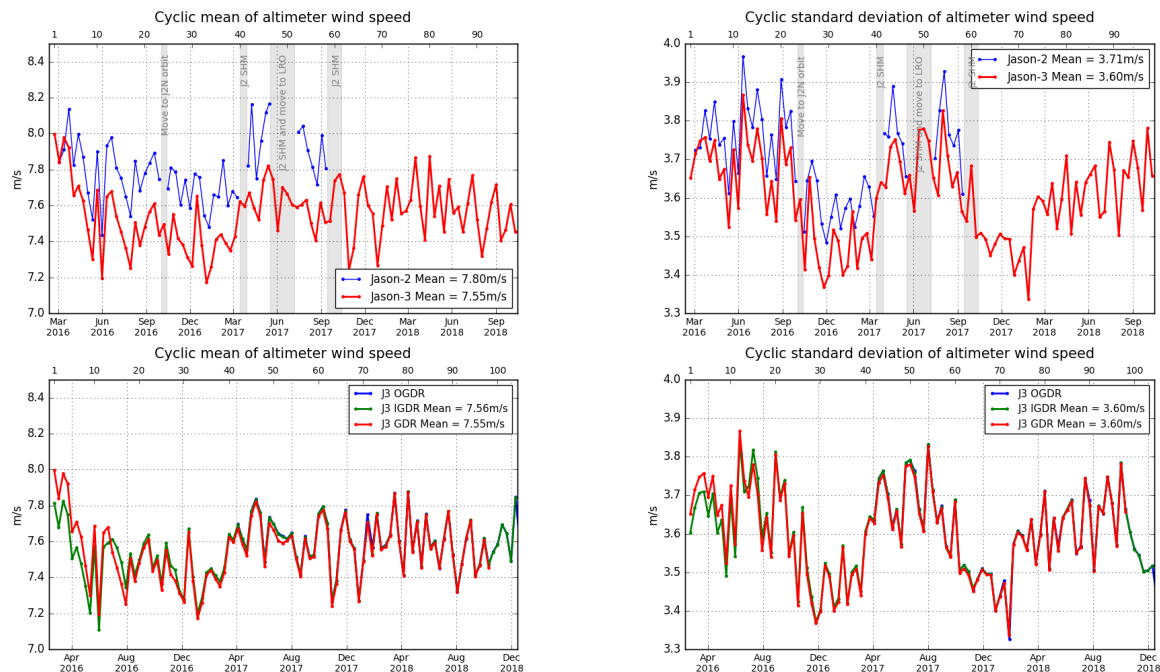


Figure 38 – Cyclic monitoring of altimeter wind speed mean (left) and standard deviation (right). **Top:** for Jason-2 and Jason-3. **Bottom:** for Jason-3 GDR, IGDR and OGDR data.

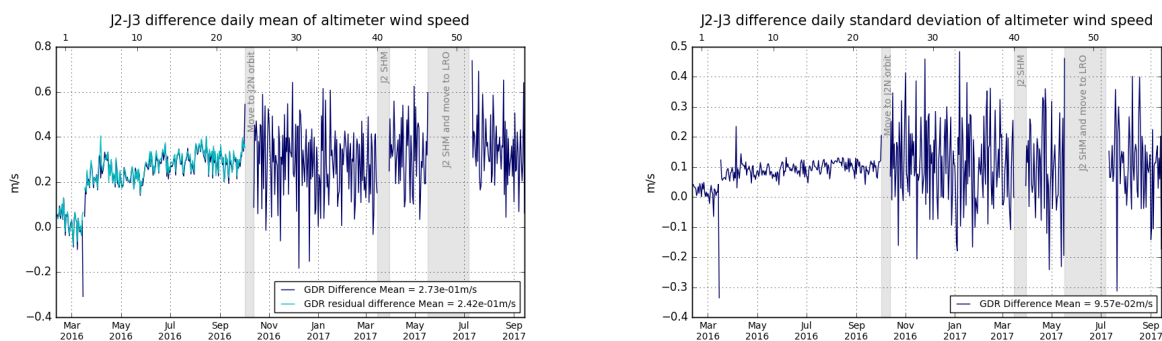


Figure 39 – Jason-2 - Jason-3 difference daily monitoring of altimeter wind speed mean (left) and standard deviation (right).

4.9. Sea state bias

GDR Sea state bias (SSB) in Ku band from Jason-3 (-8.39 cm) and Jason-2 (-8.44 cm) present an excellent agreement both in average and in standard deviation (4.62 cm vs 4.61 cm, respectively).

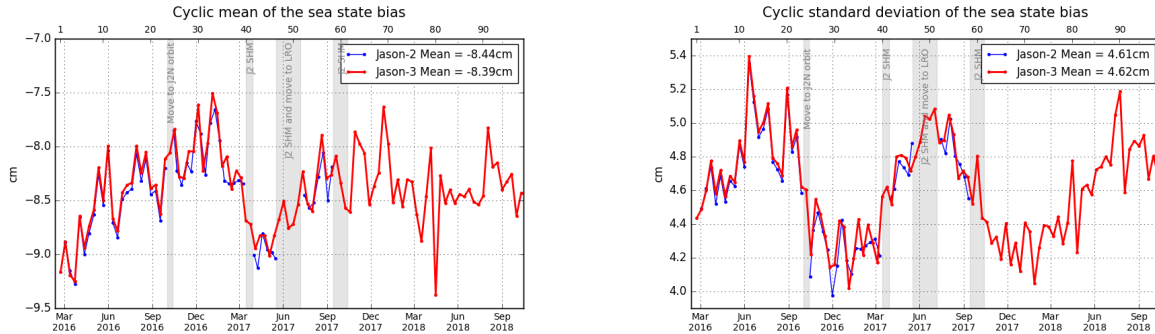


Figure 40 – Cyclic monitoring of the sea state bias mean and standard deviation for Jason-2 and Jason-3

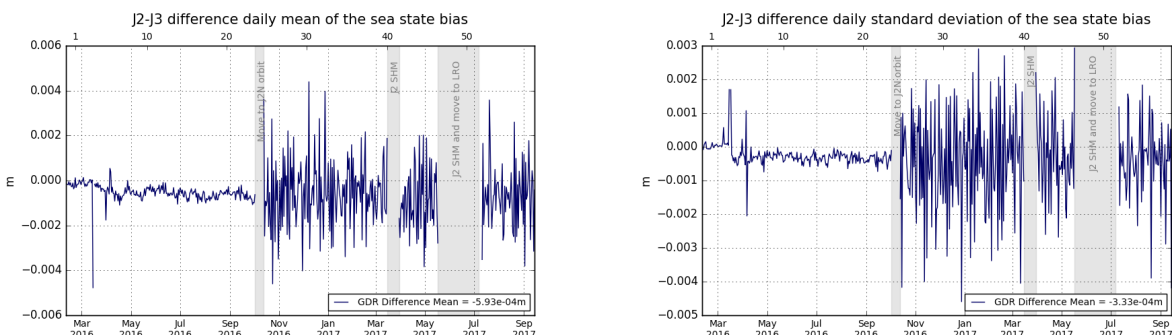


Figure 41 – Jason-2 - Jason-3 difference daily monitoring of the sea state bias mean (left) and standard deviation (right).

Improving the continuity of the Jason SSB time-series (Tran&al. work [120])

Most of the operational versions of the Sea State Bias (SSB) correction are computed empirically with the non parametric estimation technique based on kernel smoothing described in Gaspar et al [2002]. These solutions are derived from 10-day SSH differences (i.e. collinear analysis of repeat cycles of data or from crossover differences). Since only SSB differences are observed, the SSB solution can only be determined to within a constant when solving the equation system. This leads to potentially observe some solution shift related to the imposed constraint to have a SSB value equal to 0 for a flat surface between two versions of the SSB correction. This (constant) shift can reach a few centimeters when the SSB correction version is updated to consider SSH standard changes due to large uncertainty in data-poor region close to (SWH=0, WS=0) to correctly constrain the estimation of SSB(0, 0). This causes annoying disturbances every time that SSB solutions are updated for the monitoring of multi-mission altimeter biases at in-situ Cal/Val sites or for the intermission bias alignment needed to tie up the different global mean sea level time-series together. Tran &al. [120] propose changes in SSB model development to tackle/reduce the SSB constant shift issue that exists between different correction versions for a same altimetric mission or for different missions all operating at a same radar frequency and having the same data processing. The work focused on the Jason altimeters time-series, both Ku-band MLE4 and C-band data, to better connect the past and current missions. Tests with other data have also been performed (Sentinel-3A data) along with update of the 3D

SSB computation approach based on SSH differences data [Tran et al, 2016].

They concluded when the processing of the altimeter data is the same for different missions in Ku-band, the associated SSB solutions computed with the 2018 version of the non-parametric approach display very good agreement at the mm level.

5. SSH crossover analysis

5.1. Overview

SSH crossover differences are the main tool to estimate the whole altimetry system performances. They allow us to analyze the SSH consistency between ascending and descending passes. However in order to reduce the impact of oceanic variability, we select crossovers with a maximum time lag of 10 days. Mean and standard deviation of SSH crossover differences are computed from the valid dataset to perform maps or a cycle by cycle monitoring over all the altimeter period. In order to monitor the performances over stable surfaces, additional editing is applied to remove shallow waters (bathymetry above -1000m), areas of high ocean variability (variability above 20 cm rms) and high latitudes ($> |50|deg$). SSH performances are then always estimated with equivalent conditions. The main SSH calculation for Jason-3 (and Jason-2) are defined below.

$$SSH = Orbit - Altimeter\ Range - \sum_{i=1}^n Correction_i$$

with $Jason - 3\ Orbit = CNES\ orbit$ for GDR products, and

$$\begin{aligned} \sum_{i=1}^n Correction_i &= Dry\ troposphere\ correction \\ &+ Dynamical\ atmospheric\ correction \\ &+ Radiometer\ wet\ troposphere\ correction \\ &+ Dual\ frequency\ ionospheric\ correction \\ &+ Non\ parametric\ sea\ state\ bias\ correction \\ &+ Ocean\ tide\ correction\ (including\ loading\ tide) \\ &+ Earth\ tide\ height \\ &+ Pole\ tide\ height \end{aligned}$$

In this part, performance indicators from IGDR input products or IGDR L2P (used in DUACS system) are presented. L2P updates that are then applied (ocean tide correction, mean sea surface model, mog2d dynamical atmospheric correction) are detailed in [123]. Note that comparisons between Jason-3 and Jason-2 have been done from Jason-3 cycle 1 to 58 only (Jason-2 cycles 281 to 506).

5.2. Mean of SSH crossover differences

The cycle by cycle mean of SSH differences is plotted in figure 42 for Jason-3 for OGDRs, IGDRs and GDRs. Mean of SSH differences at crossovers for Jason-3 IGDR products has noticeable negative values in average (-0.21cm for IGDR versus -0.03cm for GDR). A 120 day signal is visible for Jason-3 data, with a greater amplitude on GDR than IGDR (the investigation part 8.3. is dedicated to this topic.)

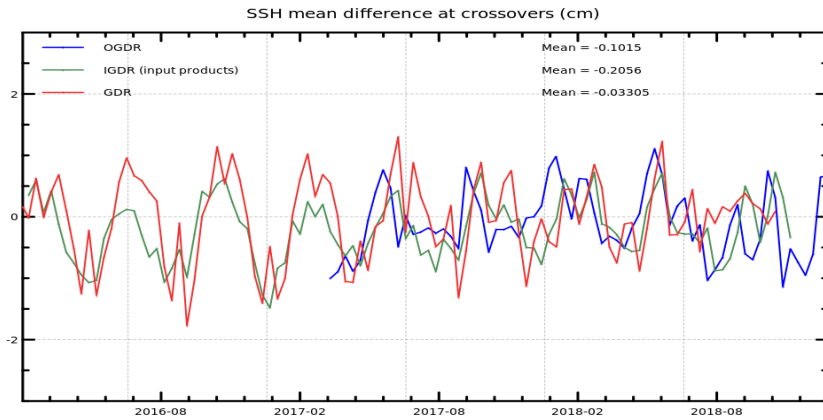


Figure 42 – Monitoring of mean of Jason-3 SSH crossover differences for OGDRs, IGDRs and GDRs. Only data with $|latitude| < 50^\circ$, bathymetry $< -1000m$ and low oceanic variability were selected.

This signal is not visible on Jason-2 GDR (left side of figure 43), but when updating ocean tide solution to FES2014 (right side of figure 43), there is such a signal for both missions. Note that even if FES correction appears to increase the SSH difference between ascending and decending observations, this does not mean that this correction degrades the data quality. This is also detailed in part 8.3..

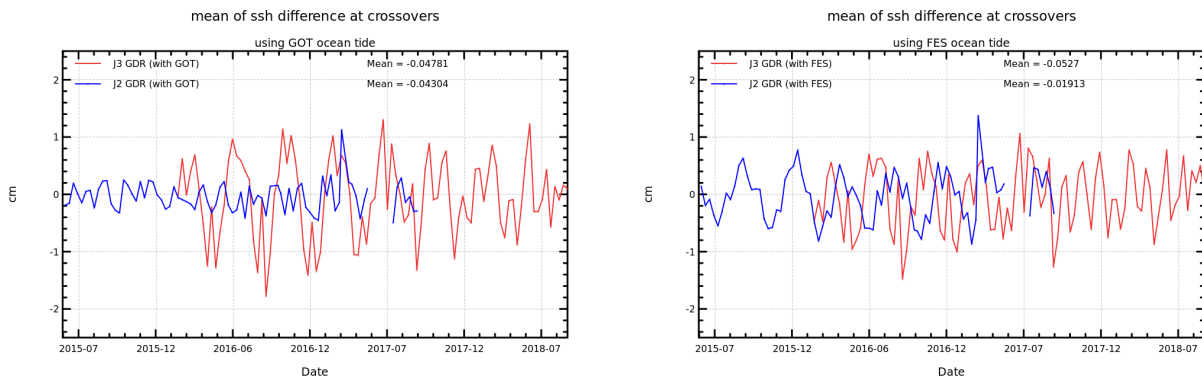


Figure 43 – Monitoring of mean of SSH crossover differences for Jason-2 and Jason-3 for GDRs. Only data with $|latitude| < 50^\circ$, bathymetry $< -1000m$ and low oceanic variability were selected, computed with got ocean tide (left) or fes ocean tide (right)

Investigations were performed during 2018 on this 120 days signal (see part 8.3.): Sea Surface Height is computed using different orbit solutions: CNES POE-E, CNES POE-F, CNES MOE, JPL POE and JPL POE release18a (available for cycles 1 to 94), and several ocean tide solutions are also used: GOT4.8, GOT4.10,

FES14a, FES14b or pure hydrodynamical model FES.

The maps of mean SSH crossover differences on figure 44 were calculated using GDR products for Jason-3 and Jason-2. These maps highlight equivalent small geographic patterns for Jason-3 and Jason-2.

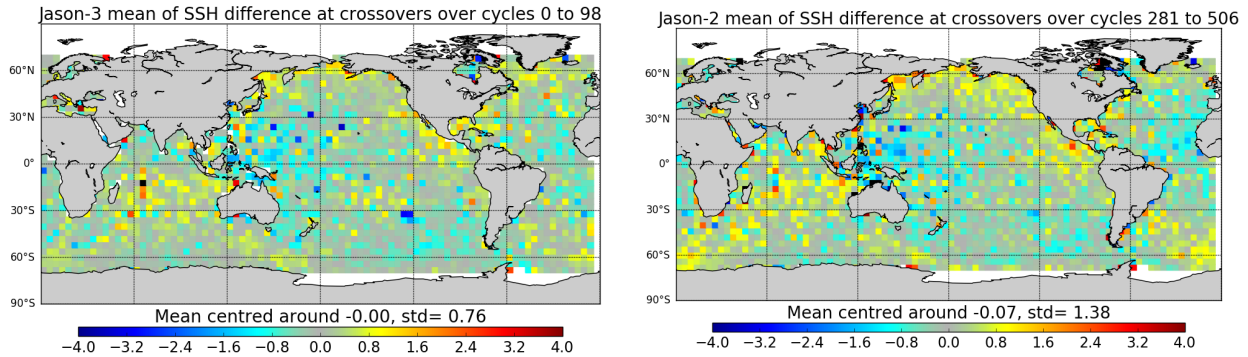


Figure 44 – Map of SSH crossovers differences mean for Jason-3 cycle 0 to 98(left) and for Jason-2 cycle 281 to 506 (right)

Dual-mission crossover performances are computed between Jason-3 and Jason-2 and presented figure 45. Mean SSH differences at Jason 3/Jason 2 crossovers is quite stable and around 3cm in average. The geographical pattern indicates some hemispheric biases, positive to the west, negative to the east. It corresponds to orbital signatures observed on sea surface height (right side of figure 45). Note that these 3 cm are due to processing differences as colocated Jason-2 minus Jason-3 non-corrected SLA (orbit - range - MSS) differences averaged over the period of tandem phase (cycle 001 to 023) shows an equivalent bias (left side of figure 49).

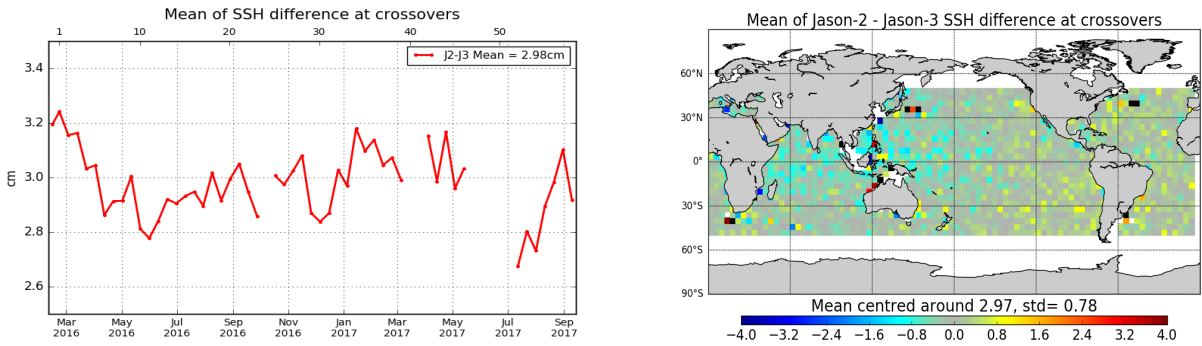


Figure 45 – Cyclic monitoring of Jason-2 - Jason-3 SSH crossover differences mean (left) and map over cycle 1 to 58 (right). Only data with $|latitude| < 50^\circ$, bathymetry $< -1000m$ and low oceanic variability were selected.

5.3. Standard deviation of SSH crossover differences

The cycle by cycle standard deviation of SSH crossovers differences are plotted for Jason-3 and Jason-2 in figure 46 after applying geographical criteria (bathymetry, latitude, oceanic variability). Both missions show very good performances, very similar and stable in time. No anomaly is detected. In GDR, the average figure is equivalent for both missions (4.92 cm rms for Jason-3, and 4.91 cm rms for Jason-2). This metric allows to estimate the system noise by dividing by $\sqrt{2}$ (3.48 cm).

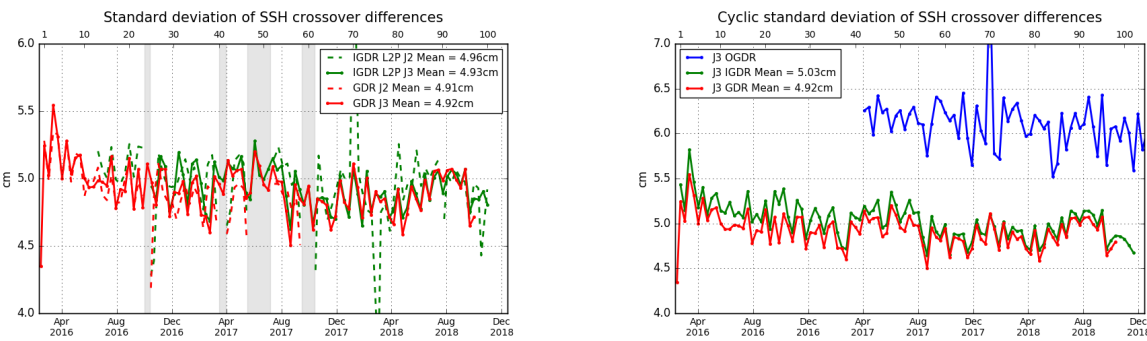


Figure 46 – Cycle by cycle standard deviation of SSH crossover differences for Jason-2 and Jason-3 (left), and for Jason-3 using OGDRs, IGDRs and GDRs (right). Only data with $|latitude| < 50^\circ$, bathymetry $< -1000m$ and low oceanic variability were selected.

5.4. Estimation of pseudo time-tag bias

The pseudo time tag bias (α) is found by computing at SSH crossovers a regression between SSH and orbital altitude rate (\dot{H}), also called satellite radial speed: $SSH = \alpha \dot{H}$.

This empirical method allows us to estimate the potential real time tag bias but it can also absorb other errors correlated with \dot{H} . Therefore it is called “pseudo” time tag bias. The monitoring of this coefficient estimated at each cycle is performed for Jason-2 and Jason-3 in figure 47. Both curves are very similar highlighting an almost 59-day signal with almost no bias (close to -0.04 ms for Jason-3). Both missions present 59 and 117 day signals. However, a near 90-day signal appears for Jason-3: such a signal is not visible for Jason-2.

Using FES2014 ocean tide correction in SSH computation shows a reduction of 59-days signal and no 90-days signal (purple curve).

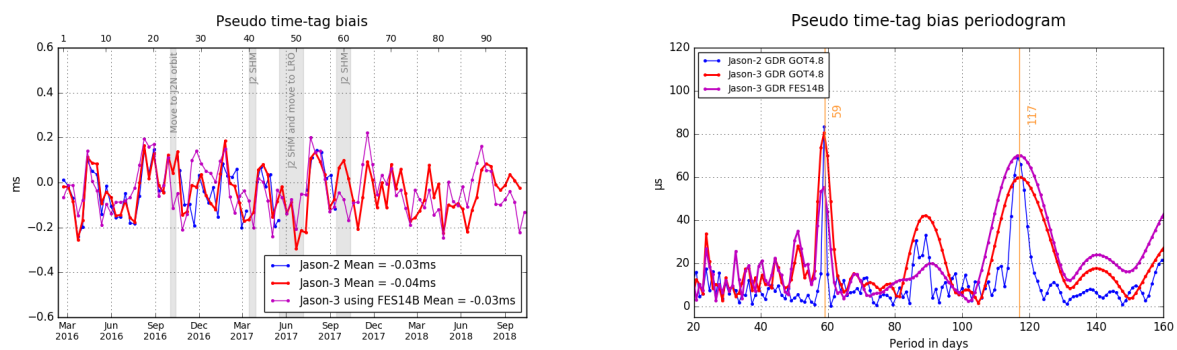


Figure 47 – Monitoring (left) and periodogram (right) of pseudo time-tag bias estimated cycle by cycle from GDR products for Jason-2 and Jason-3

6. Sea Level Anomalies (SLA) Along-track analysis

6.1. Overview

The Sea Level Anomalies (SLA) are computed along track from the subtraction of the mean sea surface to the SSH, with the SSH calculated as defined in previous section 5.1. : $SLA = SSH - MSS$. SLA analysis is a complementary indicator to estimate the altimetry system performances. It allows us to study the evolution of SLA mean (detection of jump, abnormal trend or geographical correlated biases), and also the evolution of the SLA variance highlighting the long-term stability of the altimetry system performances. In order to take advantage of the Jason-3/Jason-2 tandem flight (cycles 1 to 23), we performed direct SLA comparisons between both missions during this period.

6.2. Mean of SLA differences between Jason-3 and Jason-2

The daily monitoring of mean SLA differences between Jason-2 and Jason-3 data over the tandem phase is plotted on figure 48, where this SSH bias is computed with and without the SSH corrections. During this period, both types of curves are very similar and stable in time with variations close to 1 mm rms, except that they are spaced out by a 0.75 cm bias (0.61 cm when using ECMWF model wet troposphere correction). This bias can result from differences between Jason-3 and Jason-2 sea state bias model used, and to a small amount due to ionosphere correction differences. The global average SSH bias is close to 2.98 cm using SSH corrections (2.84 cm when using ECMWF instead of radiometer wet troposphere correction) and 2.23 cm without. However, the more crucial point for scientific applications is to insure that there is no drift between both missions, since the global bias can be corrected a fortiori.

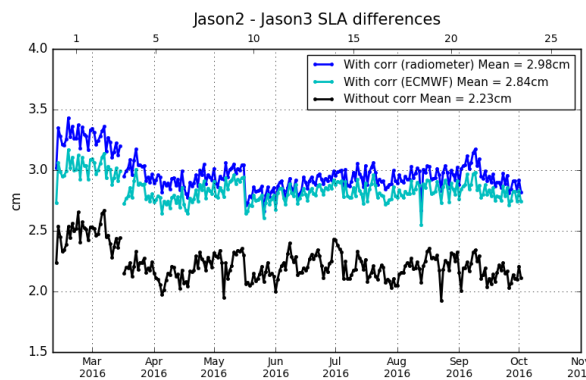


Figure 48 – Daily monitoring of SSH bias between Jason-2 and Jason-3 before Jason-2 moved to interleaved ground-track in October 2016: SSH bias without applying geophysical corrections (**black**) and with corrections using radiometer wet troposphere correction (**blue**) or using ECMWF model wet troposphere correction (**cyan**).

Colocated Jason-2 minus Jason-3 SLA differences averaged over the period of tandem phase (cycle 001 to 023) are shown on left side of figure 49. As both satellites measure the same oceanic features only 1'20" apart, only a weak hemispheric bias is visible (likely due to differences in orbit processing). Since Jason-2 has moved to its new interleaved orbit, maps of direct Jason-2 minus Jason-3 SLA measurements are no longer available. But differences of gridded SLA for Jason-2 and Jason-3 can be made. This difference is quite noisy for one cycle, especially as both satellites are shifted in time and sea state changes especially

in regions of high ocean variability. Therefore figure 49 shows an average over SLA grid differences from Jason-3 cycles 025 to 058. High variability regions as Gulf Stream and Antarctic circumpolar current are visible.

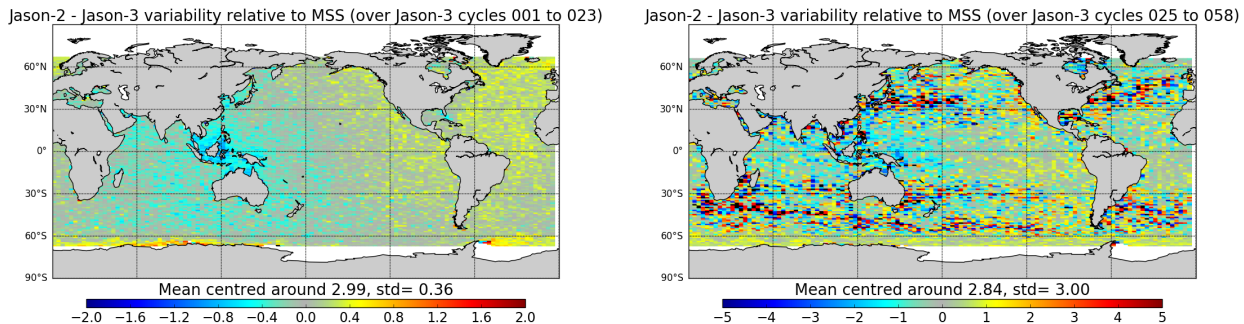


Figure 49 – GDR data. Caution: color map ranges are different between the two figures. Left: Map of SLA difference between Jason-2 and Jason-3 over tandem phase Right: Map of Jason-2 and Jason-3 SLA differences for Jason-3 cycles 025 to 058

6.3. Standard deviation of SLA differences between Jason-3 and Jason-2

The monitoring of SLA standard deviation has been computed for both missions (figure 50).

Note that this metric is very dependant to the MSS reference solution used to compute SLA. Standard deviation of SLA (green curves) from L2P products are lower than with IGDR or GDR thanks to L2P updates that include a change from product MSS referenced on 7 years to a solution referenced on 20 years. In addition, Jason-2 MSS solution in GDR product (red dotted line on right part of figure 50) moved from MSS CNES/CLS 2011 with a 7 years reference to MSS CNES/CLS 2015 (20 years reference) when move to LRO: that explains a better performance on Jason-2 GDR dataset from July 2017 onwards. The change of reference period from 7 years to 20 years integrates the evolution of the sea level in terms of trends, but also in terms of interannual signals at small and large scales (e.g. Niño/Niña) in the additional 13 years: changing from a 7 to 20 years reference period leads to better interannual signals and oceanic anomalies (see [98] for more details about the change on reference period).

Cartography of standard deviation of spatial Jason-3 minus Jason-2 SLA differences (not shown here) does not show any anomaly. It varies indeed in function of noise on measurements, which depends on significant wave height. Therefore, standard deviation of SLA differences is higher in regions with important significant wave heights.

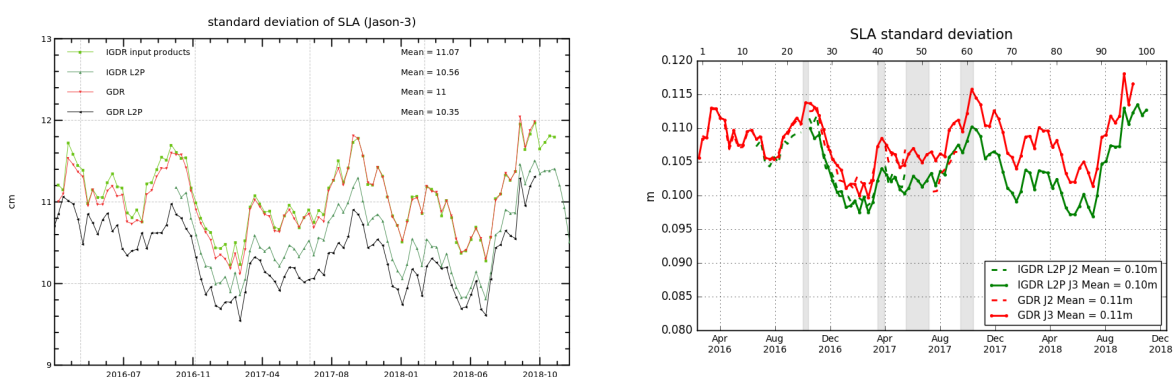


Figure 50 – Cyclic monitoring of along-track SLA standard deviation. Jason-3 OGDRs, IGDRs and GDRs (**left**). Jason-2 and Jason-3 GDRs (**right**)

6.4. Sea level seasonal variations

From Sea Level Anomalies computed relative to the Mean Sea Surface CNES-CLS 2011, the surface topography seasonal variations have been mapped in table 7 for the overall Jason-3 data set. Major oceanic signals are shown clearly by these maps: it allow us to assess the data quality for oceanographic applications.

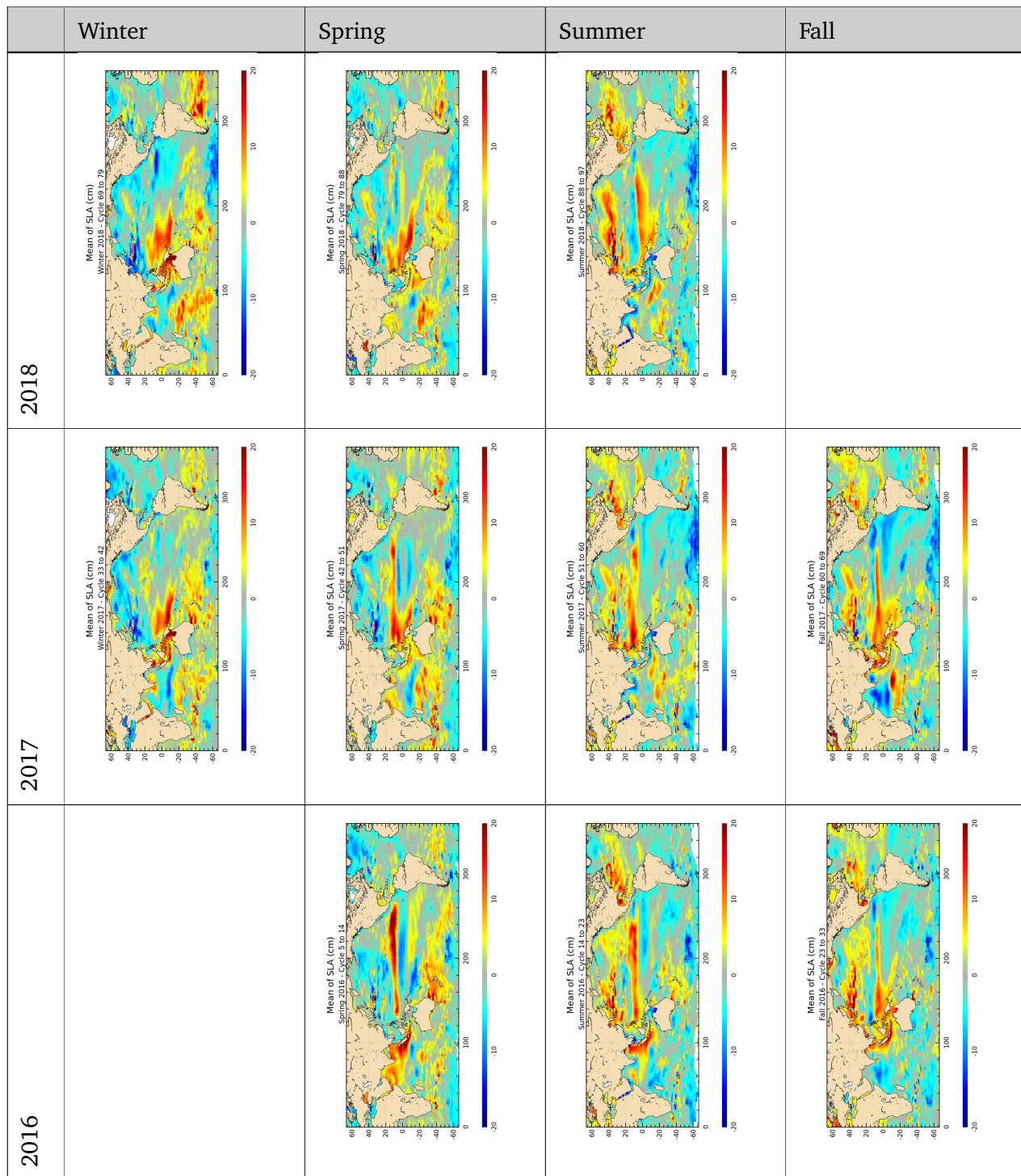


Table 6 – Seasonal variations of Jason SLA (cm) for years 2016 to 2018

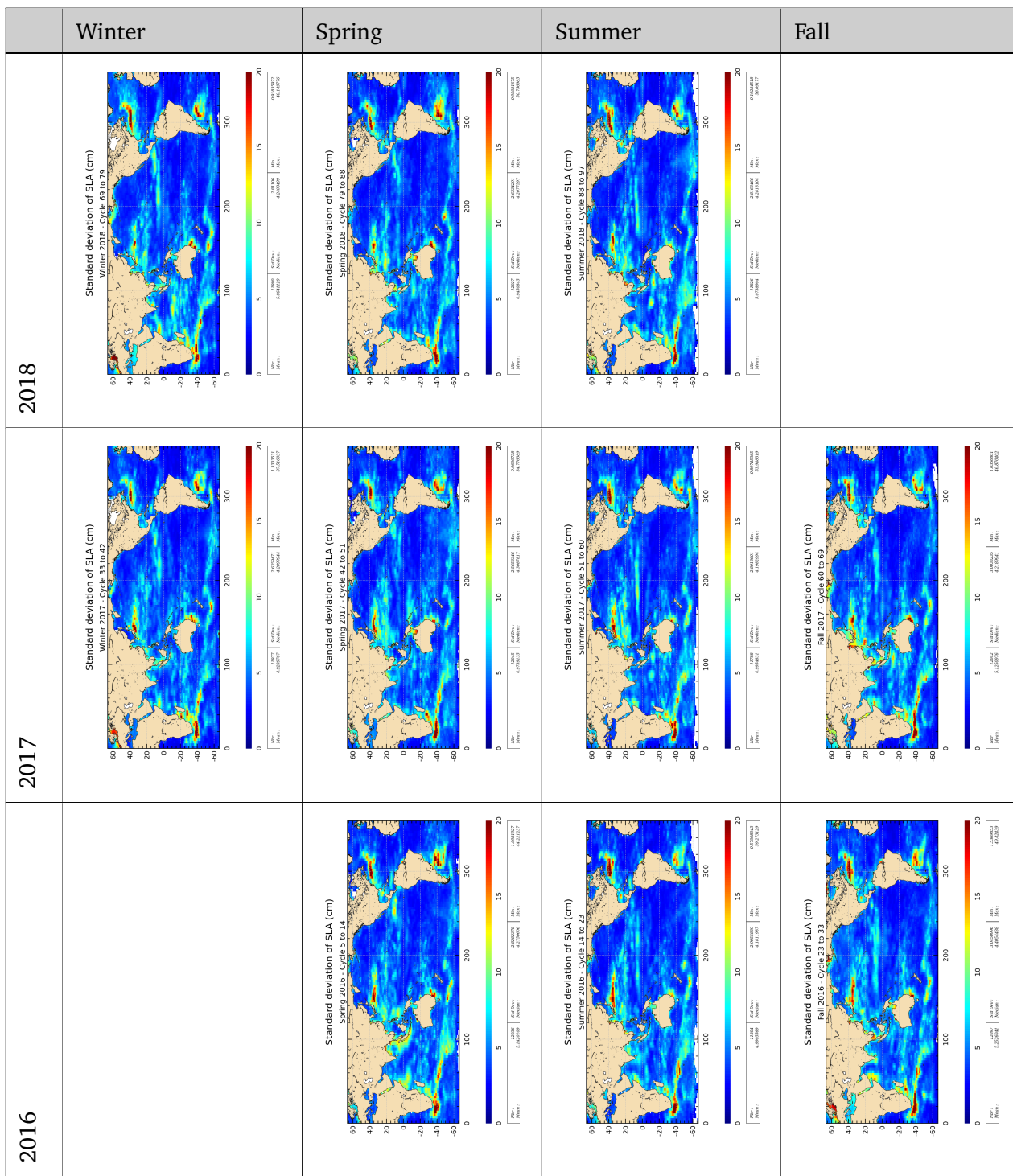


Table 7 – Seasonal variations of Jason SLA standard deviation (cm) for years 2016 to 2018

7. Mean Sea Level (MSL) calculation

For more details about Mean Sea Level studies method, see dedicated annual report of activities [116]. This report includes the description of the Mean Sea Level indicator, the comparisons between altimetry and tide gauges measurements, the comparisons between altimetry and ARGO+GRACE measurements and specific studies linked with MSL activities.

7.1. Mean sea level (MSL) calculation of reference time serie and regional MSL trends

Data from Jason-3 mission were introduced in DUACS system end of September 2016 (when Jason-2 moved to its new interleaved orbit). Over the tandem phase of Jason-3 (till cycle 023), both Jason-2 and Jason-3 satellites flew on the same ground track, only 1mn20s apart. They therefore measured the same features, allowing to calibrate Jason-3. This allowed to link precisely the MSL time series of Jason-2 and Jason-3. The uncertainty of the bias value between the two time series is less than 1 mm. The evolution of the ocean mean sea level can therefore be precisely observed on a continual basis since 1993 thanks to the 4 reference missions: TOPEX/Poseidon, Jason-1 (from may 2002 to october 2008), Jason-2 (from october 2008 to may 2016) and now Jason-3 (since june 2016).

Wet troposphere correction, inverse barometer correction, GIA (-0.3 mm/yr) are applied to calculate the MSL and the data series are linked together accurately thanks to the tandem flying phases. The following global bias are applied: -2.260 cm between T/P&Jason-1, 3.900 cm between Jason-1/Jason-2 and 2.880 cm between Jason-2/Jason-3. An exhaustive overview over possible errors impacting the MSL evolution is given in [116]. Furthermore, annual and semi-annual signals are removed from the time serie and a 2-month filter is applied. For more details, see MSL Aviso Website: <http://www.aviso.altimetry.fr/msl>.

Though mean sea level trend is globally positive, it is inhomogeneous distributed over the ocean: locally, sea level rise or decline up to ± 10 mm/yr are observed on right panel of figure 51 (note that this map of regional MSL trends is estimated from multi-mission grids (Ssalto/DUACS products) in order to improve spatial resolution).

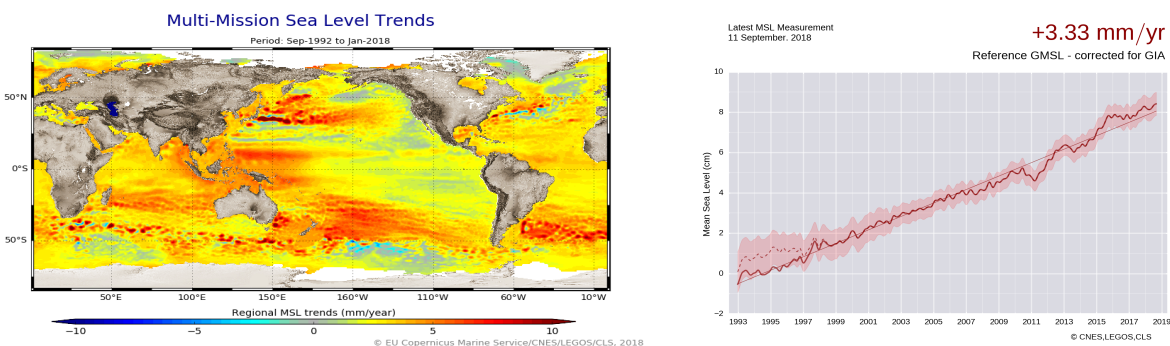


Figure 51 – Global (right) and regional (left) MSL trends from 1993 onwards.

7.2. External data comparisons with tide gauges

In order to assess the global MSL trend, comparisons to independent in-situ datasets are of great interest. Method and data used for MSL comparisons between altimetry and tide gauges measurements are detailed in [116] part 3. Comparisons of MSL time series between altimetry and Tide Gauges are done from L2P products with CMEMS 2018 standards. Compared to 2017 results, slight differences are due to an update of GMSL computation method, thanks to a better understanding of the uncertainties in the satellite GMSL record (see [117]). As concerned Jason-3 comparisons, a positive drift of about $+1.7\text{mm/yr}$ is detected but not reliable due to the short time period used (2.3 years): uncertainty is higher than 3mm/yr over such a short period.

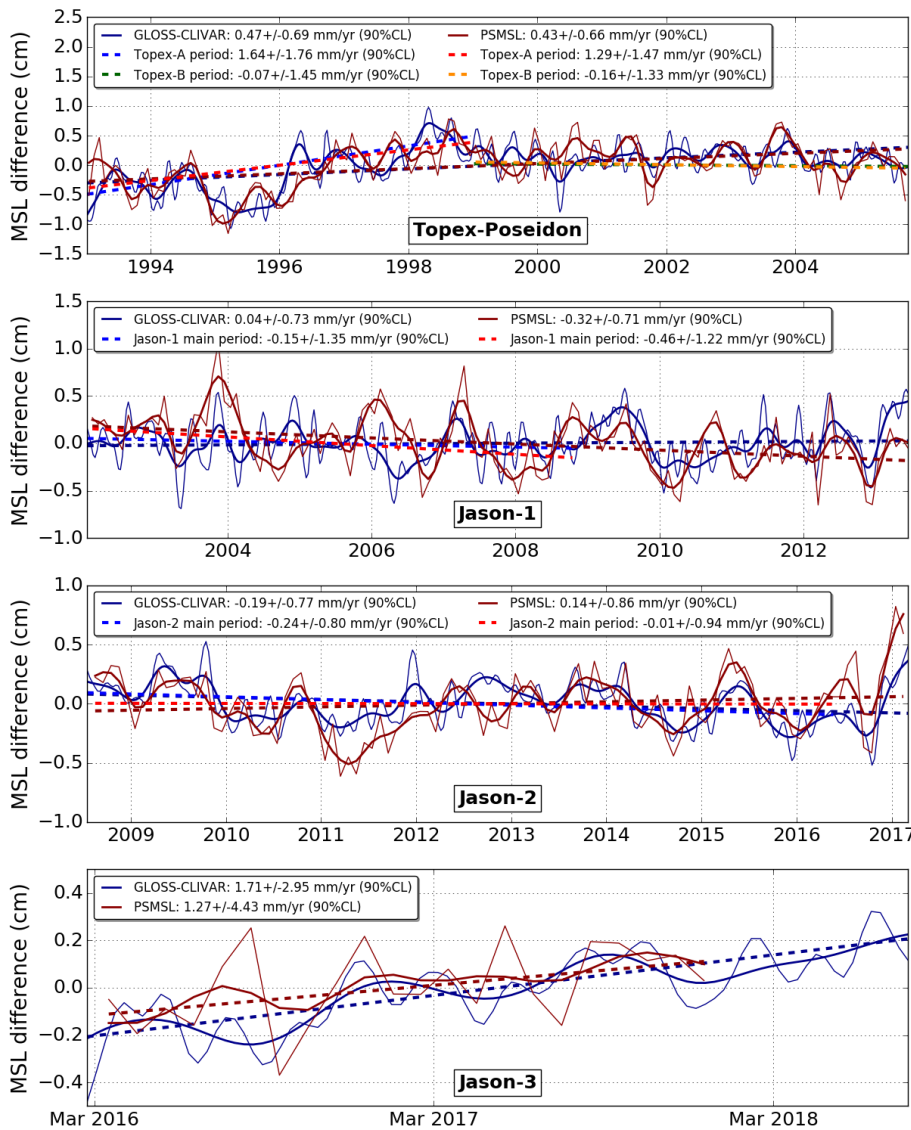


Figure 52 – Evolution of GMSL differences between altimeter and tide gauges for reference missions used in the GMSL indicator calculation (TOPEX/Poseidon, Jason-1, Jason-2 and Jason-3) with the GLOSS/CLIVAR network (blue line) and the PSMSL network (red line). Signal lower than 2 months and annual signals have been removed. The blue dashed line is the trend obtained applying a generalized least square method.

From end of 2016, Jason-3 has become the reference mission for GMSL. Linked to the TOPEX-Poseidon/Jason-1/Jason-2 serie, comparisons are done to the reference missions AVISO GMSL indicator. The MSL differences presented in figure 53 shows a global drift very slightly positive ($< 0.1\text{mm/yr}$) over the full period with an uncertainty of 0.4mm/yr to 0.5mm/yr (against tide gauges network that are used).

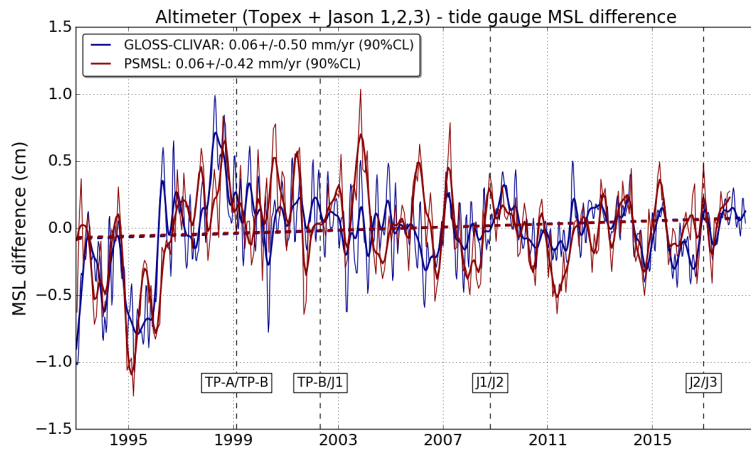


Figure 53 – Evolution of global MSL differences from altimeter / tide gauges comparisons (GLOSS/CLIVAR and PSMSL network) from TOPEX/Poseidon, Jason-1, Jason-2 and Jason-3 L2P products linked together.

8. Particular points and investigations

8.1. Caution about qual_inst_corr_1hz_sig0_ku

The Jason-3 O/I/GDR products provide a quality flag, qual_inst_corr_1hz_sig0_ku, for the Ku-band sigma-0 instrument correction, net_instr_corr_sig0_ku.

This flag is set when net_instr_corr_sig0_ku values exceed a threshold of 1 dB, which was specified at the beginning of the mission. Due to the nominal evolution (aging) of the altimeter's point target response (PTR), the instrument correction values have increased, and now often exceed the 1 dB threshold. When the 1 dB threshold is exceeded the qual_inst_corr_1hz_sig0_ku flag is set (in red on left of the figure 54). On Jason-3 it happened over ocean from cycle 072 onwards. The same behaviour was observed on Jason-2 mission, but from cycle 170 onwards (February 2013). The ageing of both missions is monitored through the evolution of the total PTR power on the right of figure 54.

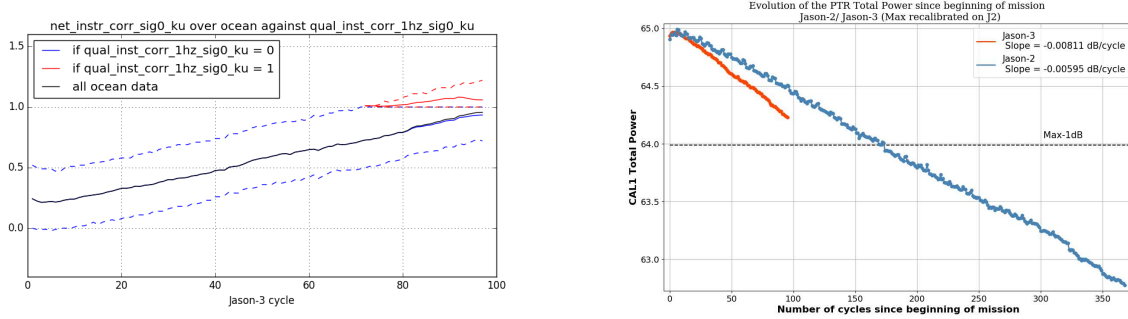


Figure 54 – Left: Jason-3 net_instr_corr_sig0_ku flag. Right: Jason-2 and Jason-3 evolution of PTR power.

Until cycle 71, no ocean data were flagged with this qual_inst_corr_1hz_sig0_ku flag (see cycle 070 on left part of figure 55). From cycle 072 until change in the processing chain, the number of flagged data is increasing over ocean (see cycle 095 on right part of figure 55).

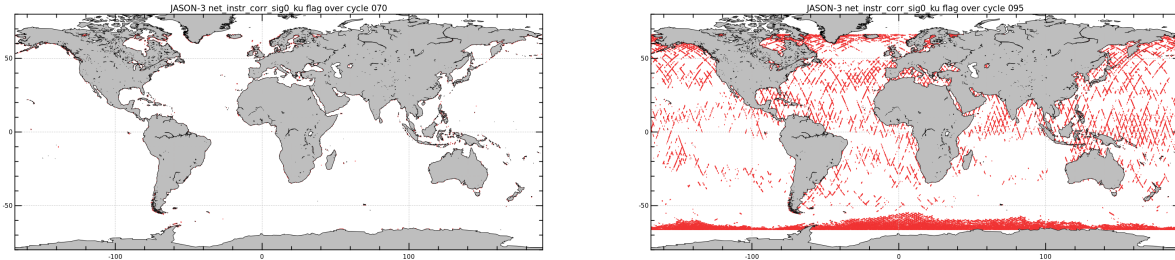


Figure 55 – Jason-3 net_instr_corr_sig0_ku flag over ocean. Left: Jason-3 cycle 070. Right: Jason-3 cycle 095.

Users are advised to ignore this flag during their processing of the Jason-3 products. The quality flag for the Ku-band sigma-0 itself, qual_alt_1hz_sig0.ku, is a sufficient editing criterion. The threshold in the processing chain has been adjusted from cycle 99 onwards, so the flag won't constantly be set.

8.2. Impact of the centering of the echo on sigma0 std

On 31st August 2017 after an DEM (Digital Elevation Model) upload, the echo centering has been updated but some onboard parameters have not been modified. It has a negligible impact on the standard deviation of the backscatter coefficient (small jump on the mean of the sigma0_std parameter, see left of figure 56) but it has no significant impact on performance indicators. On 30th of May 2018 (cycle 085) the correction in onboard parameters has been applied. The echo centering is then back to the same level as at the beginning of the mission. (see figure 56)

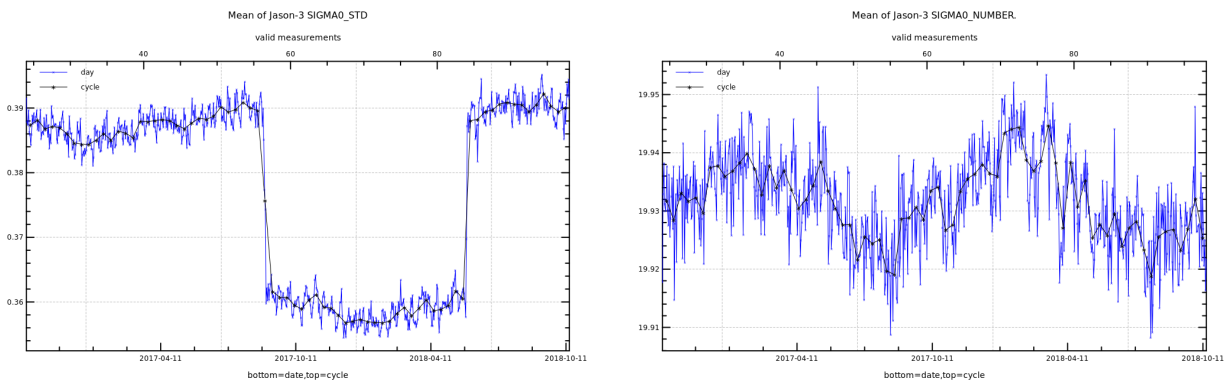


Figure 56 – Left: Mean per day (blue) or per cycle (black) of standard deviation of sigma0 (left) and number of 20Hz measurements used to compute 1Hz sigma0 (right).

8.3. 120 day signal on SSH difference at crossovers

8.3.1. Introduction

Difference of SSH at crossover points is monitored as SSH crossover differences are the main tool to estimate the whole altimetry system performances. They allow us to analyze the SSH consistency between ascending and descending passes. However in order to reduce the impact of oceanic variability, we select crossovers with a maximum time lag of 10 days. Mean and standard deviation of SSH crossover differences are computed from the valid dataset to perform maps or a cycle by cycle monitoring over all the altimeter period. In order to monitor the performances over stable surfaces, additional editing is applied to remove shallow waters (bathymetry above -1000m), areas of high ocean variability (variability above 20 cm rms) and high latitudes ($> |50|deg$). SSH performances are then always estimated with equivalent conditions.

Cyclic monitoring of mean differences at crossover points (with geophysical selection applied to remove shallow waters (bathymetry above -1000m), areas of high ocean variability (variability above 20 cm rms) and high latitudes ($> |50|deg$)) shows on Jason-3 a 120 days signal (see left of figure 57): **a first step of this dedicated study was detailed in [22]**.

This chapter deals with the results of the investigations done on this signal during year 2018.

Please note that until 06/09/2018, (end of Jason-3 cycle 094), POE-E (MOE-E) orbit standard is available in GDR (IGDR) products. From Jason-3 cycle 095 onwards, orbit standard “F” is used for both POE and MOE.

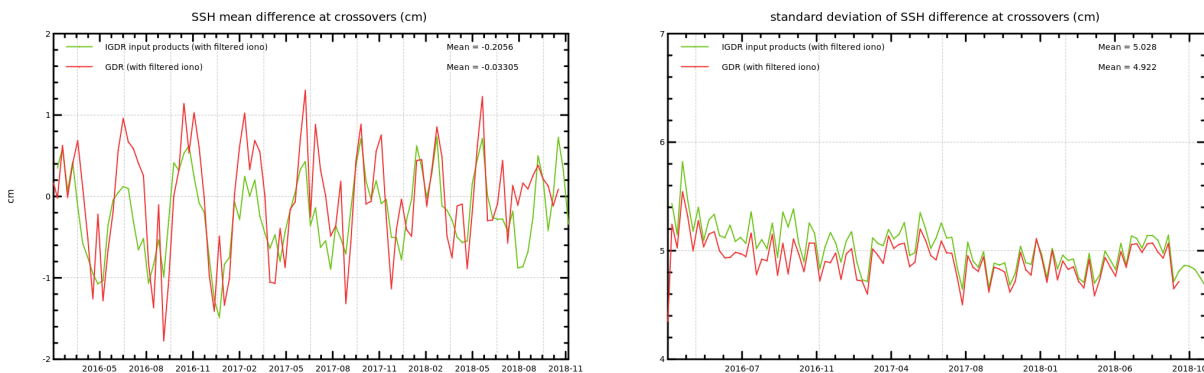


Figure 57 – Mean and standard deviation of SSH difference at crossovers with geographical selection for Jason-3 GDR and IGDR reference data (using ocean tide sol1 = GOT4.8)

Sea Surface Height is here computed using different orbit solutions: **CNES POE-E** **CNES POE-F**, **CNES MOE**, **JPL POE** and **JPL POE release18a** (available for cycles 1 to 94). Several ocean tide solutions are also used: GOT4.8, GOT4.10, FES14a, FES14b or pure hydrodynamical model FES.

8.3.2. Ocean tide solution impact

During this study, several ocean tide solutions are used to compute SSH: GOT4.8, GOT4.10, FES14 (versions A and B), and FES pure hydrodynamic model. As explained by Zawadski and al. in [118], GOT and FES ocean tide models are based on different approaches: GOT is an empirical model based on direct tidal analyses of altimetry measurements, whereas FES is a hydrodynamic model with assimilation of altimetry and in situ data. This suggests that GOT is theoretically more impacted by altimetry errors than FES, depending on the relative weighting between merging altimetry versus fitting hydrodynamics as employed in the FES solutions.

Note that as concerned 120 days signal, results (not shown here) are identical for GOT4.8 and GOT4.10 ocean tide versions (differences are only observed for 60 days signal, see [118] for details about this error). In the same way - about 120 days signal - results are identical for FES14A and FES14B ocean tide versions (not shown here). Finally, the FES pure hydrodynamic model solution leads to equivalent results for 120 days signal as FES14A or FES14B solutions. FES pure hydrodynamic model is totally free from altimetry data assimilation and shows equivalent results to FES14B solution about linked to orbit signals, so that FES model will be used in the following analysis of orbit solution impacts.

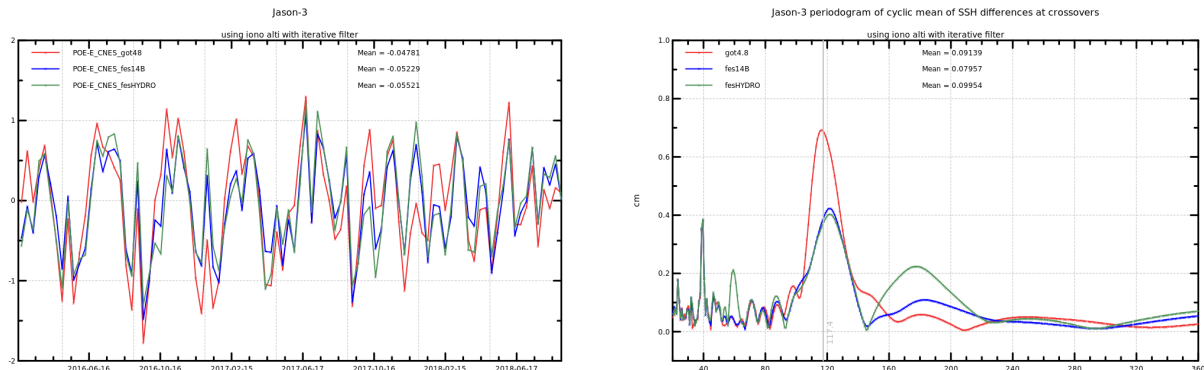


Figure 58 – Periodogram for different orbit solutions using FES pure hydrodynamic model.

8.3.3. Orbit solution impact

A signature on crossover during ‘yaw fix’ time periods is visible using **CNES POE-E** solution. The last standard version (**CNES POE-F** solution) allows to correct this dependance. It is visible on the right part of figure 59 as **red peak (POE-E)** around 40days does not exist on **blue periodogram (POE-F)**.

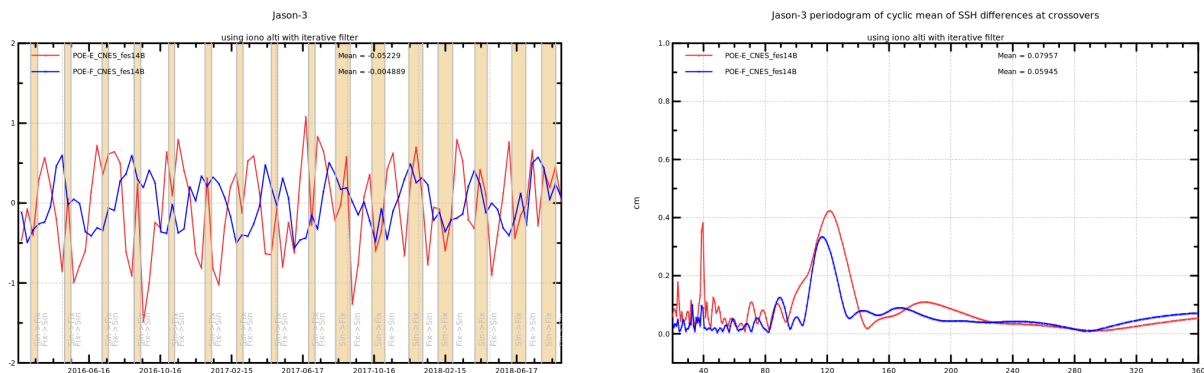


Figure 59 – Yaw fix period impact

In addition, mean difference of SSH at crossovers has also been computed using two different JPL POE solutions (**operational** or **release18a** (available for cycles 1-94)), and **CNES MOE** solution for comparison (see figure 60). The 120 days signal at crossovers answer differs against the orbit solution. The observed signal is reduced using JPL solutions compared to **CNES POE-E**. **CNES POE-F** standard allows to correct dependance to yaw fix periods and 120 days signal is slightly reduced. Note that compared to **CNES POE-E**, the **CNES POE-F** solution takes into account a better way to use GPS data.

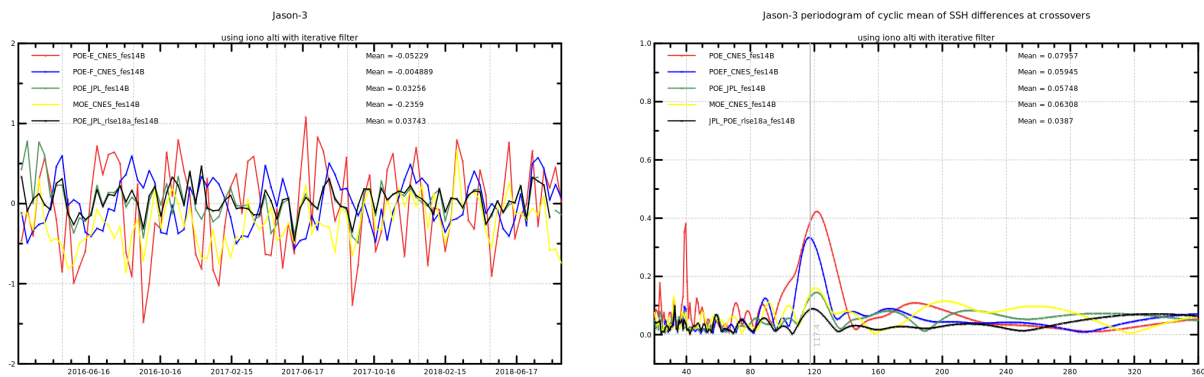


Figure 60 – 120 days signal against orbit solution

8.3.4. Variance at crossovers

Variance of SSH differences at crossovers are compared using different solutions as a key performance indicator. In our cases, a gain of 0.2cm² using CNES POE-F compared to CNES POE-E indicates an improvement with the last solution, with no significant geographically correlated patterns (see figure 61). The variance of SSH differences at crossovers level is equivalent using JPL or CNES POE-F or JPL release18a as differences from each JPL solution to CNES POE-F solution are lower than 0.1cm² (see figure 62).

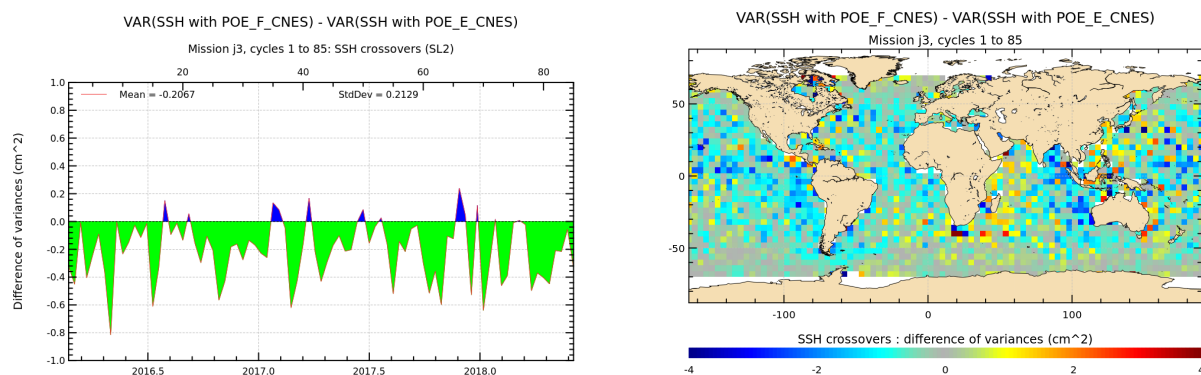
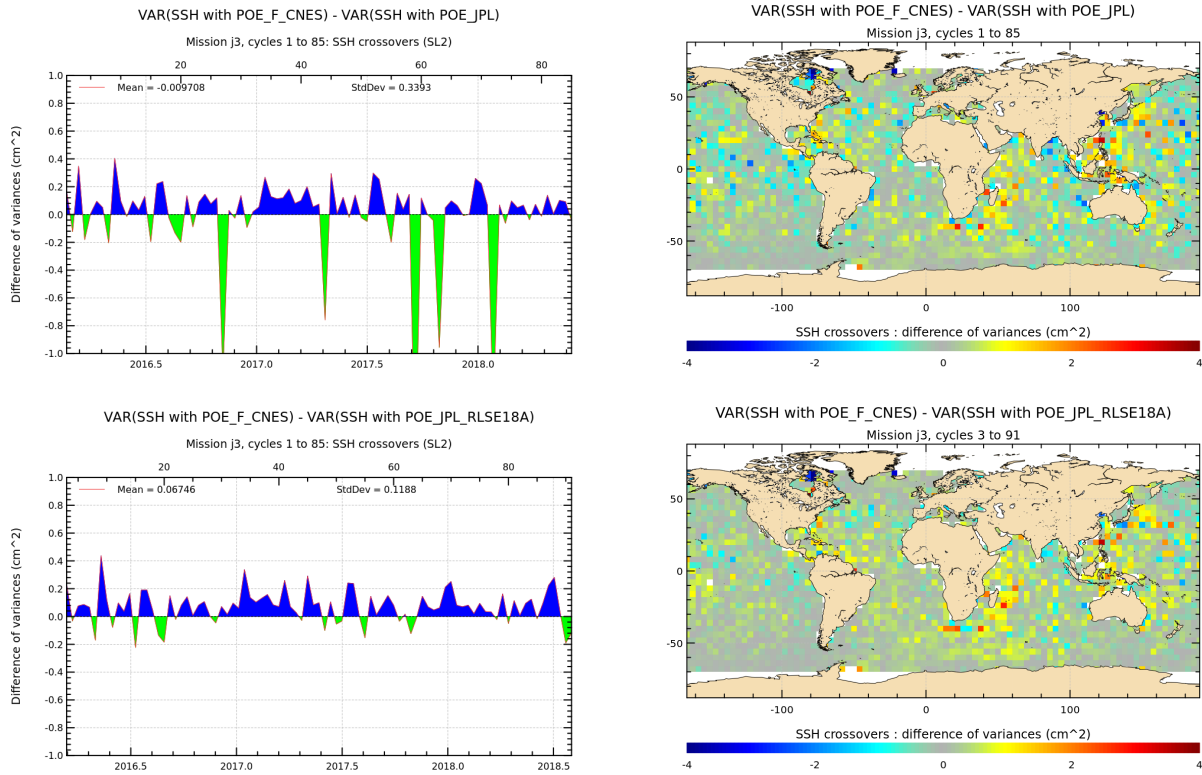


Figure 61 – difference of variance at crossovers between CNES POE-E and CNES POE-F (OceanTide=FES14B, Ionospheric correction=filtered dual-freq. alti)



*Figure 62 – difference of variance at crossovers between CNES POE-F or JPL solutions (OceanTide=FES14B, Ionospheric correction=filtered dual-freq. alti). **top:** with operational JPL POE, **bottom:** with release18a JPL POE*

8.3.5. Impact on SLA along-track

The 120 days signal on mean of differences at crossover points has no impact on along-track SLA trends. It is only due to differences between ascending and descending passes that are averaged taking into account all passes on the global point of vue (as shown on the red curves on the left part of figure 63 for Jason-3 with CNES POE-F orbit solution). This difference of behaviour is visible directly by comparing the two solutions separating odd and even passes: 120 days signal is visible on both, but opposed between ascending and descending passes (see figure 64).

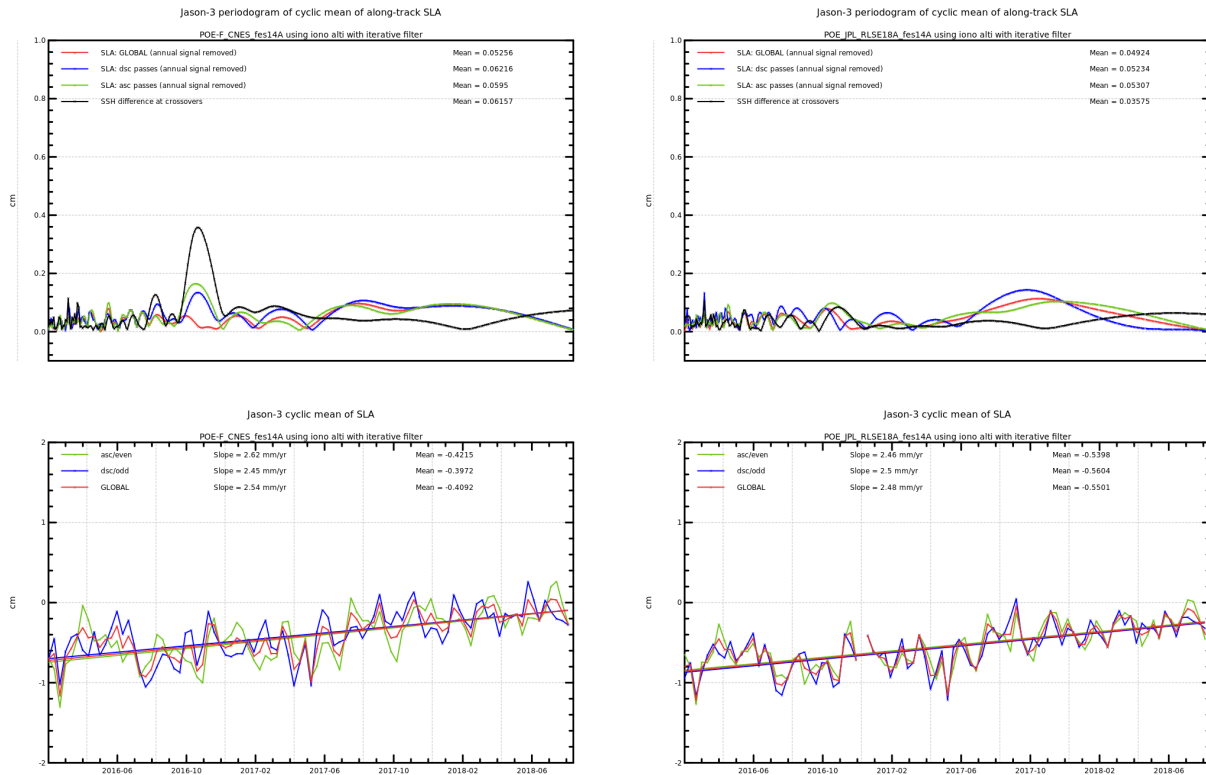


Figure 63 – Top : periodogram of along-track SLA cyclic mean (in green, blue and red - after remove of annual signal) and of cyclic mean of difference at crossovers (black). **Bottom :** along-track SLA cyclic mean (green for ascending passes only, blue for descending passes only and red taking into account all passes) after remove of annual signal - Ocean Tide = FES **Left :** CNES POE-F **Right :** JPL POE release18a

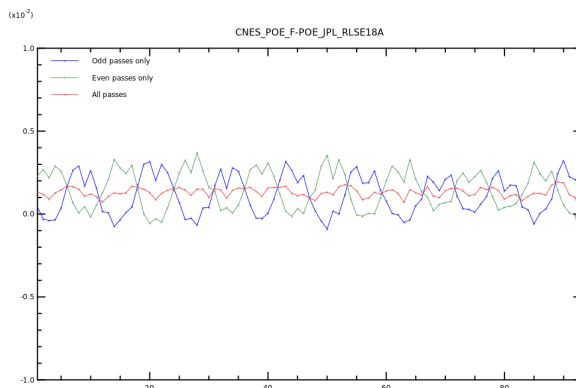


Figure 64 – Difference between CNES POE-F and JPL POE release18a, separating odd and even passes

8.4. Internal tide solution

OSTST community recommended to use internal tide solutions computed by Zaron (see [124]).

In this chapter, altimeter performance indicators are computed with or without taking into account internal tide model as a correction of range. The results presented are computed with Zaron model for M2, K1, O1 and S2 waves. Over Jason-3 period, there is no significant impact on SSH difference at crossover points or on Global Mean Sea Level trend estimation taking into account internal tides or not (not shown here).

Variance of SSH differences at crossovers are compared using different solutions as a key performance indicator. In our cases, a global gain close to 0.5cm² using internal tides compared to SSH without taking into account this correction indicates an improvement (see figure 65), with significant geographically correlated patterns where internal tides areas are defined.

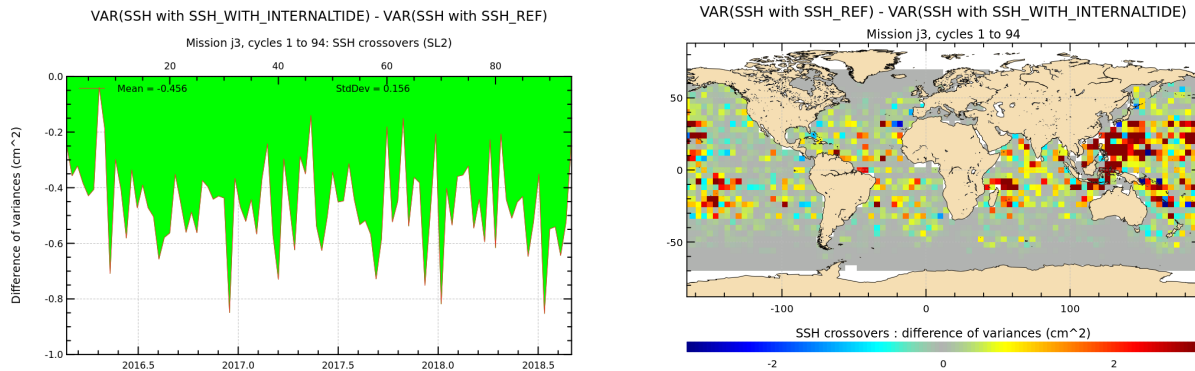


Figure 65 – difference of variance at crossovers for SSH computed with or without internal tide solution

In the same way, a reduction is visible in case of global along-track SLA variance (figure 66), with geographical patterns.

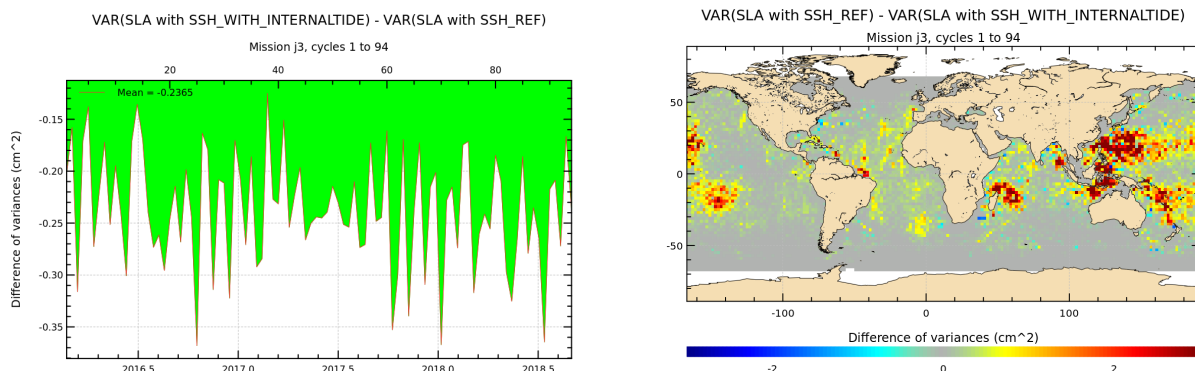


Figure 66 – Difference of variance of along-track SLA for SSH computed with or without internal tide solution

8.5. Pole tide solution

The pole tide altimeter correction is used to correct the response of the solid Earth and Oceans to the polar motion. The Wahr (1985) model has been used for all missions since TOPEX and another model is now available (Desai 2015). Legeais et al. [127] showed the last model has a significant positive impact on the regional mean sea level trends and the comparison with independent in-situ data (Argo profiles) has demonstrated that the use of this model reduces the amplitude of the annual signal of the global mean sea level. A new recommandation for Mean Pole Location equation was done in 2017. This equation has been applied to both Wahr (1985) and Desai (2015) models (see [125] and [126]).

The model for the linear mean pole is recommended based on a linear fit to the IERS C01 time series spanning 1900 to 2015: in milliarcsec, $X_p = 55.0 + 1.677 \cdot dt$ and $Y_p = 320.5 + 3.460 \cdot dt$ where $dt = (t - t_0)$, $t_0 = 2000.0$ and assuming a year = 365.25 days.

The new mean pole location equation has a significant impact on the regional mean sea level trends thanks to the remove of the long term mean pole drift in pole tide computation (see figure 67). The impact on Global Mean Sea Level is negligible (not shown here).

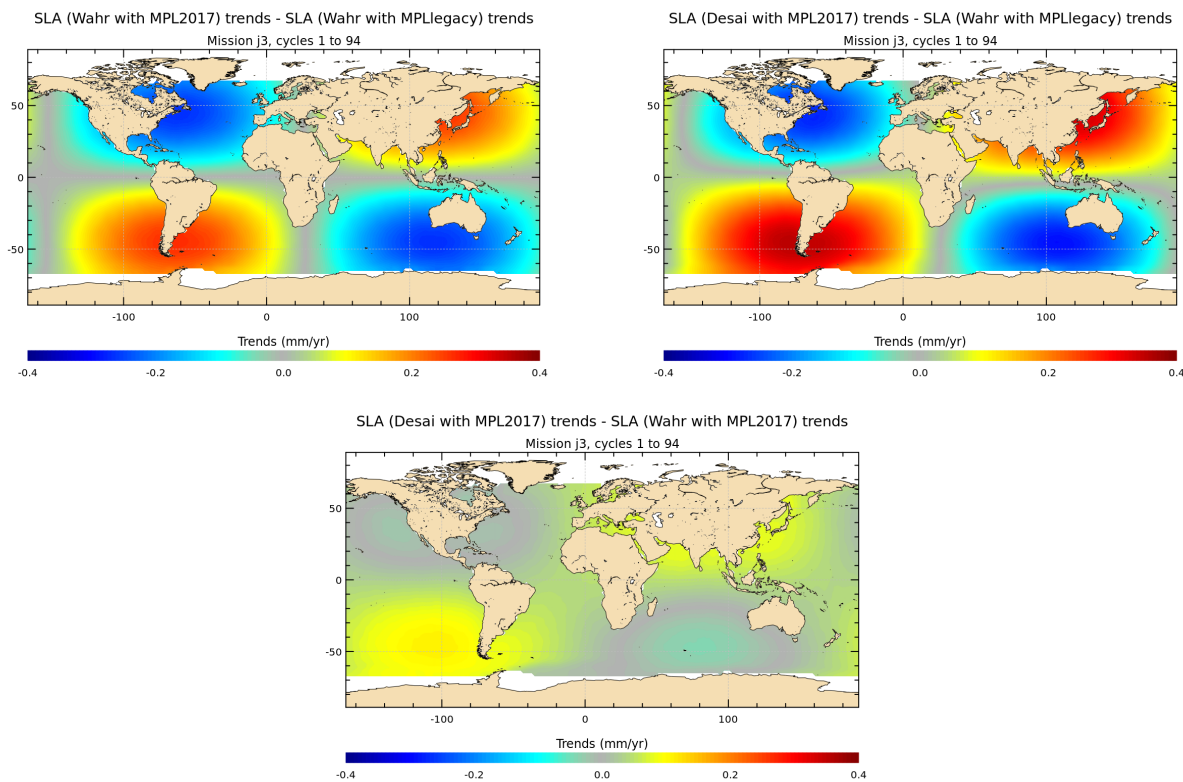


Figure 67 – Difference of trends for : Top left: SLA using Wahr85 with MPL2017 - SLA using GDR (Wahr85 and MPL legacy), Top right: SLA using Desai2015 with MPL2017 - SLA using GDR (Wahr85 and MPL legacy), Bottom: SLA using Wahr85 with MPL2017 - SLA using Desai2015 with MPL2017

9. Conclusion

Jason-3 was launched on January 17th, 2016. Since February 12th, Jason-3 was on its operational orbit following Jason-2 with 80 seconds delay on the same ground track. OGDR/IGDR products were opened to users end of June 2016, whereas the GDR products (GDR-D) were available from November 2016 onwards (NB: GDR-T are also equivalent to GDR-D).

The verification phase allowed extensive analysis and validation of the data, as both satellites observed the same geophysical phenomena until October 2nd 2016 when Jason-2 was moved to its interleaved ground track. This tandem flight phase has shown that Jason-3 data quality is excellent, at least of the same order as the Jason-2 one.

The main points of the performance assessment are summarized below:

- Ocean data availability is excellent and similar between Jason-3 and Jason-2 with a percentage greater than 99.9% after removing specific events.
- Data quality is also very good with only 3.4% of measurements not consistent with altimeter and radiometer parameters threshold criterion. Jason-2 presents an equivalent percentage of edited data.
- The altimetry parameters analysis highlights a similar behaviour compared to Jason-2. Some biases exist as between dual-frequency ionosphere correction, but they are stable.
- At crossovers, Jason-3 shows performance similar to Jason-2 with a standard deviation lower than 5 cm. However mean difference analysis highlights a 120-days signal, which is present for both missions and could be further reduced by alternative orbit solutions.
- At crossovers between Jason-3 and Jason-2, SSH performance presents excellent results with an SLA biais of about 3 cm. The consistency between both SLA is good with a small geographically correlated signal (lower than 0.5 cm in GDR) due to orbit quality.

Thanks to these good results, Jason-3 became the reference mission to ensure the continuity of Global Mean Sea Level monitoring on September 2016.

A future version of GDR including the update of mean sea surface, pole tide, internal tides, ocean tides and sea state bias will allow to significantly improve the quality of Jason-3 products.

9.1. Poster on Global Jason-2 and Jason-3 Performances at OSTST

Global Jason-2 and Jason-3 Performances

H. Roinard¹, L. Michaud¹, S. Labroue¹, N. Picot²

Contact: equipe-calval-jason@cls.fr

1. CLS, Toulouse, France

2. CNES, Toulouse, France

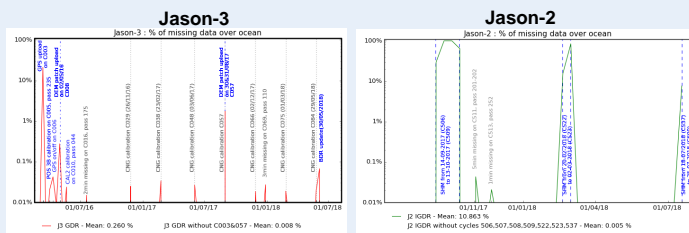


TOPEX/Poseidon, Jason-1, Jason-2, and then Jason-3 have allowed to build a high-precision ocean altimetry data record on historical ground track. Two altimeters of those are still in flight (Jason-2 and Jason-3). Their data are analyzed and monitored in order to assess the quality of the products.

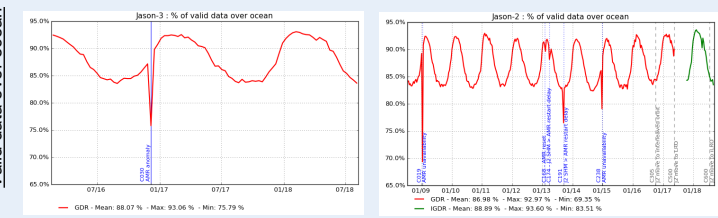
Over the last 2 years many events occurred on Jason-2 mission. A first move of orbit occurred in October 2016 from TOPEX/Jasons historical ground track to the interleaved with Jason-3 one at the same altitude. In July 2017, Jason-2 was moved to a Long Repeat Orbit (LRO), approximately 27 km below the previous orbit still used by Jason-3. At the end of the first Long Repeat Orbit in July 2018, Jason-2 was moved to a new interleaved LRO orbit. Since July 2017, SHM has occurred by three times (in September 2017, February 2018, and July 2018). How are the system performance and data quality affected (or not) by these events?

Since May 17th, 2017, Jason-3 is the only satellite on the TOPEX/Jasons historical ground track. A precise knowledge of Jason-3 data quality and errors is a key activity to ensure a reliable service to scientists involved in climate change studies as well as operational oceanography. We aim at presenting the overall performance of Jason-3 mission through different metrics highlighting the high-level accuracy of this mission.

Data coverage and quality



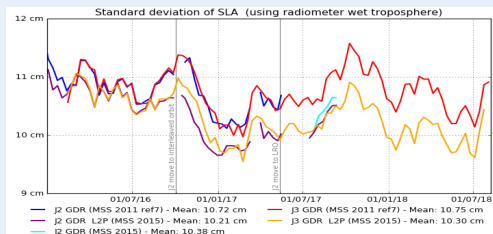
Very good data availability over ocean for both mission : 99.7% for Jason-3 GDR and 89% for Jason-2 IGDR on LRO cycle (including SHM periods)



An annual signal due to ice coverage cycle is visible (~9% of rejected data in average). Out of these rejected points, the editing process removes between 3% and 4% of data when no anomaly.

Level is consistent for Jason-2 over each period (historical ground track, interleaved, then LRO and i-LRO).

Standard deviation of Sea Level Anomaly



CNES/CLS2015 solution significantly improves this performance metric as 20 years of data are used instead of 7 years.

Standard deviation of SLA is 10.7cm in average for both Jason-2 and Jason-3 GDR-D products. This is significantly reduced using more recent MSS solutions.

SLA from current GDR use CNES/CLS2011 ref7 years solution (**J3** and **J2 repetitive**) whereas L2P products contain CNES/CLS2015 solution (**J3** and **J2**).

Note that from Jason-2 move to LRO onwards, MSS solution in operational GDR is CNES/CLS15 (**J2-LRO**),

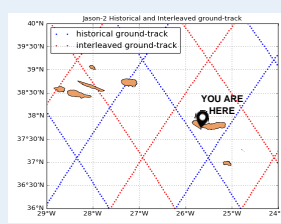
Focus on Jason-2

Topex/Jason historical orbit
C001 → C303
12/07/08 → 02/10/16

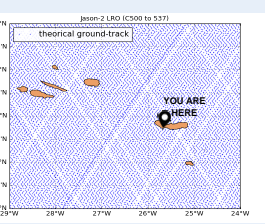
Interleaved orbit
C305 → C327
13/10/16 → 17/05/17

First drifting orbit
C500 → C537
11/07/17 → 18/07/18

Second drifting orbit
C600 → C...
From 25/07/18



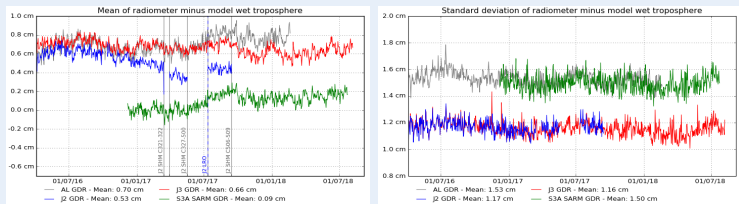
Cycle 001 to 303 Cycle 305 to 327



First LRO, Cycle 500 to 537

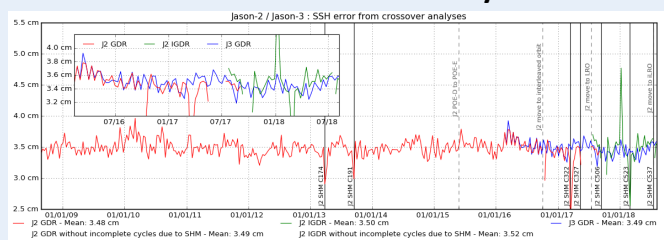
The Jason-2 Long Repeat Orbit is approximately 27 km below the historical T/P orbit still used by Jason-3. The very long repeat cycle yields a fine grid : thanks to 1 year on Long Repeat Orbit, spatial resolution from J2 data is approximately 8-km: it is beneficial for marine geodesy (e.g. improvement of bathymetry and mean sea surface models).

Radiometer behavior



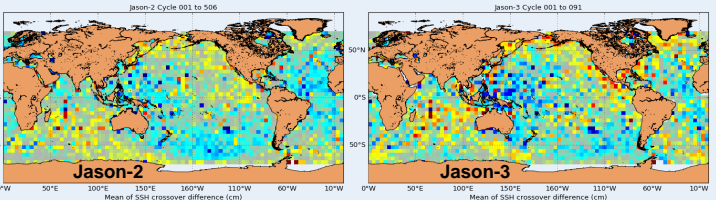
Compared to Jason-3 and AltiKa, Jason-2 radiometer wet troposphere correction minus ECMWF model difference is drifting over the first quarter of year 2017. Also, each SHM on Jason-2 introduces jumps of radiometer minus wet tropospheric correction. Jason-3 and AltiKa behaviors differ from July 2017 onwards. Taking into account standard deviation of this difference, Jason-2 and Jason-3 show similar levels, lower than AltiKa (GDR-C) and Sentinel-3A.

Error from crossovers analysis



Sea Surface Height (SSH) error for Jason-2 and Jason-3 is deduced from crossovers analysis using radiometer data and selecting $| \text{latitudes} | < 50^\circ$, bathy-<1000m, oceanic variability < 20 cm. \Rightarrow SSH error is close to 3.5 cm.

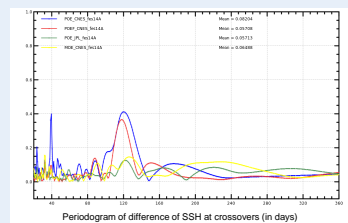
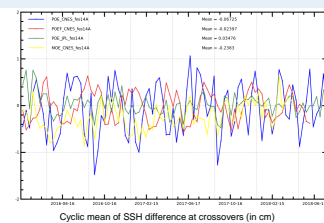
Spatial distribution of mean SSH differences shows geographically correlated patterns with differences remaining below 2 cm.



\Rightarrow Crossovers analysis demonstrates the good performance of both missions Jason-2 and Jason-3.

Focus on Jason-3

Despite the good quality of Jason-3 orbit solution, a 120-days signal remains on Jason-3 SSH differences at crossovers with GDR data. This signal disappear (JPL POE) or is reduced using alternative orbit solutions.
(see dedicated poster on orbit poster session)



Conclusions :

Jason-2 and Jason-3 missions show both excellent performances in terms of data availability and quality.

Jason-2 LRO data quality will allow to improve mean sea surface models out of historical ground track

Thanks to long term stability, Jason-3 is still the reference mission to Global Mean Sea Level (not shown here - <https://www.aviso.altimetry.fr/en/data/products/ocean-indicators-products/mean-sea-level.html>)

10. References

References

- [1] Ablain, M., A. Cazenave, G. Valladeau, and S. Guinehut. 2009 : A new assessment of the error budget of global mean sea level rate estimated by satellite altimetry over 1993-2008. *Ocean Sci*, **5**, 193-201. Available at <http://www.ocean-sci.net/5/193/2009/os-5-193-2009.pdf>
- [2] Ablain, M., S. Philipps, 2006, TOPEX/Poseidon 2005 annual validation report, TOPEX/Poseidon validation activities, 13 years of T/P data (GDR-Ms).
- [3] Ablain, M., S. Philipps, M. Urvoy, N. Tran, and N. Picot (2012) Detection of Long-Term Instabilities on Altimeter Backscattering Coefficient Thanks to Wind Speed Data Comparisons from Altimeters and Models, *Marine Geodesy*, **35:S1**, 258-275. Available at <http://www.tandfonline.com/doi/pdf/10.1080/01490419.2012.718675>
- [4] Ablain, M., G. Larnicol, Y. Faugère, A. Cazenave, B. Meyssignac, N. Picot, J. Benveniste, 2012. Error Characterization of altimetry measurements at Climate Scales. Oral presentation at OSTST meeting, Venice, Italy, 27-28 September 2012. Available at: http://www.aviso.altimetry.fr/fileadmin/documents/OSTST/2012/oral/02_friday_28/04_errors_uncertainties_I/03_EU1_Ablain.pdf
- [5] AVISO and PODAAC User Handbook. IGDR and GDR Jason-1 Products. Edition 4.1, October 2008. SMM-MU-M5-OP-13184-CN (AVISO), JPL D-21352 (PODAAC). Available at http://www.aviso.oceanobs.com/fileadmin/documents/data/tools/hdbk_j1_gdr.pdf.
- [6] Beckley, B. D. , Zelensky, N. P. , Holmes, S. A. , Lemoine, F. G. , Ray, R. D. , Mitchum, G. T. , Desai, S. D. and Brown, S. T. (2010) Assessment of the Jason-2 Extension to the TOPEX/Poseidon, Jason-1 Sea-Surface Height Time Series for Global Mean Sea Level Monitoring, *Marine Geodesy*, **33:1**, 447 - 471. Available at http://pdfserve.informaworld.com/96442_925511460.pdf
- [7] Bertiger, Willy , Desai, Shaile D. , Dorsey, Angie , Haines, Bruce J. , Harvey, Nate , Kuang, Da. , Sibthorpe, Ant and Weiss, Jan P. (2010) Sub-Centimeter Precision Orbit Determination with GPS for Ocean Altimetry. *Marine Geodesy*, **33:1**, 363 - 378. Available at http://pdfserve.informaworld.com/858128_925510150.pdf
- [8] Bertiger, Willy , Desai, Shaile D. , Haines, Bruce J., R. DeCarvalho, and A. Dorsey (2010) Jason-2/OSTM Precision Orbit Determination with GPS *Oral presentation at OSTST meetting, Lisbon, Portugal*, Available at http://www.aviso.oceanobs.com/fileadmin/documents/OSTST/2010/oral/19_Tuesday/bertiger.pdf
- [9] E. Bronner and G. Dibarboire, May 24th, 2012: Technical Note about the Jason-1 Geodetic Mission. *SALP-NT-MA-EA-16267-CNv1.0*. Available at: http://www.aviso.oceanobs.com/fileadmin/documents/data/duacs/Technical_Note_J1_Geodetic_Mission.pdf
- [10] Valladeau, G., S. Philipps. Jason-1 validation and cross calibration activities (Annual report 2009).SALP-RP-MA-EA-21795-CLS, CLS.DOS/NT/10-005.
- [11] Valladeau, G., S. Philipps. Jason-1 validation and cross calibration activities (Annual report 2010).SALP-RP-MA-EA-21903-CLS, CLS.DOS/NT/10-332.

- [12] Roinard H., Philipps S., Ablain M., Valladeau G., and Legeais J.-F., Jason-1 validation and cross calibration activities (Annual report 2013). Reference: CLS.DOS/NT/13-226. Nomenclature: SALP-RP-MA-EA-22269-CLS. Available at http://www.aviso.oceanobs.com/fileadmin/documents/calval/validation_report/J1/annual_report_j1_2013.pdf.
- [13] Roinard H., Philipps S.: Jason-1 GDR-E release. Global assessment over ocean. SALP-RP-MA-EA-22426-CLS. Available at http://www.aviso.altimetry.fr/fileadmin/documents/calval/validation_report/J1/Jason1_ReprocessingReport_GDR_E.pdf
- [14] Philipps, S., M. Ablain, G. Valladeau, and J.-F. Legeais. Jason-2 validation and cross calibration activities (Annual report 2011). Reference: CLS.DOS/NT/12-005. Nomenclature: SALP-RP-MA-EA-22042-CLS. Available at http://www.aviso.oceanobs.com/fileadmin/documents/calval/validation_report/J2/annual_report_j2_2011.pdf.
- [15] Philipps, S., M. Ablain, G. Valladeau, and J.-F. Legeais. Jason-2 validation and cross calibration activities (Annual report 2012). Reference: CLS.DOS/NT/12-223. Nomenclature: SALP-RP-MA-EA-22141-CLS. Available at http://www.aviso.oceanobs.com/fileadmin/documents/calval/validation_report/J2/annual_report_j2_2012.pdf.
- [16] Roinard, H., Philipps S., Jason-2 reprocessing impact on ocean data (cycles 001 to 020). Comparison of Jason-2 Gdr-D with Gdr-T, as well as with Jason-1 Gdr-C. SALP-RP-MA-EA-22118-CLS. CLS.DOS/NT/12.138. Available at ftp://avisoftp.cnes.fr/AVISO/pub/jason-2/documentation/gdr_d_calval_report/JA2_GDR_D_validation_report_cycles1to20_V1_1.pdf
- [17] Roinard, H., S. Philipps. Jason-2 reprocessing impact on ocean data (cycles 001 to 145). Comparison of Jason-2 Gdr-D with Gdr-T, as well as with Jason-1 Gdr-C and Envisat Gdr v2.1. SALP-RP-MA-EA-22140-CLS. CLS.DOS/NT/12.222.
- [18] Philipps, S., H. Roinard, M. Ablain, G. Valladeau, and J.-F. Legeais. Jason-2 validation and cross calibration activities (Annual report 2013). Reference: CLS.DOS/NT/13-227. Nomenclature: SALP-RP-MA-EA-22270-CLS. Available at http://www.aviso.oceanobs.com/fileadmin/documents/calval/validation_report/J2/annual_report_j2_2013.pdf.
- [19] Philipps, S., H. Roinard, M. Ablain, G. Valladeau, and J.-F. Legeais. Jason-2 validation and cross calibration activities (Annual report 2014).
- [20] Philipps, S., H. Roinard, M. Ablain, G. Valladeau, and J.-F. Legeais. Jason-2 validation and cross calibration activities (Annual report 2015).
- [21] Lauret O. Jason-3 validation and cross calibration activities (Annual report 2016). SALP-RP-MA-EA-23060-CLS.
- [22] Roinard H.. Jason-3 validation and cross calibration activities (Annual report 2017). SALP-RP-MA-EA-23187-CLS. https://www.aviso.altimetry.fr/fileadmin/documents/calval/validation_report/J3/SALP-RP-MA-EA-23187-CLS_Jason-3_AnnualReport2017_v1-2.pdf
- [23] Roinard H.. Jason-3 validation and cross calibration activities (Annual report 2018). SALP-RP-MA-EA-23248-CLS.
- [24] Ollivier A., M. Guibbaud. Envisat RA2/MWR ocean data validation and cross-calibration activities. Yearly report 2012. SALP-RP-MA-EA-22163-CLS, CLS.DOS/NT/12-292.
- [25] A. Ollivier. M. Guibbaud. Envisat RA2/MWR ocean data validation and cross calibration activities (Yearly report 2013). Reference: CLS.DOS/NT/13-290. Nomenclature: SALP-RP-MA-EA-22293-CLS.

-
- [26] M. Guibbaud. A. Ollivier. Envisat RA2/MWR ocean data validation and cross calibration activities (Yearly report 2014). Reference: CLS.DOS/NT/14-253. Nomenclature: SALP-RP-MA-EA-22396-CLS.
- [27] S. Philipps. Saral/AltiKa validation and cross calibration activities (Annual report 2013). Reference: CLS.DOS/NT/13-228. Nomenclature: SALP-RP-MA-EA-22271-CLS.
- [28] P. Prandi. Saral/AltiKa validation and cross calibration activities (Annual report 2014). Reference: CLS.DOS/NT/14-234. Nomenclature: SALP-RP-MA-EA-22418-CLS.
- [29] P. Prandi. Saral/AltiKa validation and cross calibration activities (Annual report 2015). Reference: CLS.DOS/NT/15-064. Nomenclature: SALP-RP-MA-EA-22957-CLS.
- [30] P. Prandi. Saral/AltiKa validation and cross calibration activities (Annual report 2016). Nomenclature: SALP-RP-MA-EA-23073-CLS.
- [31] G. Jettou. Saral/AltiKa validation and cross calibration activities (Annual report 2017). Nomenclature: SALP-RP-MA-EA-23188-CLS.
- [32] A. Ollivier Yearly report 2017 as parts as SALP activities (Annual report 2017).
- [33] Valladeau, G.. Validation of altimetric data by comparison with tide gauge measurements for TOPEX/Poseidon, Jason-1, Jason-2 and Envisat. SALP-NT-MA-EA-22157-CLS, CLS.DOS/NT/12-259.
- [34] Legeais J.-F. and S. Dupuy. 2012 annual report: Validation of altimeter data by comparison with in-situ T/S Argo profiles for T/P, Jason-1, Jason-2 and Envisat missions. CLS-DOS/NT/12-261. SALP-RP-MA-EA-22176-CLS.
- [35] Valladeau G. and Prandi P., 2013:Validation of altimeter data by comparison with tide gauge measurements for TOPEX/Poseidon, Jason-1, Jason-2 and Envisat (Annual report 2013). [CLS.DOS/NT/13-262].
- [36] Legeais J.F. and Ablain M., 2013: Validation of altimetric data by comparison with in-situ T/S Argo profiles (Annual Report 2013) [SALP-RP-MA-EA-22281-CLS, CLS.DOS/NT/13-256]
- [37] Prandi P., Valladeau G., 2014:Validation of altimeter data by comparison with tide gauge measurements for TOPEX/Poseidon, Jason-1, Jason-2 and Envisat (Annual report 2014). [SALP-RP-MA-EA-22419-CLS, CLS.DOS/NT/15-020].
- [38] Prandi P., Legeais J.F. and Ablain M., 2014: Validation of altimetric data by comparison with in-situ T/S Argo profiles (Annual Report 2014) [SALP-RP-MA-EA-22406-CLS, CLS.DOS/NT/15-007]
- [39] Prandi P., Valladeau G., 2015:Validation of altimeter data by comparison with tide gauge measurements for TOPEX/Poseidon, Jason-1, Jason-2 and Envisat (Annual report 2015). [SALP-RP-MA-EA-22956-CLS, CLS.DOS/NT/15-062].
- [40] Prandi P., Legeais J.F. and Ablain M., 2015: Validation of altimetric data by comparison with in-situ T/S Argo profiles (Annual Report 2015) [SALP-RP-MA-EA-22966-CLS, CLS.DOS/NT/15-068]
- [41] Prandi P., Debout V.: Validation of altimeter data by comparison with tide gauges measurements: yearly report 2016 for TOPEX/Poseidon, Jason-1, Jason-2, ERS-2, Envisat and SARAL/AltiKa. SALP-RP-MA-EA-23082-CLS.
- [42] Zawadzski L., Taburet N.: Validation of altimeter data by comparison with in-situ T/S Argo profiles (Annual Report 2016). SALP-RP-MA-EA-22966-CLS.

- [43] Valladeau, G., J.F. Legeais, M. Ablain, S. Guinehut, and N. Picot, 2012: Comparing altimetry with tide gauges and Argo profiling floats for data quality assessment and Mean Sea Level studies. *Marine Geodesy* 2012, DOI: 10.1080/01490419.2012.718226.
- [44] Legeais J.-F., P. Prandi, M. Ablain and S. Guinehut: Analyses of altimetry errors using Argo and GRACE data. *Ocean Science Discussion*, doi:10.5194/os-2015-111, in review, 2016.
- [45] Bond, N. A., M. F. Cronin, H. Freeland, and N. Mantua (2015), Causes and impacts of the 2014 warm anomaly in the NE Pacific. *Geophys. Res. Lett.*, 42, 3414–3420. doi: 10.1002/2015GL063306.
- [46] Boening, C., J. K. Willis, F. W. Landerer, R. S. Nerem, and J. Fasullo (2012), The 2011 La Niña: So Strong, the Oceans Fell, *Geophys. Res. Lett.*, doi:10.1029/2012GL053055, in press.
- [47] John T. Fasullo , C. Boening, F. W. Landerer, R. S. Nerem (2013), Australia's Unique Influence on Global Sea Level in 2010-2011, doi:10.1002/grl.50834, in press.
- [48] Boy, François and Jean-Damien Desjonquieres. 2010. Note technique datation de l'instant de reflexion des échos altimètres pour POSEIDON2 et POSEIDON3 Reference: TP3-JPOS3-NT-1616-CNES
- [49] Brown G.S., “The average impulse response of a rough surface and its application”, *IEEE Transactions on Antenna and Propagation*, Vol. AP 25, N1, pp. 67-74, Jan. 1977.
- [50] Brown S., S. Desai, and W. Lu “Initial on-orbit performance assessment of the advanced microwave radiometer and performance of JMR GDR-C”, *Oral presentation at OSTST meeting, Nice, France, 9-12 november 2008*. Available at http://www.aviso.oceanobs.com/fileadmin/documents/OSTST/2008/oral/brown_calval.pdf
- [51] Brown, S., S. Desai, W. Lu, and A. Sibthorpe. 2009. Performance Assessment of the Advanced Microwave Radiometer after 1 Year in Orbit. *Oral presentation at OSTST meeting, Seattle, USA*. Available at: <http://www.aviso.oceanobs.com/fileadmin/documents/OSTST/2009/oral/Brown.pdf>
- [52] S. Brown. 2010. A Novel Near-Land Radiometer Wet Path-Delay Retrieval Algorithm: Application to the Jason-2/OSTM Advanced Microwave radiometer. *IEEE TGRS vol. 48 n°4*. Available at ftp://podaac.jpl.nasa.gov/allData/ostm/preview/L2/AMR/docs/Brown_TGARS_2010.pdf
- [53] Cerri, L. , Berthias, J. P. , Bertiger, W. I. , Haines, B. J. , Lemoine, F. G. , Mercier, F. , Ries, J. C. , Willis, P. , Zelensky, N. P. and Ziebart, M. (2010) Precision Orbit Determination Standards for the Jason Series of Altimeter Missions, *Marine Geodesy*, **33:1**, 379 - 418. Available at http://pdfserve.informaworld.com/816985_925509111.pdf
- [54] Cerri, L., A. Couhert, S. Houry, F. Mercier. 2011. Improving the long-term stability of the GDR orbit solutions. *Oral presentation at OSTST meeting, San Diego, USA*. Available at http://www.aviso.oceanobs.com/fileadmin/documents/OSTST/2011/oral/02_Thursday/Splinter3POD/05_Cerri.pdf.
- [55] Chambers, D., P., J. Ries, T. Urban, and S. Hayes. 2002. Results of global intercomparison between TOPEX and Jason measurements and models. *Paper presented at the Jason-1 and TOPEX/Poseidon Science Working Team Meeting, Biarritz (France), 10-12 June*.
- [56] Collard, F. (2005). Algorithmes de vent et période moyenne des vagues JASON à base de réseaux de neurones. BO-021-CLS-0407-RF. Boost Technologies.
- [57] Commien, L., S. Philipps, M. Ablain and N. Picot. 2009. SSALTO CALVAL Performance assessment Jason-1 GDR “C”/GDR “b”. *Poster presented at OSTST meeting, Seattle, USA*. Available at: <http://www.aviso.oceanobs.com/fileadmin/documents/OSTST/2009/poster/commien.pdf>

- [58] Couhert, A., L. Cerri, F. Mercier, S. Houry. 2010. Status of Jason-1 and Jason-2 GDR orbits. *Talk presented at OSTST meeting, Lisbon, Portugal.* Available at: <http://www.aviso.oceanobs.com/fileadmin/documents/OSTST/2010/oral/couhert.pdf>
- [59] DeCarvalho, R., S. Brown, B. Haines and S. Desai. 2009. Global cross calibration and validation of the Jason-1 and Jason-2/OSTM data products. *Oral presentation at OSTST meeting, Seattle, USA.* Available at: <http://www.aviso.oceanobs.com/fileadmin/documents/OSTST/2009/oral/deCarvalho.pdf>
- [60] Desjonquieres, J.-D., G. Carayon, J.-L. Courriere, and N. Steunou “POSEIDON-2 In-Flight results”, *Oral presentation at OSTST meeting, Nice, France, 9-12 november 2008.* Available at <http://www.aviso.oceanobs.com/fileadmin/documents/OSTST/2008/oral/desjonquieres.pdf>
- [61] Desjonquères, J. D. , Carayon, G. , Steunou, N. and Lambin, J. (2010) Poseidon-3 Radar Altimeter: New Modes and In-Flight Performances, *Marine Geodesy*, **33**:1, 53 - 79. Available at http://pdfserve.informaworld.com/542982_925503482.pdf
- [62] Dettmering, Denise and Bosch, Wolfgang (2010) Global Calibration of Jason-2 by Multi-Mission Crossover Analysis, *Marine Geodesy*, **33**:1, 150 - 161. Available at http://pdfserve.informaworld.com/315039_925510361.pdf
- [63] - Dibarboire, G., F. Boy, J. D. Desjonquieres, S. Labroue, Y. Lasne, N. Picot, J. C. Poisson, and P. Thibaut, 2014: Investigating short-wavelength correlated errors on low-resolution mode altimetry. *J. Atmos. Oceanic Technol.*, **31**, 1337–1362, doi:10.1175/JTECH-D-13-00081.1
- [64] Dorandeu.,J., M. Ablain, Y. Faugère, F. Mertz, 2004 : Jason-1 global statistical evaluation and performance assessment. Calibration and cross-calibration results. *Marine Geodesy* **27**: 345-372.
- [65] - Dufau, C., M. Orsztynowicz,G. Dibarboire, R. Morrow, and P.-Y. Le Traon (2016), Mesoscale resolution capability of altimetry:Present and future, *J. Geophys. Res.Oceans*, **121**, doi:10.1002/2015JC010904.
- [66] Faugère, Y. et al. 2009. The SLOOP project: preparing the next generation of altimetry products for open ocean. *Poster presented at OSTST meeting, Seattle, USA.* Available at: <http://www.aviso.oceanobs.com/fileadmin/documents/OSTST/2009/poster/Faugere2.pdf>
- [67] Faugère, Y. et al. 2010. CROSS-CALIBRATION between ENVISAT and JASON-1/2. *Oral presentation at OSTST meeting, Lisbon, Portugal.* Available at: http://www.aviso.oceanobs.com/fileadmin/documents/OSTST/2010/oral/19_Tuesday/Tuesday_afternoon/faugere.pdf
- [68] Jason-2 Version “T” Geophysical Data Records : Public Release, August 2009. Available at : http://www.aviso.oceanobs.com/fileadmin/documents/data/products/Jason-2_GDR_T_disclaimer.pdf
- [69] Renaudie C., S. Philipps, 2014: Comparison of the latest GSFC SLR/DORIS std1204 orbits with current orbits for TP,J1 and J2. CLS Ramonville St Agne.
- [70] Gourrion, J., Vandemark, D., Bailey, S., Chapron, B., Gommenginger, G.P., Challenor, P.G. and Srokosz, M.A., 2002: A two-parameter wind speed algorithm for Ku-band altimeters, *Journal of Atmospheric and Oceanic Technology*. **19**(12) 2030-2048.
- [71] http://grgs.obs-mip.fr/grace/variable-models-grace-lageos/mean_fields

- [72] Dumont, J.-P., V. Rosmorduc, N. Picot, S. Desai, H. Bonekamp, J. Figa, J. Lillibridge, R. Sharroo, 2011: OSTM/Jason-2 Products Handbook. CNES: SALP-MU-M-OP-15815-CN. EUMETSAT: EUM/OPS-JAS/MAN/08/0041. JPL: OSTM-29-1237. NOAA/NESDIS: Polar Series/OSTM J400. Available at http://www.aviso.oceanobs.com/fileadmin/documents/data/tools/hdbk_j2.pdf
- [73] Hernandez, F. and P. Schaeffer, 2000: Altimetric Mean Sea Surfaces and Gravity Anomaly maps inter-comparisons. AVI-NT-011-5242-CLS, 48 pp. CLS Ramonville St Agne.
- [74] Huffman, G. and D.T.Bolvin, 2009: TRMM and Other Data Precipitation Data Set Documentation. Available at ftp://precip.gsfc.nasa.gov/pub/trmmdocs/3B42_3B43_doc.pdf
- [75] Imel, D.A. 1994. Evaluation of the TOPEX/POSEIDON dual-frequency ionospheric correction. *J. Geophys. Res.*, **99**, 24,895-24,906.
- [76] Jalabert,E., A.Couhert, J. Moyer, F. Mercier, S. Houry, S. Rios-Bergantinos. 2015. JASON-2, SARAL AND CRYOSAT-2 STATUS. *Talk presented at OSTST meeting, Reston, USA, 20-23 October 2015.*http://meetings.aviso.altimetry.fr/fileadmin/user_upload/tx_ausyclsseminar/files/OSTST2015/POD-01-Jalabert.pdf
- [77] Lemoine, F.G., Zelensky N.P., Chinn, D.S., et al. (2010), Towards development of a consistent orbit series for TOPEX, Jason-1, and Jason-2 Adv. Space Res., 46(12), 1513–1540, doi: 10.1016/j.asr.2010.05.007 (updated).
- [78] Lemoine, F., N.P. Zelensky, S. Melachroinos, D.S. Chinn, B.D. Beckley, D.D. Rowlands, and S.B. Luthcke. 2011. GSFC OSTM (Jason-2), Jason-1 & TOPEX POD Update. *Oral presentation at OSTST meeting, San Diego, USA.* Available at http://www.aviso.oceanobs.com/fileadmin/documents/OSTST/2011/oral/02_Thursday/SplinterPOD/03Lemoine_et.al_SWT2011_v01.pdf.
- [79] Lemoine F., N.P. Zelensky, D.S. Chinn, B.D. Beckley, D.E. Pavlis, J. Wimert, O. Bordyugov. 2014 : New GSC POD Standards for TOPEX/Poseidon, Jason-1, Jason-2 (OSTM). *Oral presentation at OSTST meeting, Konstanz, Germany.* Available at <http://www.aviso.altimetry.fr/fr/coin-utilisateur/equipes-scientifiques/sci-teams.html>.
- [80] Le Traon, P.-Y., J. Stum, J. Dorandeu, P. Gaspar, and P. Vincent, 1994: Global statistical analysis of TOPEX and POSEIDON data. *J. Geophys. Res.*, **99**, 24619-24631.
- [81] MSEs (CNES, NASA, NOAA, EUMETSAT). 2011. GDR Status. *Oral presentation (by N. Picot) at OSTST meeting, San Diego, USA.* Available at http://www.aviso.oceanobs.com/fileadmin/documents/OSTST/2011/oral/03_Friday/Plenary/GDRProducts/02PicotGDR_status_2011.pdf.
- [82] Aviso one-satellite-based Mean Sea Level reprocessing, http://www.aviso.altimetry.fr/fileadmin/documents/data/products/indic/msl/MSL_reprocessing_201402.pdf.
- [83] Moyer J., E. Jalabert, A. Couhert, S. Rios-Bergantinos, F. Mercier, S.Houry. 2014 : Jason-2 POD status. *Oral presentation at OSTST meeting, Konstanz, Germany.* Available at <http://www.aviso.altimetry.fr/fr/coin-utilisateur/equipes-scientifiques/sci-teams.html>.
- [84] Obligis, E., L. Eymard, M. Ablain, B. Picard, J.F. Legeais, Y. Faugere and N. Picot, 2010. The wet tropospheric correction for altimetry missions: A mean sea level issue. *Oral presentation at OSTST meeting, Lisbon, Portugal.* Available at http://www.aviso.oceanobs.com/fileadmin/documents/OSTST/2010/oral/19_Tuesday/OBLIGIS.pdf.

- [85] Ollivier A., Faugere Y., Granier N., 2008: Envisat RA-2/MWR ocean data validation and cross-calibration activities. Yearly report. Technical Note CLS.DOS/NT/09.10, Contract N° SALP-RP-MA-EA-21633-CLS http://www.aviso.oceanobs.com/fileadmin/documents/calval/validation_report/EN/annual_report_en_2008.pdf
- [86] Ollivier A., Faugere Y., P. Thibaut, G. Dibarboire, and J.-C. Poisson, 2008: Investigation on the high frequency content of Jason-1 and Jason-2. CLS.DOS/NT/09-027
- [87] Ollivier A., M. Guibbaud, Faugere Y. Envisat RA2/MWR ocean data validation and cross-calibration activities. Yearly report 2011. SALP-RP-MA-EA-22062-CLS, CLS.DOS/NT/12-021.
- [88] Ollivier A., A. Couhert, V. Pignot, C. Renaudie, S. Phillips, N. Picot, 2014 : Assessment of orbit quality through the SSH calculation towards GDR-E standards. *Oral presentation at OSTST meeting, Constance, Germany*. Available at <http://www.aviso.altimetry.fr/fr/coin-utilisateur/equipes-scientifiques/sci-teams.html>
- [89] Ollivier A., S. Philipps, M. Ablain, A. Edwell, L. Cerri, N. Picot, 2013 : Assessment of Orbit Quality through the Sea Surface Height calculation, New insight in resolving long term and inter-annual signal for climate studies. *Oral presentation at OSTST meeting, Boulder, USA*. Available at <http://www.aviso.altimetry.fr/fr/coin-utilisateur/equipes-scientifiques/sci-teams.html>
- [90] Ollivier A., Dibarboire G., Picard B., Ablain M., OSTST2014, Konstanz - Germany, "Spectral analysis of altimetric signal and errors Towards a spectral error budget of Nadir Altimetric missions" http://meetings.aviso.altimetry.fr/fileadmin/user_upload/tx_ausyclsseminar/files/30Ball0900-2_Pres_OSTST2014_J2_ErrorBugdet_Spectra_Ollivier.pdf
- [91] Otten M., C. Flohrer, T. Springer, and W. Enderle. 2011. Generating precise and homogeneous orbits for Jason-1 and Jason-2. *Oral presentation at OSTST meeting, San Diego, USA*. Available at http://www.aviso.oceanobs.com/fileadmin/documents/OSTST/2011/oral/03_Friday/Splinter6POD/01_Otten.pdf.
- [92] Peltier, 2004, Global Glacial Isostasy And The Surface of The Ice-Age Earth: The ICE-5G (VM2) Model and GRACE. *Annual Review of Earth and Planetary Sciences*, May 2004, Vol. 32, Pages 111-149, doi: 10.1146/annurev.earth.32.082503.144359
- [93] Philipps, S., M. Ablain, J. Dorandeu, P. Thibaut, N. Picot and J. Lambin. 2006. SSALTO CALVAL Performance assessment Jason-1 GDR 'B'/GDR 'A'. *Poster presented at OSTST meeting, Hobart, Australia*. Available at: <http://www.aviso.oceanobs.com/fileadmin/documents/OSTST/2006/ablain1.pdf>
- [94] Picot, N., P. Thibaut, N. Tran, S. Philipps, J.C. Poisson, T. Moreau, and E. Bronner. 2010. New Jason-2 GDR-C standards. *Oral presentation at OSTST meeting, Lisbon, Portugal*. Available at http://www.aviso.oceanobs.com/fileadmin/documents/OSTST/2010/oral/PThibaut_Jason2.pdf.
- [95] Picot, N., P. Thibaut, N. Tran, S. Philipps, J.C. Poisson, E. Bronner, C. Garcia and many others. 2011. Jason-2 GDR-D standards. *Oral presentation at OSTST meeting, San Diego, USA*. Available at http://www.aviso.oceanobs.com/fileadmin/documents/OSTST/2011/oral/02_Thursday/Splinter5IP/05NPicot_et_al_OSTST_2011_J2-GDRD-Standards.pdf.
- [96] Schaeffer, P., A. Ollivier, Y. Faugere, E. Bronner, and N. Picot. The new CNES CLS 2010 Mean Sea Surface. *Oral presentation at OSTST meeting, Lisbon, Portugal, 18-20 october 2010*. Available at http://www.aviso.oceanobs.com/fileadmin/documents/OSTST/2010/oral/19_Tuesday/Schaeffer.pdf.

- [97] Schaeffer, P., Y. Faugere, J.-F. Legeais, A. Ollivier, T. Guinle, and N. Picot (2012). The CNES_CLS11 Global Mean Sea Surface Computed from 16 Years of Satellite Altimeter Data. *Marine Geodesy* **35**: sup1, 3-19. Available at <http://www.tandfonline.com/doi/abs/10.1080/01490419.2012.718231>
- [98] DUACS/Aviso team 'A new version of SSALTO/Duacs products available in April 2014' <http://www.aviso.altimetry.fr/fileadmin/documents/data/duacs/Duacs2014.pdf>
- [99] Scharroo, R., J. Lillibridge, and W.H.F. Smith, 2004: Cross-calibration and long-term monitoring of the Microwave Radiometers of ERS, TOPEX, GFO, Jason-1 and Envisat. *Marine Geodesy*, 97.
- [100] Solar Radio Flux (10.7cm) (daily solar data). Available at http://www.swpc.noaa.gov/ftpmenu/indices/old_indices.html
- [101] Thibaut, P. O.Z. Zanifé, J.P. Dumont, J. Dorandeu, N. Picot, and P. Vincent, 2002. Data editing: The MQE criterion. *Paper presented at the Jason-1 and TOPEX/Poseidon Science Working Team Meeting, New-Orleans (USA), 21-23 October.*
- [102] Thibaut, P., J.-C. Poisson, A. Ollivier, S. Philipps, and M. Ablain: "Jason-2 waveforms, tracking and retracking analysis", *Oral presentation at OSTST meeting, Nice, France, 9-12 november 2008*. Available at <http://www.aviso.oceanobs.com/fileadmin/documents/OSTST/2008/oral/thibaut.pdf>
- [103] Moreau, T., P. Thibaut, 2009. Etude dépointage Poseidon-3: optimisation de l'angle d'ouverture d'antenne. CLS-DOS-NT-09-028. 15 pp, CLS Ramonville St. Agne.
- [104] P. Thibaut. Bilan des activités d'expertise altimétriques menées en 2009 : Lot 2D. SALP-RP-MA-EA-21808-CLS, CLS-DOS-NT-10-029.
- [105] Tran, N. , Labroue, S. , Philipps, S. , Bronner, E. and Picot, N. (2010) Overview and Update of the Sea State Bias Corrections for the Jason-2, Jason-1 and TOPEX Missions, *Marine Geodesy*,**33:1, 348 - 362**. Avialable at http://pdfserve.informaworld.com/804727_925502357.pdf
- [106] Tran, N., P. Thibaut, J.-C. Poisson, S. Philipps, E. Bronner, and N. Picot. Jason-1, Jason-2 and TOPEX Sea State Bias. Overview and Updates. *Oral presentation at OSTST meeting, Lisbon, Portugal, 18-20 october 2010*. Avialable at <http://www.aviso.oceanobs.com/fileadmin/documents/OSTST/2010/oral/TRAN.pdf>
- [107] N. Tran, S. Philipps, J.-C. Poisson, S. Urien, E. Bronner, and N. Picot. Impact of GDR_D standards on SSB corrections. *Oral presentation at OSTST meeting, Venice, Italy, 27-28 September 2012*. Available at http://www.aviso.oceanobs.com/fileadmin/documents/OSTST/2012/oral/02_friday_28/01_instr_processing_I/01_IP1_Tran.pdf.
- [108] Zlotnický, V. 1994. Correlated environmental corrections in TOPEX/POSEIDON, with a note on ionospheric accuracy. *J. Geophys. Res.*, **99**, 24,907-24,914
- [109] Edward D. Zaron , Robert deCarvalho, 2016. Identification and Reduction of Retracker-Related Noise in Altimeter-Derived Sea Surface Height Measurements. *Journal of Atmospheric and Oceanic Technology*, p201-210, doi:10.1175/JTECH-D-15-0164.1
- [110] Zawaszki, L., M. Ablain, A. Cazenave, B. Meyssignac. 2014. Confidence envelop of the Global MSL time-series deduced from Jason-1 and Jason-2 altimetric missions. *Poster presentation at OSTST meeting, Constance, Germany, 28-31 October 2014*, Available at http://meetings.aviso.altimetry.fr/fileadmin/user_upload/tx_ausyclsseminar/files/Poster_OSTST14_GMSLUncertainty.pdf
- [111] World Meteorological Organization, 2010: El Nino/ La Nina Update (30 March 2010). Available at http://www.wmo.ch/pages/prog/wcp/wcasp/documents/El_Nino_Mar10_Eng.pdf.

- [112] World Meteorological Organization, 2011: El Nino/ La Nina Update (25 January 2011). Available at http://www.wmo.ch/pages/prog/wcp/wcasp/documents/El-Nino_Jan11_Eng.pdf.
- [113] World Meteorological Organization, 2015: El Nino/ La Nina Update (16 November 2015). Available at http://www.wmo.int/pages/prog/wcp/wcasp/documents/WMO_ENSO_Nov15_Eng.pdf
- [114] Correction Troposphérique Humide pour le radiomètre Jason-3 : approche neuronale. CLS-J3PROTO-15-0002. Projet CNES PEACHI-J3
- [115] H. Roinard, E. Cadier. Jason-2 validation and cross calibration activities (Annual report 2017). Reference: SALP-RP-MA-EA-23186-CLS. Available at https://www.aviso.altimetry.fr/fileadmin/documents/calval/validation_report/J2/SALP-RP-MA-EA-23186-CLS_Jason-2_AnnualReport2017_v1-2.pdf.
- [116] M. Ablain. N. Taburet. L. Zawadski. R. Jugier. M. Vayre. SALP annual report (2017) of Mean Sea Level Activities. Reference: SALP-RP-MA-EA-23189-CLS. Available at https://www.aviso.altimetry.fr/fileadmin/documents/calval/validation_report/SALP-RP-MA-EA-23189-CLS_AnnualReport_2017_MSL.pdf.
- [117] Uncertainty in Satellite estimate of Global Mean Sea Level changes, trend and acceleration. Michaël Ablain, Benoit Meyssignac, Lionel Zawadzki, Rémi Jugier, Aurélien Ribes, Anny Cazenave, and Nicolas Picot <https://doi.org/10.5194/essd-2019-10>
- [118] Lionel Zawadzki , Michaël Ablain, Loren Carrere, Richard D. Ray, Nikita P. Zelensky, Florent Lyard, Amandine Guillot, and Nicolas Picot. Investigating the 59-Day Error Signal in the Mean Sea Level Derived From TOPEX/Poseidon, Jason-1, and Jason-2 Data With FES and GOT Ocean Tide Models
- [119] Ngan Tran (CLS, France); Doug Vandemark (UNH, USA); Hui Feng (UNH, USA); Fabrice Ardhuin (LOPS, France); Lotfi Aouf (Meteo-France, France); Sophie LeGac (CNES, France); Nicolas Picot (CNES, France) Updated Jason-3 wind speed and SSB solutions (2D and 3D). Abstract: https://cpaess.ucar.edu/sites/default/files/images/abstracts_book-OSTST-2017-2.pdf, Poster number: IPC_001. https://meetings.aviso.altimetry.fr/fileadmin/user_upload/tx_ausyclsseminar/files/Poster OSTST17_SSB_tran.pdf
- [120] Ngan Tran (CLS, France), Gerald Dibarboure (CNES, France), Nicolas Picot (CNES, France). Improving the continuity of the Jason SSB time-series. https://meetings.aviso.altimetry.fr/fileadmin/user_upload/tx_ausyclsseminar/files/Poster OSTST18_SSB_tran.pdf
- [121] https://meetings.aviso.altimetry.fr/fileadmin/user_upload/tx_ausyclsseminar/files/2017-10-25_Le_Gac_Jason-3_DEM_validation_OSTST2017_FINAL_OSTST.pdf
- [122] https://meetings.aviso.altimetry.fr/fileadmin/user_upload/tx_ausyclsseminar/files/Pres OSTST2017_Jason3_HRoinard.pdf
- [123] <https://www.aviso.altimetry.fr/en/data/product-information/updates-and-reprocessing/ssaltoduacs-product-changes-and-updates.html>
- [124] https://meetings.aviso.altimetry.fr/fileadmin/user_upload/CLOS_10_Ray.pdf
- [125] Wahr JM (1985) Deformation induced by polar motion. J Geophys Res 90(B11):9363–9368. doi:10.1029/JB090iB11p09363
- [126] Revisiting the pole tide for and from satellite altimetry. Desai S., Wahr J., Beckley B., J Geod (2015) 89: 1233. <https://doi.org/10.1007/s00190-015-0848-7>

[127] Climate Change Initiative conclusions and recommandations about Pole Tide (2015) 1-http://www.esa-sealevel-cci.org/webfm_send/389 2-http://www.esa-sealevel-cci.org/webfm_send/400 3-http://www.esa-sealevel-cci.org/webfm_send/549 4-http://www.esa-sealevel-cci.org/webfm_send/539